8-2010

Application of Signal Advance Technology to Electrophysiology

Chris M. Hymel

The TMC LIBRARY
Health Sciences Resource Center

APPLICATION OF SIGNAL ADVANCE TECHNOLOGY
TO ELECTROPHYSIOLOGY

by

Chris M. Hymel, B.S., M.Eng.

Houston, Texas

APPROVED:

_____
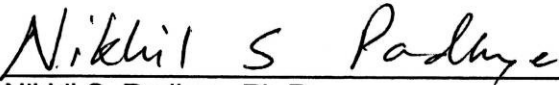
Khader M. Hasan, Ph. D., Supervisory Professor

_____
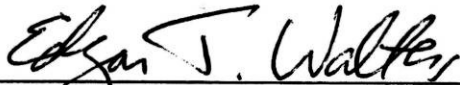
James A. Bankson, Ph. D.

_____

Victoria P. Knutson, Ph.D.

_____

Nikhil S. Padhye, Ph.D.

_____
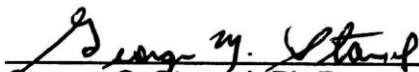
Edgar T. Walters, Ph.D.

_____

Richard E. Wendt, Ph. D.

APPROVED:

_____

George C. Stancel, Ph.D.
Dean, The University of Texas
Graduate School of Biomedical Sciences at Houston

APPLICATION OF SIGNAL ADVANCE TECHNOLOGY
TO ELECTROPHYSIOLOGY

by

Chris M. Hymel, B.S., M.Eng.
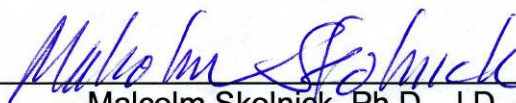
Houston, Texas

We have guided and mentored Mr. Hymel through the design, implementation and analysis of his dissertation. We are pleased to be recognized for the part we have played in his scientific development.

_____

Michael E. Brandt, Ph.D.

_____

Malcolm Skolnick, Ph.D., J.D.

_____

H. Martin Blacker. M.D.

APPLICATION OF SIGNAL ADVANCE TECHNOLOGY
TO ELECTROPHYSIOLOGY

A

DISSERTATION

Presented to the Faculty of
The University of Texas
Health Science Center at Houston
and
The University of Texas
M. D. Anderson Cancer Center
Graduate School of Biomedical Sciences

in Partial Fulfillment

of the Requirements

for the Degree of

DOCTOR OF PHILOSOPHY

by

Chris M. Hymel, B.S., M.Eng.
Houston, Texas

August, 2010

Dedication

To G_d,

His Son,

the Holy Spirit,

and Milinda

Acknowledgements

I have come to realize that the completing the dissertation is so much more and an individual effort – it took a team of caring and dedicated people.

I would first like to express my heartfelt appreciation for the support provided by Michael Brandt and Malcolm Skolnick. You spent countless hours providing inspiration, guidance, insight and support over the years, well beyond serving in any official capacity. You encouraged and motivated me to strive for excellence and without your selfless commitment, this work may never have been completed.

I also wish to thank my advisor, Hasan Khader and the other members of my supervisory committee, James Bankson, Victoria Knutson, Nikhil Padhye, Edgar T. Walters and Richard Wendt III. You generously gave your time and guidance and pushed me further than I thought possible under challenging circumstances. Your collective input greatly improved the dissertation.

I further wish to thank Ron Stubbers, H. Martin Blacker, Harold Russell and Jon Wiener for your encouragement and assistance through this process.

To my mom, dad and siblings, thank you for your continued encouragement.

To my daughters Andrea, Ashley, Emma and Evan, thank you for your love and support.

To my wife, Milinda, please know just how much I appreciate your unyielding and unconditional love and patience, and the sacrifices made to allow me to finish this work – often believing in me when I struggled to believe in myself. I love you all.

Abstract

Medical instrumentation used in diagnosis and treatment relies on the accurate detection and processing of various physiological events and signals. While signal detection technology has improved greatly in recent years, there remain inherent delays in signal detection/ processing. These delays may have significant negative clinical consequences during various pathophysiological events. Reducing or eliminating such delays would increase the ability to provide successful early intervention in certain disorders thereby increasing the efficacy of treatment.

In recent years, a physical phenomenon referred to as Negative Group Delay (NGD), demonstrated in simple electronic circuits, has been shown to temporally advance the detection of analog waveforms. Specifically, the output is temporally advanced relative to the input, as the time delay through the circuit is *negative*. The circuit output precedes the *complete* detection of the input signal. This process is referred to as signal advance (SA) detection.

An SA circuit model incorporating NGD was designed, developed and tested. It imparts a constant temporal signal advance over a pre-specified spectral range in which the output is almost identical to the input signal (i.e., it has minimal distortion).

Certain human patho-electrophysiological events are good candidates for the application of temporally-advanced waveform detection. SA technology has potential in early arrhythmia and epileptic seizure detection and intervention. Demonstrating reliable and consistent temporally advanced detection of electrophysiological waveforms may enable intervention with a pathological event (much) earlier than previously possible. SA detection could also be used to improve the performance of neural computer interfaces, neurotherapy applications, radiation therapy and imaging.

In this study, the performance of a single-stage SA circuit model on a variety of constructed input signals, and human ECGs is investigated. The data obtained is used to quantify and characterize the temporal advances and circuit gain, as well as distortions in the output waveforms relative to their inputs.

This project combines elements of physics, engineering, signal processing, statistics and electrophysiology. Its success has important consequences for the development of novel interventional methodologies in cardiology and neurophysiology as well as significant potential in a broader range of both biomedical and non-biomedical areas of application.

TABLE OF CONTENTS

LIST OF ILLUSTRATIONS

Chapter V:

Chapter VI

Appendix A:

LIST OF TABLES

Appendix C:

Chapter I

Introduction

There are numerous biomedical applications where an electrophysiological signal is transduced, analyzed and then returns information that is useful therapeutically or diagnostically for the purpose of interventional or therapeutic control. The process of acquiring and utilizing physiological data requires its detection as an analog signal typically followed by additional processing steps such as signal amplification, filtering, conversion to digital form, signal interpretation and response generation. Each of these steps takes a certain amount of time to perform, thereby delaying the use of the acquired signal for possible treatment or as an intervention.

In addition, a number of responsive biomedical applications rely on the ability to separate electrophysiological signal features or components based on specific spectral characteristics. Often, features of interest overlap or are masked by other activity in the bioelectric waveform complicating needed feature extraction. As with any signal processing operation, spectral separation delays the use of the processed data, thus potentially reducing its effective use in a responsive biomedical system.

The performance of signal acquisition technology used in electronic systems to acquire and process signals continues to improve. The inherent delays between the detection of electrophysiologically generated signals, their subsequent processing and use however, remain an obstacle with respect to further progress in treatment-intervention.

To address this problem and provide a possible method for improving responsive system performance, this dissertation describes the development of a circuit model, based on a phenomenon in physics referred to as Negative Group Delay (NGD) that can be used to offset signal processing delays by temporally advancing the detection of electrophysiological signals.

In Chapter II (Background and Significance) the subject of NGD which signifies the temporal advance of a circuit transit time in electronics, is introduced. Electronic circuitry has been developed to produce an NGD that has been shown to temporally advance (i.e. reduce or negate the time delay) the detection of a range of signals including Gaussian pulses, sine waves and audio signals that contain multiple frequency components. Further, this effect has been demonstrated in both narrow and broad frequency bands using electronic circuitry.

Given the counterintuitive nature of the concept of temporally advancing signal detection, the issue of causality/superluminality is also addressed in Chapter II. Further, the possibility of increasing the temporal advance through the cascading of multiple single-stage signal advance (SA) circuits is discussed. Experimental results from a number of studies for signals ranging in frequency from 0.2 to over 3,000 Hertz (Hz) are summarized, compared and used to project anticipated results for the present study.

The circuit response results obtained from the investigator's early physical circuits and preliminary theoretical circuit models are presented, including circuit models designed for different frequency ranges. A practical discussion of SA utility based on the performance and response times of current analog and digital electronics is also presented. Finally, a rationale for development of an SA circuit designed to operate over the spectral range of 1 to 25 Hz for the purpose of temporally advancing the detection of electrocardiograms (ECG) is provided.

In order to take advantage of current feature selection methodologies used in online signal processing systems, any temporally advanced output must have minimal signal distortion of the features of interest. In the case of electrocardiology, a number of clinical indications are related to variations in the timing of events, as well as ECG amplitude

variations. As such, the timing of signal components and signal distortion are important considerations.

Hypotheses

Based on the background information, results of previous studies and the investigator's preliminary results, the following working hypothesis is put forth:

ECG waveform detection (specifically, individual heartbeats) can be temporally advanced at least 5 ms ($\pm$ 5%/0.25 ms) using a single-stage SA circuit model. In addition, the output signal distortion with respect to the input signal will be ten percent or less.

Stated as a null hypothesis, ECG waveform detection temporal advance obtained using a single-stage SA circuit model is less than or equal to 4.75 ms and the output distortion is greater than 10%.

In order to test these hypotheses, the SA circuit model should meet the following performance goals:

1) Temporal advance of ECG waveforms by 5 ms ($\pm$ 0.25 ms) with a coefficient of variation (Cv) of less than 5%,

2) Mean gain of $1.0 \pm 10\%$ with a Cv of less than 10%,

3) Distortion ratio of less than 10%,

4) A statistically insignificant increase in variance (based on the F-test comparing multiple input and output ECG waveform features),

5) Input/output waveform dissimilarity of less than 1%

In order to achieve these goals, it is necessary to quantify the effects of temporally advanced signal detection in terms of the actual advance achieved and any resulting signal distortions. This is accomplished by comparing the temporally advanced output waveforms to their respective inputs. The specific objectives of this study are:

Objective 1

To design and develop a single stage, SA circuit model optimized for the frequency range of 1 to 25 Hz using circuit analysis/simulation software. Preliminary testing of the SA circuit model is performed using the following input test signals: 1) Gaussian pulses with half amplitude pulse widths of > 0.2 s (1/2 period of 25 Hz sinusoids) and 2) single frequency sinusoidal waveforms between 1 and 25 Hz. The results obtained will be used to confirm performance of the SA circuit model design and evaluate adequacy of the constructed input test signals.

Objective 2

To test the SA circuit model using the following constructed test signals: 1) Twenty-five Gaussian pulses with widths of 0.2 to 5.0 s (1/2 period of 1 to 25 Hz sinusoids), 2) Twenty-five single frequency sinusoids ranging from 1 to 25 Hz; 3) Twenty-five tri-frequency waveforms constructed of three superposed sinusoids of varying amplitudes and frequencies.

The results are analyzed in the time-domain in order to quantify and characterize the duration and constancy of both the temporal advance and the gain of the SA circuit output with respect to its input as well as any resultant signal distortion. Cross-correlation analyses will be employed to objectively determine the temporal advance obtained based on the time associated with the maximum correlation.

The input and output signals are then subjected to spectral analysis in order to 1) characterize signal distortion in the output waveforms, 2) calculate the gain relative to

frequency for the triple frequency test signals and 3) apply correlation analysis to compare the spectral content of the outputs with their respective inputs.

Objective 3

To test the effects of SA circuitry on pre-recorded human electrocardiography (ECG) waveforms (specifically individual sinus rhythms/heartbeats), including three ECG's from subjects exhibiting normal sinus rhythms and two from subjects exhibiting tachycardia. The results are analyzed in both the time (temporal advance and gain) and frequency domains (signal distortion) using the analyses described in Objective 2. Cross-correlation analyses are employed to quantify the temporal advance achieved. Input/output distortion ratios are calculated and Fourier and correlation analyses are used to quantify morphological shape distortion.

Achieving these objectives enables the requisite results to quantify the signal detection temporal advance and characterize the effect of the SA circuitry on the ECG signals.

In Chapter III (SA Circuit Model Design and Initial Testing) the methods employed in theoretical circuit model design using SPICE circuit development and analysis software are discussed and the theoretical circuit response characteristics in terms of gain, phase and group delay with respect to frequency are presented. In addition, composition of the preliminary test signals (Gaussian pulse and sine waves) and methods used to construct them, and the initial results of their application to the SA circuit model are reviewed.

Chapter IV (SA Circuit Model Testing and Results Analyses) describes the methods for rigorous testing of the SA circuit model using constructed input test signals (Gaussian pulses, single frequency sine waves and triple frequency signals). The test signal construction and application to the SA circuit model is described. The transformation of the time domain signals into the frequency domain is explained. Finally, input and output signals are compared and analyzed in both the time and frequency domain and detailed experimental results are provided including:

- output variability relative to the input,
- the constancy and amplitude of the gain relative to frequency,
- the constancy and duration of the signal detection temporal advance,
- overall distortion, and
- waveform dissimilarity.

In Chapter V (Application to ECG Signals) the preparation and application of ECG test signals (specifically individual heartbeats) to the SA circuit model is discussed. The time and frequency domain analyses and the experimental results are also provided. Also, assumptions regarding the spectral content of the ECG signals are tested and additional variability results are presented.

In Chapter VI (Discussion) the results obtained are summarized and interpreted with respect to the original hypotheses and the SA circuit model performance goals. A number of potential applications of SA technology are described that represent both near- and long-term opportunities to potentially improve system performance. In addition, some of the study limitations and deficiencies are discussed as well as recommendations for remediation. And finally, a number of possible future studies are briefly described that address some of the study deficiencies and that may build on the results obtained in this investigation.

Chapter II
Background and Significance

Negative Group Delay

A phenomenon referred to as negative group delay (NGD) has recently been demonstrated in simple electronic circuits [1-5]. Typically, the group delay of a waveform propagating through a circuit or medium provides a measure of the transit time of the waveform envelope as it progresses through it. Thus, NGD, a counterintuitive concept, refers to a temporally advanced circuit transit time for a range of signals (i.e., the time delay is negated or reduced). Figure 2.1 shows results which demonstrate the relationship between the output of such a circuit relative to a Gaussian pulse input. Note that the detection of the output peak actually precedes the *complete* input signal peak detection.
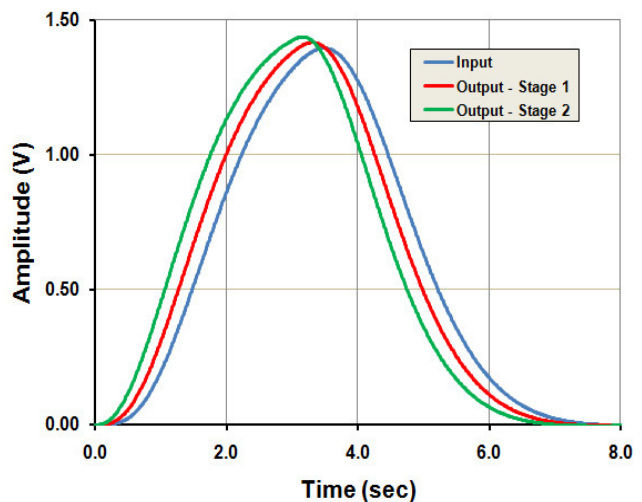
Figure 2.1: Input/advanced output

A simplified block diagram of a circuit that exhibits NGD is shown in Figure 2.2. The circuit consists of a high-gain operational amplifier (op amp) whose output is fed back to its inverting input (negative feedback) after passing through a passive linear feedback circuit. This passive linear feedback circuit consists of a combination of resistive, capacitive, or inductive components.
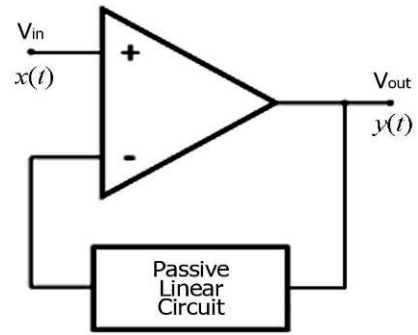
Figure 2.2: Simplified circuit block diagram.

A signal applied to a passive linear circuit typically exhibits a temporal delay as the energy from the signal is stored in the electric field of the capacitors and the magnetic field of the inductors while it passes through these circuit components. High-gain operational amplifiers function to reduce the difference between the respective signals applied to their inverting (-) and non-inverting (+) inputs. In this circuit configuration, the output signal from the op amp passes through the feedback circuit incurring a time delay before being applied to the inverting input. This slightly delayed and inverted output recursively (repeatedly) applied to the inverting input results in the leading or foremost portions of the input waveform being differentially amplified, while the lagging portions are attenuated.

The number of repeated cycles and the delay in the feedback loop are a function of the op amp response time and the overall impedance of the passive linear circuit. For a given op amp, the values of the components comprising the passive linear circuit in the feedback loop determine the overall signal transforming characteristics of the temporal advance circuitry.

Alternate explanations for NGD have been offered by other investigators. For example,

> "…for operational amplifiers with a sufficiently high gain-feedback product, the voltage difference between the two input signals arriving at the inverting and non-inverting inputs of the amplifier must remain small at all times. The operational amplifier must therefore supply a signal with a *negative* group

delay at its output, such that the *positive* delay from the passive filter is exactly canceled out by this negative delay at the inverting (-) input port." [3],

and

"…there is sufficient information in the early portion of any analytic voltage wave form to reproduce the entire waveform earlier in time.**"** [6].

Empirically, the net result is that "this negative feedback circuit will produce an output pulse whose peak leaves the output port of the circuit *before* the peak of the input pulse arrives at the input port of this circuit." [3].

Op amp configurations that effectively reverse the circuit's transfer function (mathematical representation of the relationship, as a function of frequency, between the input and output of a circuit) are not uncommon. For example, a negative impedance converter transforms a resistive load to its negative. Gyrator circuits use capacitive impedance to simulate large inductive impedances [7,8]. Thus, gyrators can be used to replace the large physical coils previously used to achieve large inductive impedance.

At first glance, the behavior of these circuits is counter-intuitive. It appears to violate causality since the temporally advanced output signal occurs before the input signal has been completely detected. This seemingly contradictory circuit behavior may be understood by recognizing that electromagnetic propagation is characterized by five different signal velocities as described by the physicist Léon Brillouin [9]. These are

- *Phase velocity* - the speed at which the phase of any one spectral frequency component of the wave travels.
- *Group velocity* **-** the speed at which the variations in the shape of the wave's amplitude (known as the modulation or envelope of the wave) propagates.
- *Front velocity* - the speed of an abrupt signal discontinuity (signal abruptly turned on or off).
- *Velocity of energy transport* - the speed of energy transfer.
- *Signal velocity*- the speed of information transfer, which, under various conditions, may be equivalent to one or more of the above four velocities.

According to Brillouin, the "front velocity will correspond to the speed at which the very first, extremely small (perhaps invisible) vibrations will occur, while the signal velocity yields the arrival of the main signal, with intensities on the order of the magnitude of the input signal." [9].

Typically, the signal velocity is equivalent to both the group and energy transport velocities. While the front velocity cannot exceed the speed of light, in special cases (e.g., media or circuitry which amplifies the initial or anterior-most portion of a waveform and attenuates the posterior portion), "… the group velocity … can be greater than the velocity of light c, can be infinite and even negative!" [9]. That is, the detection of a pulse or waveform at the output can precede its *complete* detection at the input. During the time interval between the arrival of the wave-front (front velocity) and the actual detection of the group waveform, electromagnetic energy begins to propagate through the circuit, the magnitude of which is not detectable until the oscillations achieve sufficient amplitude (Figure 2.3).
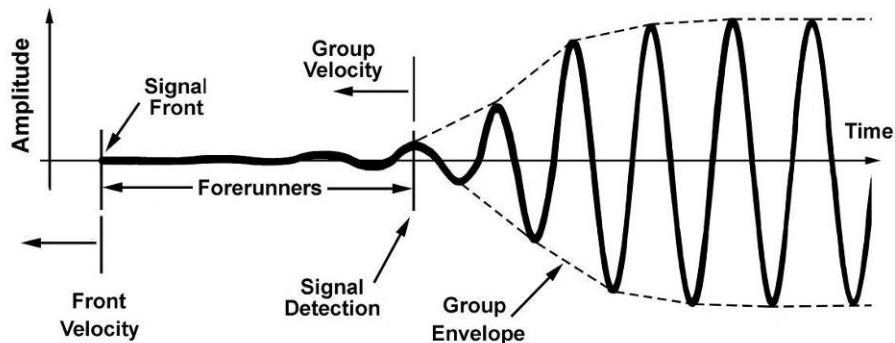
Figure 2.3: Front velocity and group velocity.

These very early, very low energy (typically undetected) perturbations (called forerunners by Brillouin) actually contain sufficient information to reproduce a temporally advanced signal. Thus, temporally advanced signal detection is accomplished by using a high-gain oscillator to amplify these earliest signal deflections. [1-3,10]. A signal temporal advance may not exceed the front velocity thereby establishing a theoretical signal detection or group velocity advance upper limit [1,3,9]. Electrophysiological signals are typically characterized by a waveform amplitude envelope that propagates at the group

velocity. Thus, for most bioelectric waveforms, the signal velocity is equivalent to the group velocity.

Causality/Superluminality

A number of articles refer to NGD as superluminal (faster than the speed of light) signal propagation [3,5,6], which raises the question, "Does NGD violate causality?" The question of superluminality and causality were addressed in studies in which the input signal was suddenly discontinued. This resulted in a simultaneous (rather than advanced) discontinuity (signal or waveform abruption) in the output demonstrating a causal relationship between the input and output waveforms [1,3,5]. The causality issue was further examined in a study in which detection of the temporally advanced output peak was used as a trigger to abruptly discontinue the input signal before reaching its peak amplitude [2] which resulted in a damped oscillation in the temporally advance output waveform, again satisfying causality.

NGD circuitry essentially imparts a phase shift to the input signal thereby advancing its detection without violating causality. NGD has been demonstrated with both sinusoidal and "complex" (comprising multiple spectral components) audio signal inputs in which, over a band-limited spectral range, the phase has a positive linear slope with respect to frequency [5].

Group delay is defined as the negative of the rate of change of phase with respect to frequency, denoted mathematically as [11]:

$$\tau(\omega) = -\delta\varphi(\omega)/\delta\omega, \tag{2.1}$$

where ω is the frequency in radians and φ is the signal phase.

As such, the negative of the derivative of a function with a positive linear slope yields an NGD that is constant over a specific frequency range.

Utilizing Fourier analysis, any signal may be decomposed into a sum of sine waves of different frequencies. Further, the output of any linear, time-invariant system is equal to the sum of the responses of the system to each of its inputs [12]. Circuitry designed to impart a linear phase shift (with respect to frequency) will produce a constant temporal advance to all of the sine wave group velocities (over a limited spectral range). The result is equivalent to detecting the signal earlier than can currently be achieved with state-of-the art electronics technology. In the remainder of this work this temporally advanced signal detection effect is referred to as Signal Advance (SA).

Circuit Cascading

The signal detection temporal advance that may be achieved in a single circuit stage appears to be limited to a fraction of the narrowest half-cycle pulse width of its input analog signal [1,4,5,13]. Serial cascading of SA circuit stages (Figure 2.4) to increase the overall temporal advance has also been demonstrated. It has further been suggested that the resulting advance could exceed the narrowest input pulse width [3,4,13] but is likely limited to a few pulse rise times [10]. As the temporal advance increases through the cascading of multiple stages, signal distortion tends to increase due possibly to "ringing" – the generation of higher frequency components close to the circuit's resonant frequency.
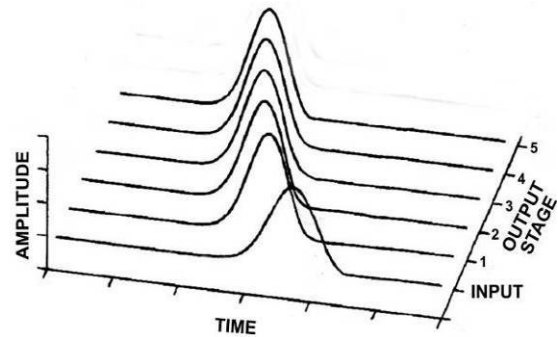
Figure 2.4: Cascading SA circuits.

The phrase "a few pulse rise times" is interpreted as two to four pulse rise times, and a "pulse rise time" as one half of a pulse width (one fourth the period - Figure 2.5). This suggests that the overall advance that may be obtained, even with sequential cascading, may be limited to about one full period of the highest frequency component of the signal.
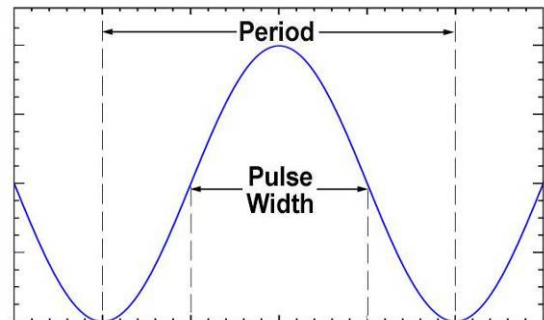
Figure 2.5: Pulse width vs. period.

Cao, et al, [13] demonstrated that cascading could increase temporal advance of the signal within a narrow bandwidth with waveform distortion limited to pulse-width compression. However, this required highly filtered input waveforms [4,13]. It has been further demonstrated that multi-pole (i.e., having multiple resonances or characteristic frequencies) NGD circuitry may be designed that exhibits a relatively constant temporal advance and gain for band-limited signals [5].

A functional block diagram of a single SA circuit is shown in Figure 2.6. Depending on the specific application, an SA circuit may include the following sub-stages:

1. A pre-filter/signal conditioning stage (analog only),
2. A temporal advance circuit stage (analog), and
3. A post-filter/signal conditioning stage (analog or digital).
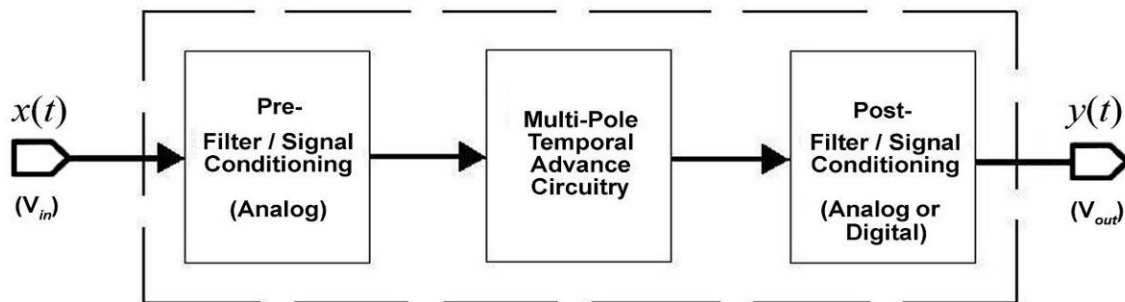
Figure 2.6 SA circuit with pre- and post- filtering/signal conditioning.

It is important to note that the pre-filter/signal conditioning stage consists of analog circuitry (not digital), whereas the post-filter/signal conditioning stage may be implemented using either analog or digital electronics. Recall that the temporal advance circuitry functions to selectively amplify the very early, signal perturbations (referred to as forerunners [9]) effectively imparting a temporal advance to the analog signal detection. If the input signal is subjected to digital filtering/signal conditioning prior to its application to the temporal advance circuit, these early, low amplitude perturbations would be lost during the conversion from analog to digital.

Pre-filtering may be used to band-limit the incoming signals and, in the case of cascaded SA circuits, reduce or eliminate distorting noise from preceding stages. Post-

filtering may be used to eliminate distortions resulting from the temporal advance circuit sub-stage.

It should also be noted that in order to achieve an overall signal detection temporal advance, any required pre- and/or post-filter stage must operate in less time than the temporal advance achieved by the SA circuit stage. Electronics technology that exhibits sufficiently short response times to achieve this will be discussed in more detail later.

Parallel arrays of narrowband SA circuits (where single SA circuits are additionally cascaded) can be configured to generate a more application specific input-output response (Figure 2.7). This parallel arrangement provides a mechanism to achieve a temporal signal advance over specific spectral frequency bands tuned to detect certain aspects of the incoming analog signal.
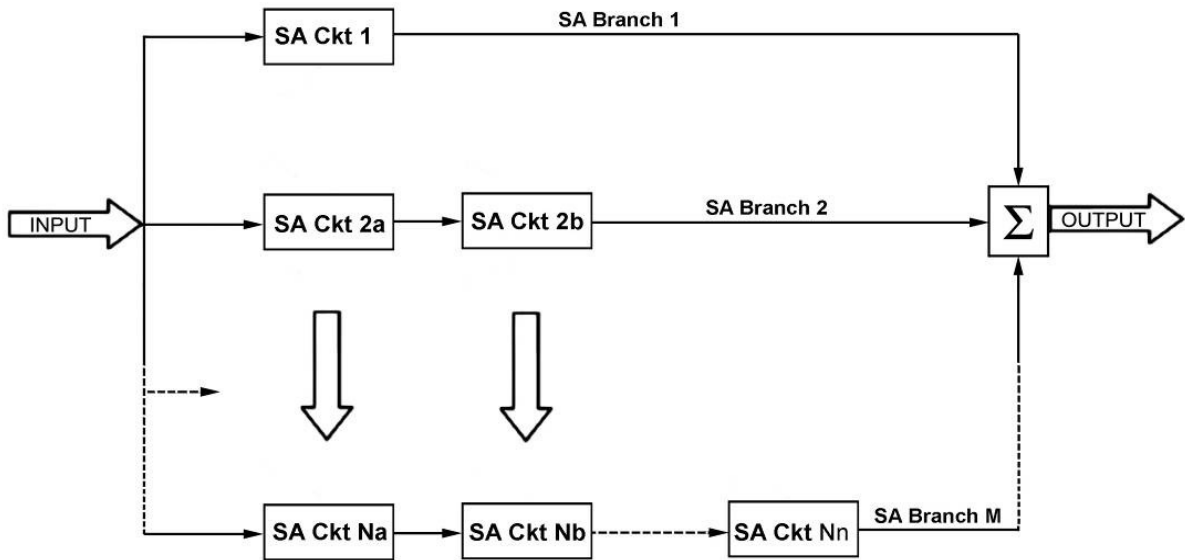
Figure 2.7: Parallel SA circuit array.

In general, the narrower the spectral band over which the SA circuit operates, the less complicated the SA circuit design. In addition, the lower the maximum frequency the greater the detection advance that can be achieved per stage, thus fewer cascade stages might be required as the obtainable advance is a function of the highest frequency (narrowest half-cycle pulse width) in the input signal.

14

Parallel configurations using narrowband SA circuits could yield a more linear input-output response in terms of gain and temporal advance over narrow spectral ranges of interest. Alternatively, they could be configured to impart varying delays/advances over certain spectral ranges, effectively acting as spectral filters resulting in temporal separation of waveform components based on their spectral content.

A number of practical applications have been described in the literature in which the use of NGD purportedly improves operational efficiency and system performance in several domains including: integrated circuit internal clocking [14,15], transistor-transistor communication [3], signal sampling and processing [16,17], microwave applications [18,19] and signal cable transmission [20]. Thus far, no references in the literature have been found reporting bioelectric applications of NGD. Moreover, the cited applications do not operate over spectral ranges that generally include electrophysiological signals nor do they exhibit response characteristics suitable for such applications. Thus, application of NGD or temporal advance to physiological signals provides a fresh and open field of investigation that may have application in interventional, control or other responsive systems.

Review of Previous NGD Investigations

The results of a number of studies investigating NGD over a range of input signals reveal a consistent relationship between their primary wavelength/pulse widths and the temporal advance that was achieved. For studies in which the input signal was sinusoidal, the period of the signal's highest frequency component (representing the minimum pulse width of the signal) was defined as the pulse width at one half amplitude of a raised cosine with a period equal to the inverse of the frequency of the sinusoid (Figure 2.5).

Table 2.1 summarizes these results for inputs with half amplitude pulse widths ranging from about 2 s to 150 µs, which corresponds to a spectral range of 0.2 Hz to 3.3 kHz. The summary shows the duration of the temporal advance obtained as a percentage of the input pulse width.

These results are depicted graphically in Figure 2.8. The advance achieved in a single stage relative to the input pulse width ranges from 30 to 40 percent; averaging about

35%. For example, for a bioelectric waveform in which the range of spectral content of interest is less than 100 Hz and the period is 10 ms, thus the half amplitude pulse width is 5 ms. As such, the signal detection temporal advance expected from a single SA circuit stage is about 1.5 ms. Similarly, for an SA circuit model designed for signals with spectral content less than 25 Hz, the expected detection temporal advance would be around 5 ms.

Table 2.1: Input pulse width/frequency and temporal advance.

Study	Pulse Width	Equivalent Frequency	Advance	Percent Advance
Hymel (2007)*	2.44 s	0.20 Hz	0.9 s	36.9%
Kitano, et al., [4]	1.95 s	0.26 Hz	0.5 s	25.6%
Chaio, et al., [3]	37.5×10^{-3} s	13 Hz	12.1×10^{-3} s	32.3%
Hymel (2008)**	20.0×10^{-3} s	25 Hz	5.3×10^{-3} s	26.5%
Hymel (2008)*	5.0×10^{-3} s	100 Hz	1.53×10^{-3} s	30.6%
Zhilu, et al., [16]	1.57×10^{-3} s	320 Hz	0.66×10^{-3} s	42.0%
Hymel (2008)*	0.67×10^{-3} s	750 Hz	0.31×10^{-3} s	46.5%
Munday, et al [5]	0.17×10^{-3} s	3000 Hz	0.078×10^{-3} s	46.8%
Erickson, et al. [19]	0.15×10^{-3} s	3300 Hz	0.047×10^{-3} s	31.7%

* See Preliminary Results (this chapter)   ** See Chapter 4 - Temporal Advance Results
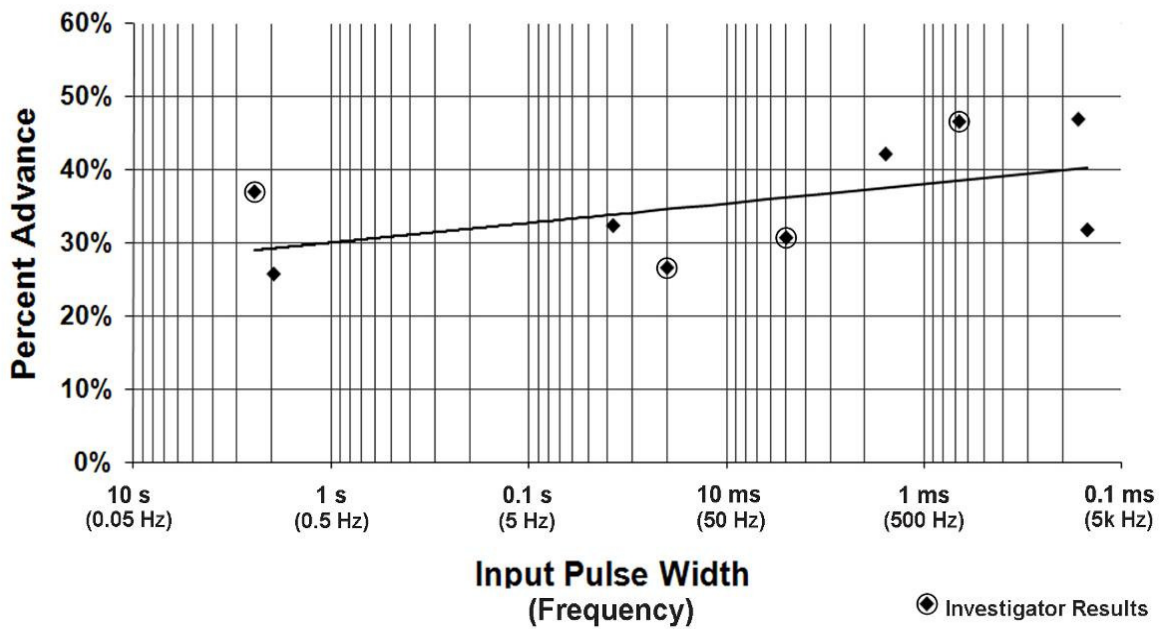
Figure 2.8: Percent advance relative to input pulse width.

16

Preliminary Results

Initial development efforts involved replicating and then later improving the response of NGD circuits described in the literature [3,4,5] using the Super-SPICE Gold Professional Circuit Analysis software package. These designs were tested using Gaussian pulse inputs and later, Gaussian-windowed sine waves. Gaussian-windowing (or filtering) was selected since the majority of the NGD studies employed Gaussian waveforms due to their rapid spectral roll-off and mathematical simplicity. Use of Gaussian-windowing also facilitates any future time-frequency analyses since the derivative of a Fourier transform of a Gaussian window is also a Gaussian function.

Based on the simulated design results, a two-stage SA circuit board (Figure 2.9) was constructed. To facilitate visual inspection, the circuit was tested using a Gaussian pulse with a half amplitude pulse width of two seconds as the input signal. Figure 2.10 is a time-lapsed image of a dual-trace oscilloscope (timescale: 0.5 s/div)

Figure 2.9: SA circuit board.

showing the temporally advanced output pulse relative to the input. The signal detection advance achieved in each stage was roughly 0.45 s resulting in a 0.9 s overall advance. Note the output distortion (narrowed pulse width and skewing) relative to the input.
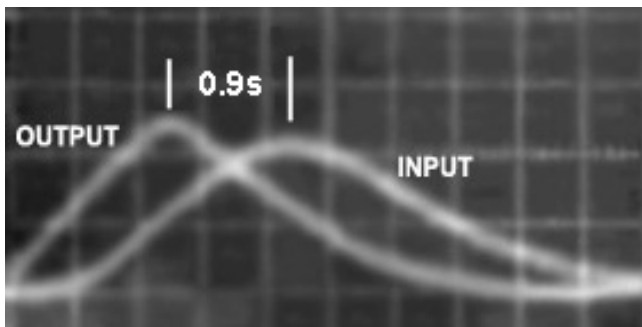
Figure 2.10: Actual SA output vs. input.

While the temporal advance obtained was over 0.5 s, it varied as a function of frequency (Figure 2.11) becoming positive (indicative of a time delay) as the frequency approached 0.45 Hz. Although these efforts convincingly demonstrate that a signal temporal advance design using NGD can be implemented in electronics, the response characteristics of this particular design would be of little utility in electrophysiology.

In order to achieve a constant temporal advance (or negative group delay) over a specific spectral range, the phase response must have a positive linear slope relative to frequency over the desired frequency range [5]. Subsequent SA circuit design efforts focused on establishing a relatively constant gain and temporal advance response over a spectral range relevant for electro-physiological signals (less than 1 kHz) that required a multi-pole design in order to linearize

Figure 2.11: Delay vs. frequency.

the circuit responses. Figure A.1 (Appendix A) is a general schematic diagram for a three stage (including a resistor voltage divider), quadruple zero and quadruple pole SA circuit (without any pre- or post-filtering). The transfer function $(\Delta \tilde{V}_{out} / \Delta \tilde{V}_{in})$ for this circuit may be expressed as

$$\left[1+\left(\frac{1}{R_2}\right)\left(\frac{1}{(R_1+i\omega L_1)^{-1}+i\omega C_1}\right)\right] \times \left[1+\left(\frac{1}{R_4}\right)\left(\frac{1}{(R_3+i\omega L_2)^{-1}+i\omega C_2}\right)\right] \times \left(\frac{R_{29}}{R_{29}+R_{30}}\right) \quad (2.2)$$

where the R's are resistors, L's are inductors, C's are capacitors, i is the imaginary number (square root of -1), and ω is frequency in radians per second.

SPICE circuit analysis software was used to numerically simulate the idealized theoretical performance of this circuit model using the program's AC analysis function. This analysis yielded data used to calculate responses in terms of the circuit model's gain, phase and group delay with respect to frequency. In the next chapter, the SPICE theoretical circuit performance/analysis is compared with an engineering-mathematical analysis of the circuit's transfer function.

In order to develop an SA circuit model that demonstrates a relatively constant signal detection advance and gain response over a specific frequency range, the circuit components used by Munday and Henderson [5], which exhibited a relatively constant response range from 1 to over 2,500 Hz, were scaled. This was followed by adjusting their values to match the available physical components.

This process provides a method for the development of SA circuit models that exhibit a relatively constant gain and signal detection temporal advance response over a particular frequency range of interest. Two interim SA circuit model designs for the frequency ranges of 1 to 500 Hz and 1 to 100 Hz were developed based on this methodology. The theoretical circuit response results obtained for each of the SA circuit model designs are described over the next few pages.

Figure 2.12 is a semi-log graph of gain vs. frequency for an SA circuit model designed to achieve a linear positive slope through the threshold frequency of interest (in this case 500 Hz). Note the constancy of the gain for spectral content through 500 Hz and the location of the poles (at just over 1,000 and 2,000 Hz), and, later, in Figure 2.16 (at just over 200 and 400 Hz).
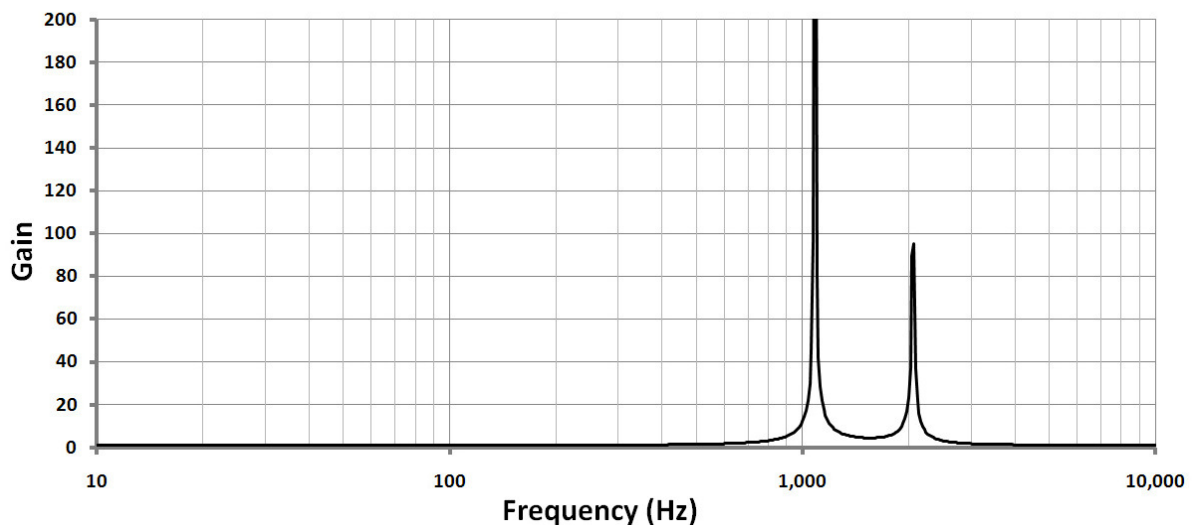
Figure 2.12: Gain vs. frequency (500 Hz SA circuit model, semi-log).

Figure 2.13 is a semi-log graph of phase vs. frequency of the 500 Hz SA circuit model. Note the phase discontinuities which correspond to the poles in Figure 2.12. Figure 2.14 is a linear-linear graph of phase vs. frequency for the same circuit model that displays the phase response over the frequency range from 1 to 1,200 Hz. Note the phase response has a positive linear slope to almost 1,000 Hz.

19
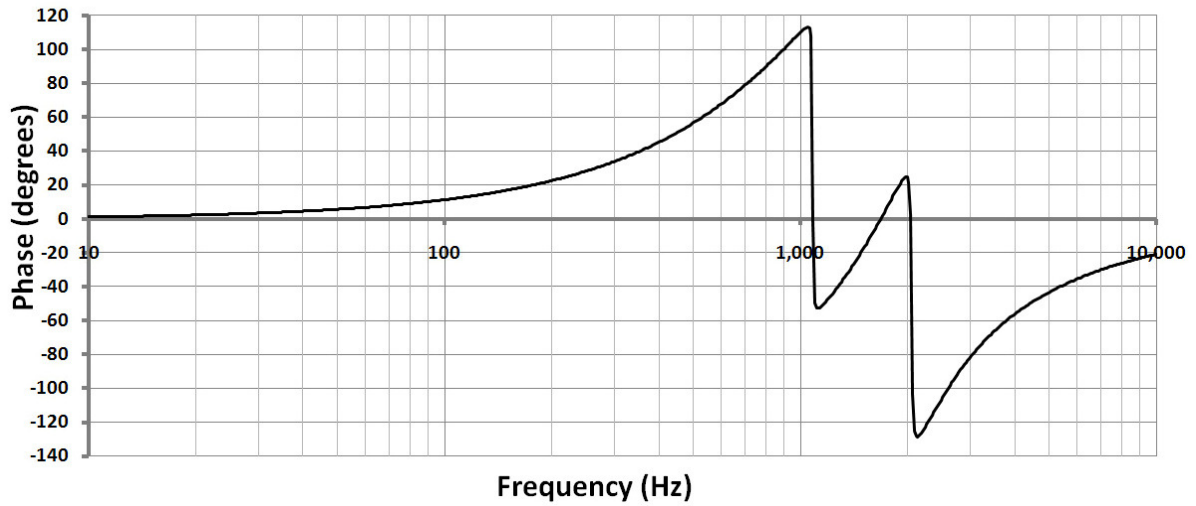
Figure 2.13: Phase vs. frequency (500 Hz SA circuit model, semi-log).
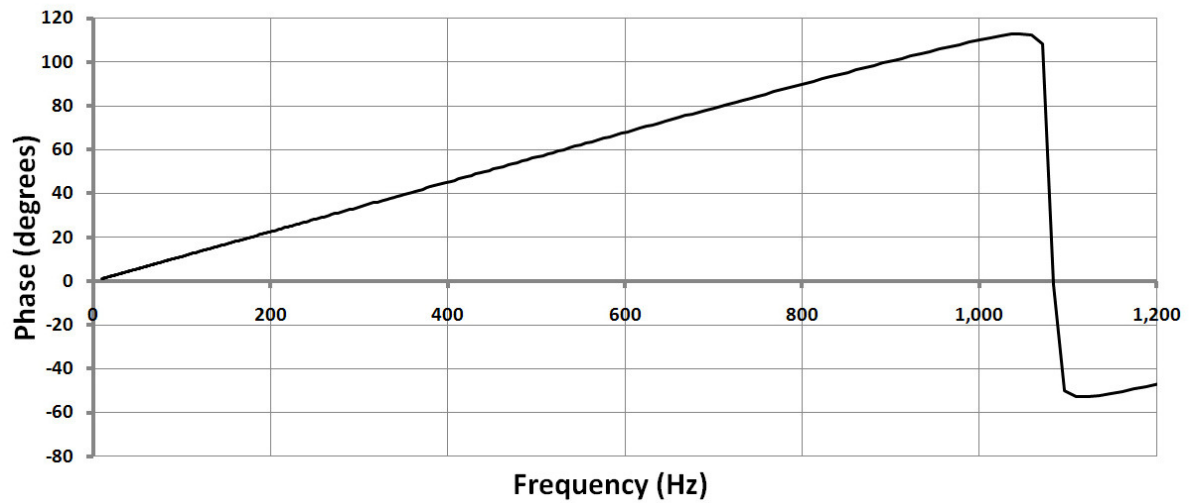
Figure 2.14: Phase vs frequency (500 Hz SA circuit model, linear).

Figure 2.15 is a semi-log graph of group delay vs. frequency for the same SA circuit. Recall that negative group delay is equivalent to a signal detection temporal advance. Note the constancy of the temporal advance (~300 µs) for spectral frequencies through 500 Hz. The discontinuities correspond to the poles in the gain plot (Figure 2.12).
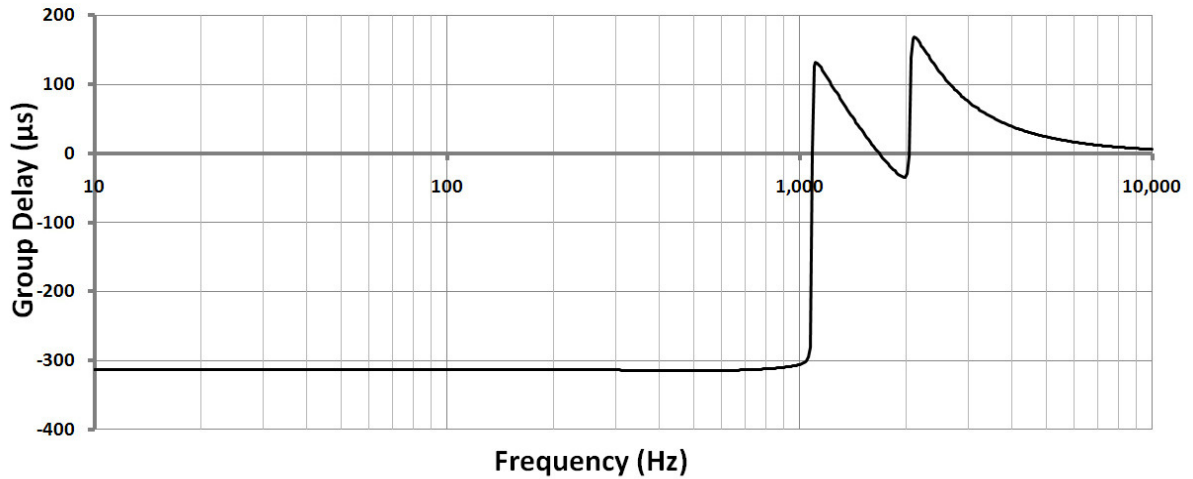
Figure 2.15: Group delay vs. frequency (500 Hz SA circuit model, semi-log).

Following successful development of the 500 Hz SA circuit model, an SA circuit design was developed to accommodate signals with spectral content in the range of 1 to 100 Hz. Figures 2.16 and 2.17 depict the gain and group delay (respectively) vs. frequency.

The signal gain and detection temporal advance are effectively constant through 100 Hz and the temporal advance (or NGD) has increased to 1.5 ms.
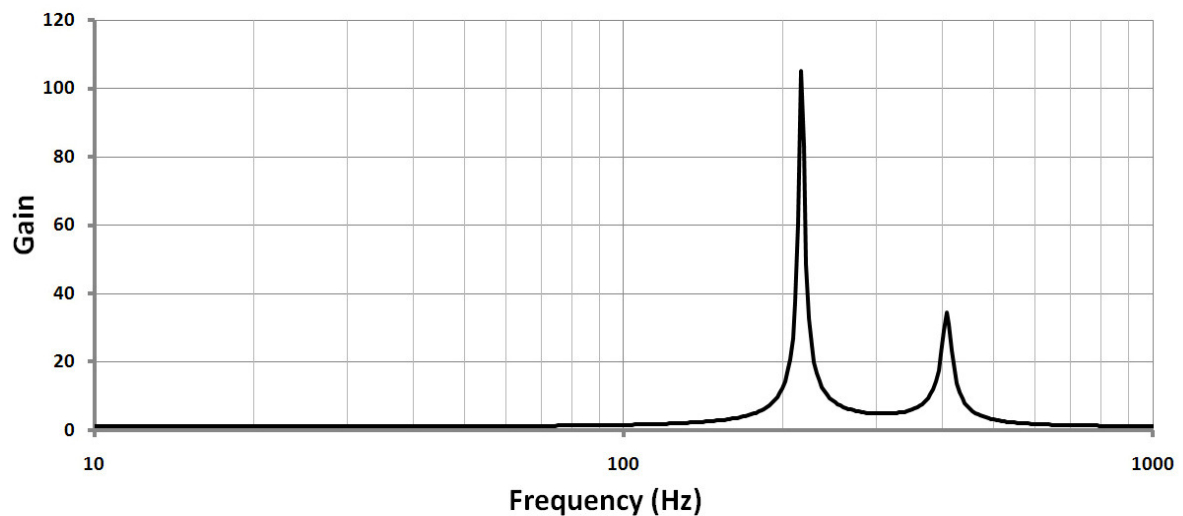
Figure 2.16: Gain vs. frequency (100 Hz SA circuit model, semi-log).

21
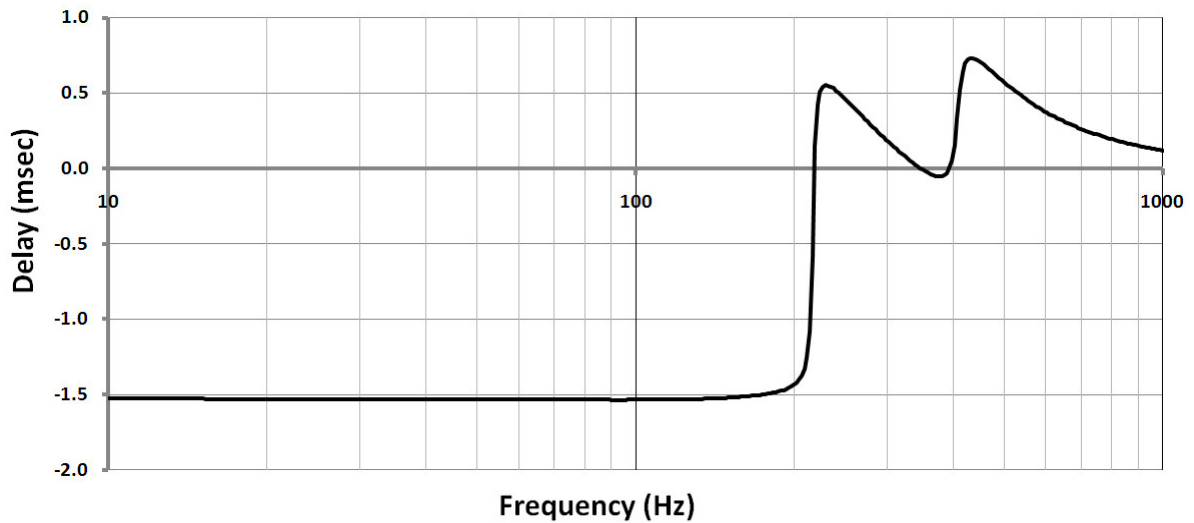
Figure 2.17: Group delay vs. frequency (100 Hz SA circuit model, semi-log).

Significance

In order to derive utility and value in the use of temporally advanced signal detection, there are functional requirements for the majority of electrophysiological applications. The length of the temporal advance achieved must 1) exceed the delay imposed for any required pre- or post-filtering, and 2) provide a sufficient temporal advance to reduce the electrophysiological signal processing time. In addition, for a number of near-term applications, the temporally advanced output must also be a high fidelity representation of the input.

Figure 2.10 shows the display from an oscilloscope of the input pulse and the temporally advanced output. It was noted that the output pulse was both narrowed and skewed (to the left). In the frequency domain, the pulse width narrowing would be manifest as a shift to a slightly higher frequency and the skewing would be indicated by the introduction of additional frequency components due to changes in shape/slope of output pulse. A refined SA circuit design was developed to provide a constant gain and signal detection advance in order to reduce these distortions.

Inspection of Figures 2.12 through 2.17 reveals that any spectral content in the input waveform above the design frequencies (500 Hz and 100 Hz, respectively) would experience disproportionate amplification. Further, in those spectral ranges, there may no longer be a temporal advance, but rather a variable temporal delay in which higher frequency spectral components would appear later in the output signal (Figure 2.15 and 2.17).

These temporal distortions could have a deleterious effect on the fidelity of the advanced output in broadband applications. This signal distortion could potentially render the advanced output unusable for some near-term clinical applications which rely on existing feature detection methods. For these applications, required signal filtering must be completed in significantly less time than the detection temporal advance achieved.

Signal conditioning to compensate for distortion in the temporally advanced output could be accomplished with either active operational amplifier (op-amp) based filters or digital signal processors with response/conversion rates that are negligible relative to the signal temporal advance obtained. Ideally, signal conditioning would eliminate all spectral content above the design cut-off with appropriate roll-off characteristics while considering tradeoffs involving circuit complexity, time delay, and efficacy. Post-filtering would minimize any disproportionately amplified frequencies above the design frequency that may be present in the advanced output generated by the temporal advancing circuitry itself. Signal conditioning filtering could result in signal delays that might inadvertently negate the subsequent temporal advance of the SA circuit. Signal conditioning was not explored in this study.

Use of high-speed op-amps could fulfill both the control response and filtering requirements. The key to successful implementation is the response (or settling) time of high-speed operational amplifiers which range from 5 μs to under 10 ns [21-26]. The time delay resulting from the use of these high-speed op amps will reduce the SA circuit temporal advance by a very miniscule amount (on the order of from 500 to 50,000 times less than a 5 ms advance achieved by the SA circuitry).

If more sophisticated algorithmic filtering or feature detection methodologies are required, digital filtering and detection methods using analog-to-digital convertors (ADCs)

and digital signal processors (DSPs) or digital controllers may be implemented. Recently announced/released ADCs and DSPs, which can be used to perform digital filtering and/or waveform reconstitution have settling times ranging from more than 400 times less (using the ADSI271 [27] or the ADS1605 [28] ADC coupled to the TMS5509 DSP [29]) to more than 6,000 times less (Freescale MC56F8023 Digital Signal Controller [30]) than the projected 5 ms waveform temporal advance. These devices are able to digitize incoming analog waveforms and execute up to forty program instructions per cycle (equivalent to the settling time).

Using the high-speed devices described above, any filtering/signal conditioning needed for most applications could be accomplished using relatively standard analog or digital filtering methods. However, the nonlinear nature of the SA circuit operation may require the development of more sophisticated algorithmic methodologies in order to reconstitute original signal characteristics and detect specific waveform features. It is important to note that while digital filtering/signal conditioning methods can be applied to the temporally advanced output signal, they cannot be applied to the incoming signal prior to its application to the temporal advance circuitry. This is because the analog-to-digital conversion process would eliminate the very early, very low energy (typically undetected) forerunners, which are preferentially amplified by signal advance technology.

Selection of ECG's for this Study

The goal of this research is to evaluate the input/output characteristics a single stage temporal advance circuit designed to impart a constant gain and temporal advance over a specific spectral range in order to facilitate its use as a research tool. Therefore, for the purposes of this study, an SA circuit model was designed to temporally advance detection of human electrocardiogram (ECG) signals.

A number of signal characteristics (Figure 2.18) make the ECG an ideal candidate for the investigation of SA technology:

- The ECG is generally a well-defined waveform containing "signature" voltage deflections designated P, Q, R, S, T, U.
- The QRS complex has a high signal-to-noise ratio (SNR)
- ECG signal amplitudes are measured in millivolts (vs. micro-volts for EEG signals).
- A number of cardiac pathologies are reflected not only by changes in ECG signal amplitudes but in deviations from normal of various time intervals.
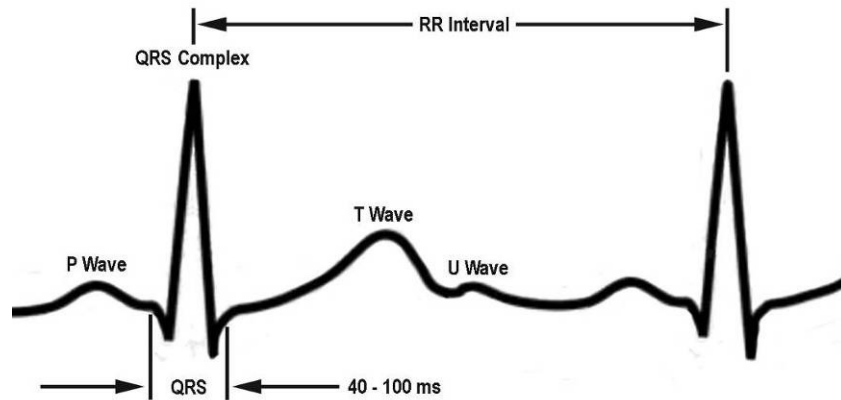
Figure 2.18: Normal sinus rhythm.

Consider a hypothetical ECG application in which the goal is simply the temporally advanced detection of the peak of the R-wave. The duration of the QRS complex of a normal human ECG sinus rhythm ranges from 0.04 to 0.10 s. A minimum 40 ms period for the QRS complex translates to maximum frequency of 25 Hz. Further, normal cardiac rhythms are broadband signals containing harmonics up to approximately 25 Hz [53]. Fourier analysis was applied to ECG recordings of human heart beats. The spectral distributions obtained from these recordings (Figure 2.19) indicate that the majority of the power contribution (> 90%) derives from spectra below 25 Hz, supporting the assertions regarding the frequency content of cardiac rhythms.

Thus, the SA circuit model used in this study to investigate the constancy of both gain and temporal advance of cardiac signals is designed for a frequency range for 1 to 25 Hz. Based on results summarized in Table 2.1 (and shown graphically in Figure 2.8) the projected temporal advance for a single-stage SA circuit model designed for ECG signals with a design cut-off of 25 Hz is expected to be approximately 5 ms.
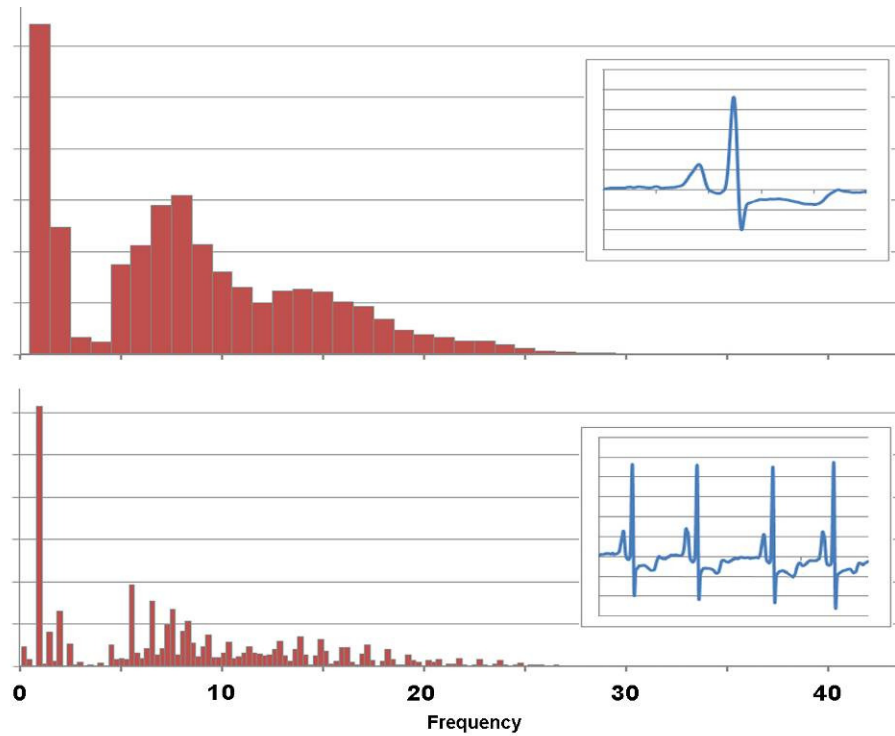
Figure 2.19: Spectral distribution of a normal sinus rhythm.

Summary

The following have been demonstrated with respect to SA circuit technology:

- Output signal detection can be temporally advanced relative to the complete detection of the input signal.

- The advance and gain may be constant over a specified spectral range.

- Wideband analog waveforms (those with multiple spectral components) can be temporally advanced.

- SA circuits are scalable to specific spectral ranges.

- Based on previous studies, the signal detection temporal advance that may be achieved is directly related to input signal pulse width and inversely related to the maximum frequency of the signal.

- Temporally advanced signal detection is not superluminal and does not violate causality.

- Temporal signal advance may be increased by cascading multiple circuit stages.

- The response time of current analog and digital electronics is significantly less than the projected signal detection temporal advance that is likely to be attainable.

- ECG waveform characteristics are well suited for a study of the effect of SA technology on electrophysiological signals.

There appears to be ample evidence that an SA circuit model can be designed that yields both nearly constant amplitude gain and signal detection temporal advance for spectral bands that include electrophysiological signals such as the ECG, EMG and EEG. Furthermore, based on direct experimentation and results obtained by other investigators, the temporal advance can be increased by cascading multiple SA circuit stages, provided that signal distortion and any introduced artifacts (particularly high frequency oscillations) can be kept to a minimum.

SA technology has potential applications in a broad range of signal detection and processing systems, both physiological and non-physiological. SA technology may be well suited for medical instruments and treatment devices as well as electrophysiological interfaces used in the detection, acquisition and processing of band-limited analog waveforms produced by the body (e.g., brainwaves - EEG/MEG; neuromuscular potentials - EMG; cardiac rhythms - ECG). The ability to provide faster, more immediate detection of and a more rapid response to anomalous signals or alarm conditions may enable more effective control or intervention.

Some potential applications include real-time artifact detection/correction, neural pacing/seizure suppression, neurofeedback/neurotherapy, brain-computer/neural interfaces and electrocardiology. Further, SA technology could enhance the performance of physiologically gated diagnostic and therapeutic applications such as imaging and radiotherapy by temporally advancing the detection of certain trigger signals thereby improving target and timing accuracy. For each of these applications, reducing response time and/or temporally separating overlapping signals could yield significant improvements in overall system performance. This may allow for more effective treatment of certain conditions, potentially opening the door to a whole new class of medical devices that respond faster than any that is currently available.

Chapter III

Signal Advance Circuit Model

Design and Initial Testing

A general systems approach was used for the circuit/signal analysis described in the following. Figure 3.1 is a top-level simplified schematic of the black box showing its input and output signals.
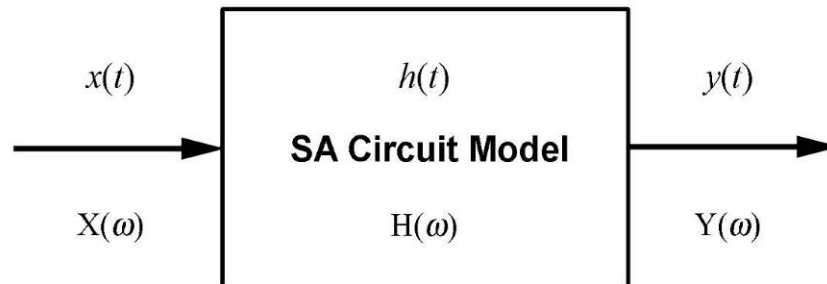
Figure 3.1: Generalized SA circuit model.

The functioning of the circuit model is fully characterized by its so-called impulse response function, $h(t)$. The signal output of the circuit $y(t)$, is the convolution of the input signal $x(t)$ with $h(t)$ or

$$y(t) = x(t) * h(t), \qquad\qquad (3.1)$$

where "*" represents the convolution operator [31]. In signal processing, time domain signals are usually transformed into their frequency domain representations - most notably using Fourier transformation. When transforming the above equation in this way, convolution in the time domain becomes multiplication in the frequency domain:

$$Y(\omega) = X(\omega)\,H(\omega). \qquad (3.2)$$

where $H(\omega)$ is the so-called transfer function of the circuit and ω is the angular frequency in radians ($\omega = 2\pi f$, where f is the regular frequency in Hertz). By convention, capital letters are used for the frequency domain representations of signals. The Fourier domain signals X and Y, and transfer function H are complex (consisting of real and imaginary portions) and can be represented as phasors or vectors, i.e., they are characterized by their magnitude (symbolized by the absolute value sign | |) and phase angle (symbolized by φ) as a function of frequency, ω [32].

The SA circuit model is designed with two architecturally identical stages in series (cascaded), each consisting of different valued components (refer to the general schematic, Figure A.1 and detailed schematics Figures A.2 through A.4 from the SPICE software in Appendix A). A third stage is a voltage divider resistor network also in series that adjusts (reduces) the overall gain of the circuit by an amount $0 < G \le 1$. Going inside the generalized circuit model shown in Figure 3.1, one arrives at the three stage systems diagram (Figure 3.2).
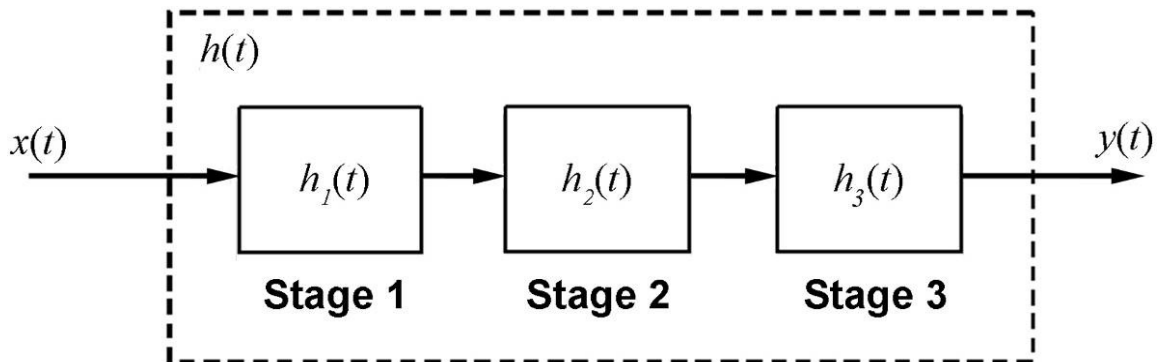
Figure 3.2: Three stage SA circuit model.

Here the overall transfer function is $H(\omega) = H_1(\omega)\, H_2(\omega)\, H_3(\omega)$, and the associated impulse response is $h(t) = h_1(t) * h_2(t) * h_3(t)$, i.e., the individual impulse responses for each stage are convolved to arrive at the impulse response for the overall circuit.

SA Circuit Model Development

SA circuit models were developed using Anasoft's Super-SPICE Gold Professional Circuit Analysis Package [33]. SPICE has been the industry standard software for circuit design for over 25 years [34]. This software tool allows for full analog electronic circuit design, development and functional modeling as well as circuit operation and performance analyses based of the same foundational analyses described above. The circuit response output from SPICE was used to generate the idealized theoretical response functions for the gain, phase and group delay relative to frequency [35,36].

The preliminary results section described a previous physical circuit which was assembled and tested as well as two (100 Hz and 500 Hz) SA circuit models that displayed constant temporal advance and gain characteristics over defined spectral ranges. It is important to recognize the difference between the development of a theoretical model and the SPICE circuit simulation. The theoretical analysis is dependent on mathematical models and assumes idealized component performance, whereas the circuit simulation requires the application of the actual signal to the circuit model and takes into account actual component performance data. Thus any theoretical results must be subsequently validated through circuit simulation and ultimately, in actual circuitry.

The theoretical 25 Hz SA circuit model (Appendix A, Figure A.1), like the 100 Hz and 500 Hz circuit models described in Preliminary Results (Chapter II), is based on a four pole (two pairs of complex conjugate poles) design in order to obtain relatively constant temporal advance and gain characteristics over the frequency band of interest. The initial 25 Hz SA circuit model used no active components in the feedback loop, but rather only resistors, capacitors and inductors. The circuit component values were determined by linearly scaling component values used in the previous SA circuit model designs and subsequently adjusting the values to correspond to the available physical components. The

SA circuit model design yielded the desired circuit transfer response characteristics, essentially a constant gain and positive linear phase response over the frequency range of 1 to 25 Hz, based on the SPICE theoretical AC analysis results.

One result of this process is that the frequency corresponding to the first (lowest resonant frequency) pole is close to 60 Hz. This frequency corresponds to the AC mains' line noise in most North American electrical systems, and is typically filtered to eliminate this source of artifact. For a majority of biomedical signal applications (ECG, EEG, EMG, ENG, etc) the signals are routinely anti-alias/low-pass filtered. In addition, these signals are notch filtered at the mains frequency (60 Hz in North America). In order to adjust the resonant frequency corresponding to the first pole of the SA circuit model, component values used in the first half of the transfer function (eq. 2.2) would need to be modified to shift the first pole to a different frequency, say down to 50-55 Hz or up to 65-70 Hz. Compensatory adjustments of the values of the circuit components affecting the second pole (higher resonant frequency) would then need to be made to retain the desired gain and phase (and therefore negative group delay) responses.

The SA circuit model performance is tested in SPICE using AC analysis to determine its theoretical gain and phase response characteristics with respect to frequency. The SPICE AC analysis uses linearized models for all non-linear circuit components and applies an AC signal with a user specified frequency range providing theoretical circuit performance results (gain and phase) relative to frequency. A few problems were encountered associated with over-reliance upon ideal components exemplified by initial circuit performance failures. Resolution required a period of "debugging" and multiple consultations with Anasoft's SPICE program developer. For example, the idealized capacitors lacked internal resistance (that give rise to voltage leakage in the real world) which was resolved by placing a 10 MΩ (meg-Ohm) resistor in parallel with each capacitor in order to simulate the voltage leakage.

From the AC analysis yielding the circuit model's frequency response, SPICE generates three columns of data accordingly. These are frequency (in radians) and the real and imaginary components of the Fourier transform of the circuit's output voltage for each frequency. From this data, the spectral magnitude of the output was calculated as the

square root of the sum of the squares of the real and imaginary parts of the discrete Fourier transform of the circuit output:

$$|Y(\omega)| = [\text{Re}(Y(\omega))^2 + \text{Im}(Y(\omega))^2]^{1/2}. \tag{3.3}$$

The gain was then found by dividing this measure by the magnitude of the circuit input at each discrete frequency. The phase is calculated by taking the arctangent of the real and imaginary output values and converting from radians into degrees:

$$\varphi(\omega) = \arctan[\text{Im}(Y(\omega))/\text{Re}(Y(\omega))]. \tag{3.4}$$

Recall that group delay is defined as the negative of the rate of change of phase relative to frequency, mathematically $-\delta\varphi(\omega)/\delta\omega$. From the phase results (using frequency in radians), the circuit's average group delay relative to frequency is numerically approximated to first-order as:

$$\tau(\omega) = -(\varphi(\omega + \varepsilon) - \varphi(\omega))/\varepsilon, \tag{3.5}$$

where ε is the frequency resolution following digitization. The gain is computed as:

$$G(f) = |H(f)| = |Y(f)|/|X(f)|, \tag{3.6}$$

where frequency (f) is in Hz.

From these formulae the gain, phase and group delay responses relative to frequency for the 25 Hz SA circuit model were determined and plotted. These responses serve as a basis for comparison with the results from the subsequent circuit model simulation studies.

These circuit responses, derived both directly, using the SA circuit model transfer function, and through the SPICE AC analysis, exhibit a relatively constant gain through 25 Hz (Figure 3.3). The poles (corresponding to the circuit resonant frequencies) are located at 62.0 and 111.7 Hz. The gain associated with the first pole is almost 27.
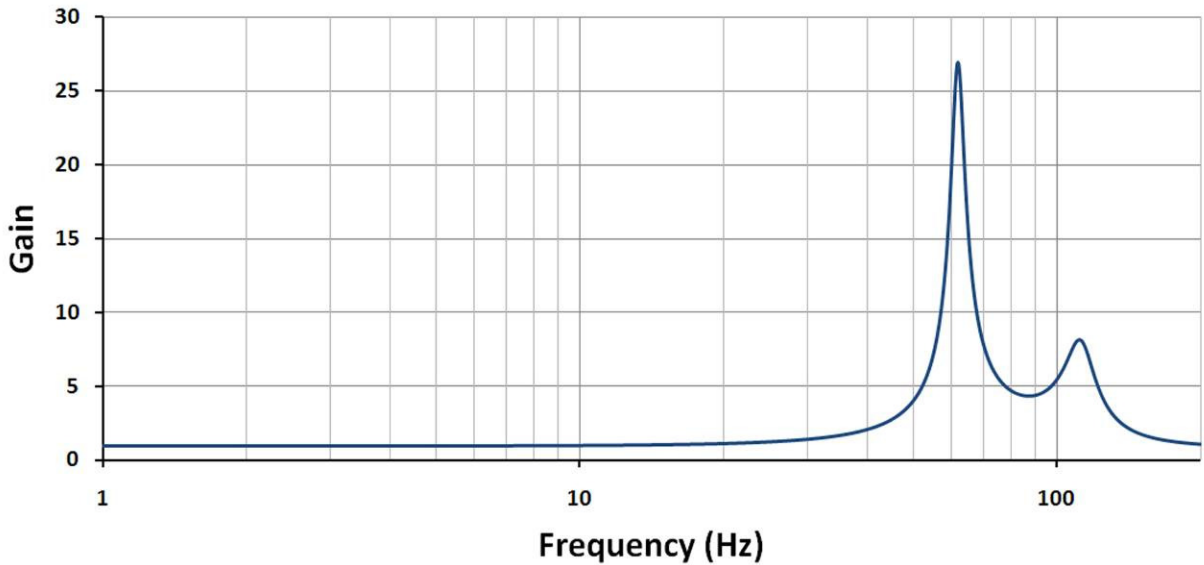
**Figure 3.3: Gain vs. frequency (semi-log plot) for the
SPICE inductor-based SA circuit model.**

The AC analysis applies sinusoids at each frequency of one volt (peak-to-peak), thus the output voltage amplitude corresponding to the peak of the first pole (62 Hz) is nearly 27 V (volts). Given supply voltages of ± 10 V (see schematics, Appendix A), output amplitudes above 10 V are not realizable thus confirming that these responses reflect idealized theoretical results.

Figure 3.4 is a semi-log graph of the theoretical phase vs. frequency for the SA circuit model designed to achieve a linear positive slope through the design frequency of 25 Hz. Note the discontinuities in the phase response that occur at the same resonant frequencies that correspond to the pole locations in the gain response plot (Figure 3.3).

Figure 3.5 is a linear-linear graph of the theoretical phase vs. frequency in which the upper frequency range is reduced to 75 Hz. In this graph, the desired linear phase response with a positive slope beyond 25 Hz is evident.
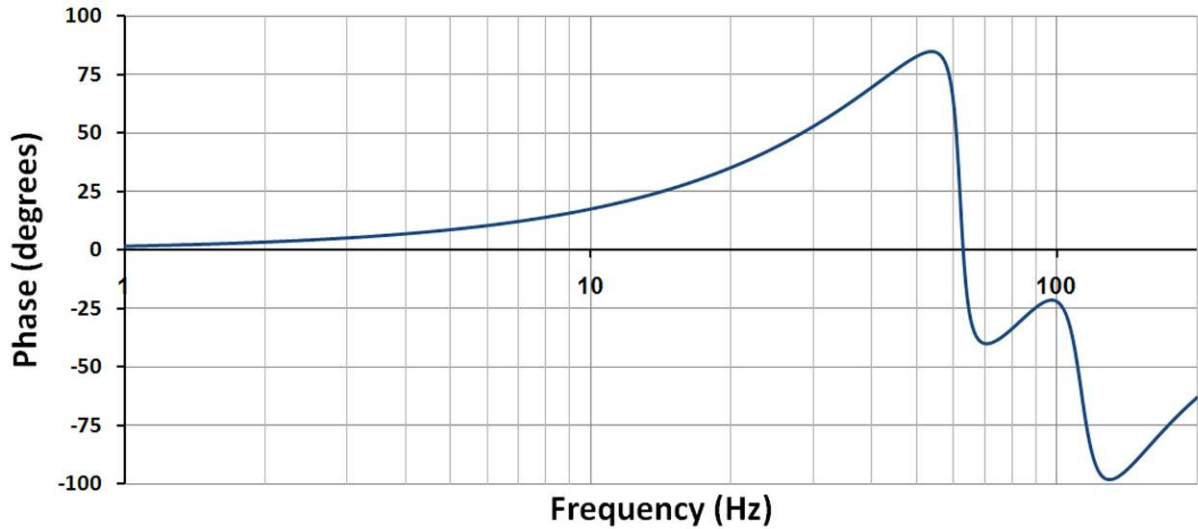
**Figure 3.4: Phase vs. frequency (semi-log plot) for the
SPICE inductor-based SA circuit model.**
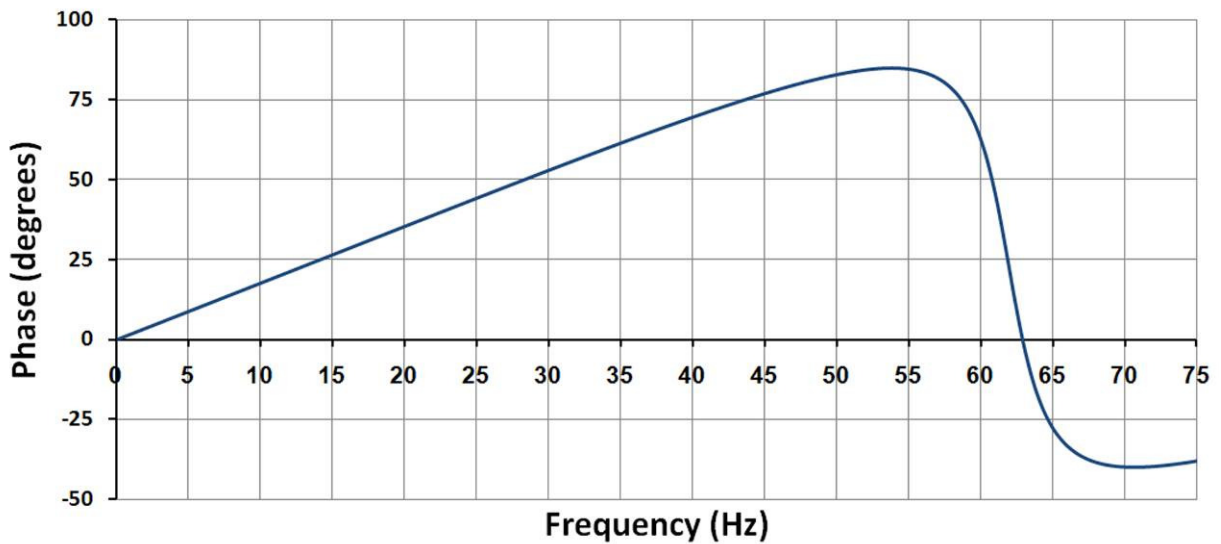
**Figure 3.5: Phase vs. frequency (linear plot) for the
SPICE inductor-based SA circuit model.**

Figure 3.6 is a graph of the theoretical group delay vs. frequency (computed from the phase vs. frequency data in Figure 3.5) that exhibits a relatively constant (just under) 5 ms (average 4.92 ms) temporal advance for a band-limited input signal in the frequency range of 1 to 25 Hz. Note the large temporal delays that occur at the poles (resonant frequencies).
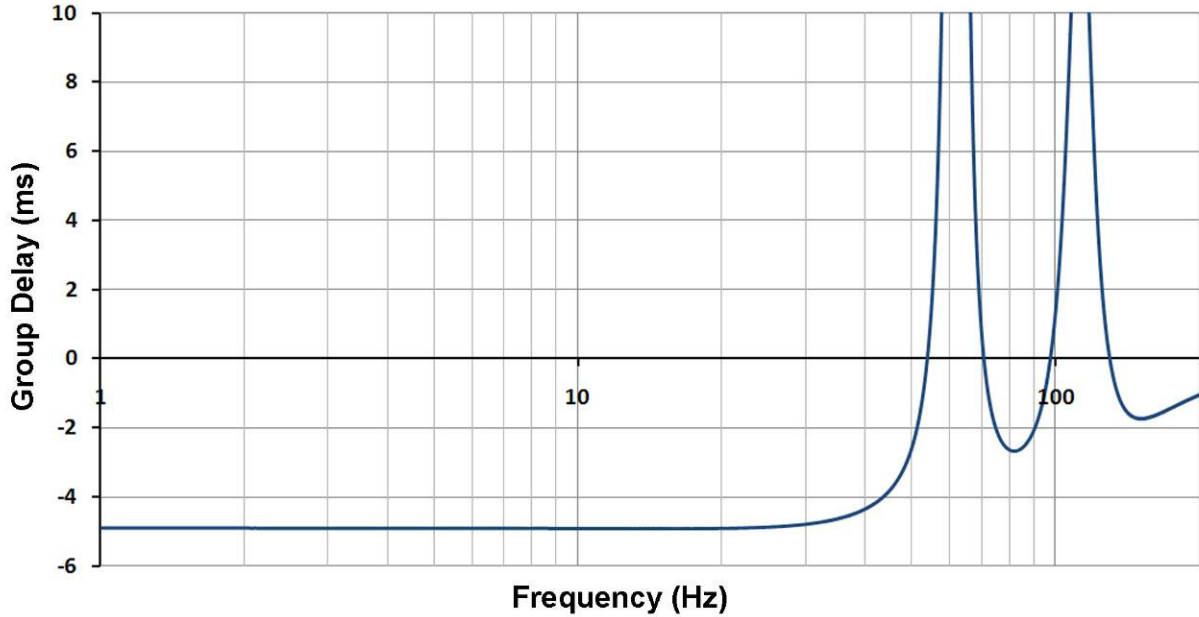
Figure 3.6: Group delay vs. frequency (semi-log plot) for the SPICE inductor-based SA circuit model.

Circuit Model Stability

The generalized transfer function for the SA circuit models (eq. 2.2) can be expressed as H(s) = [1 + N$_1$(s)/D$_1$(s)] x [1 + N$_2$(s)/D$_2$(s)] x G where s is the complex frequency variable, sometimes referred to as the Laplace variable, that replaces the term $i\omega$. The N(s)'s are the respective complex numerators for Stages 1 and 2, the D(s)'s are the respective complex denominators for Stages 1 and 2, and G is a scalar gain multiplier implemented as a voltage divider (Stage 3). Substituting components into eq. 2.2, the transfer function becomes:

$$H(s) = \left[1 + \left(\frac{1}{R_2}\right)\left(\frac{1}{(R_1 + sL_1)^{-1} + sC_1}\right)\right] \times \left[1 + \left(\frac{1}{R_4}\right)\left(\frac{1}{(R_3 + sL_2)^{-1} + sC_2}\right)\right] \times \left(\frac{R_{29}}{R_{29} + R_{30}}\right). \quad (3.8)$$

Note that the term in square brackets just to the right of the equals sign is the transfer function H$_1$(s) for Stage 1 of the circuit model and the second bracketed term is the

36

transfer function $H_2(s)$ for Stage 2 (refer back to Figure 3.2) and that $H(s) = H_1(s) H_2(s)$ $H_3(s)$, with $H_3(s) = G$. Eq. 3.8 may be simplified into the following form, from which circuit stability can be determined by solving for the zeros and the poles of $H(s)$:

$$H(s) = \left[1 + \left(\frac{1}{R_2}\right)\left(\frac{R_1 + sL_1}{s^2 L_1 C_1 + sC_1 R_1 + 1}\right)\right] \times \left[1 + \left(\frac{1}{R_4}\right)\left(\frac{R_3 + sL_2}{s^2 L_2 C_2 + sC_2 R_3 + 1}\right)\right] \times \left(\frac{R_{29}}{R_{29} + R_{30}}\right). \quad (3.9)$$

To solve this, the zeros and poles for Stages 1 and 2 are first found separately. Then, eq. 3.9 can be solved numerically (in subsequent discussion this is denoted as the "math" method) and determine the pole frequencies for (the composite) H(s). Finally, these results are compared to the numerical equivalents derived from the SPICE theoretical circuit analysis. The circuit gain (Stage 3, the resistor voltage divider) $G = 0.74$.

For each of Stages 1 and 2 there is a pair of complex conjugate zeros for a total of four. The zeros for the first two circuit stages are found by setting each of the first two bracketed terms in eq. 3.9 equal to zero and solving for the roots of the resulting quadratic equations yields the zeros:

$$z_{1,2} = \frac{-(C_1 R_1 R_2 + L_1) \pm \sqrt{(C_1 R_1 R_2 - L_1)^2 - 4 L_1 C_1 R_2^2}}{2 L_1 C_1 R_2}, \quad \text{and} \quad (3.10)$$

$$z_{3,4} = \frac{-(C_2 R_3 R_4 + L_2) \pm \sqrt{(C_2 R_3 R_4 - L_2)^2 - 4 L_2 C_2 R_4^2}}{2 L_2 C_2 R_4}. \quad (3.11)$$

Substituting in the actual component values from the 25 Hz SA circuit model into eqs. 3.10 and 3.11 then gives: $z_{1,2}$ = -347.72 $\pm$ 220.0i and $z_{3,4}$ = -332.2 $\pm$ 670.3i.

For each of Stages 1 and 2 there is a pair of complex conjugate poles for a total of four. Setting the denominator for each of these stages equal to zero and solving for the roots of the resulting quadratic equations yields the poles:

$$p_{1,2} = -\frac{R_1}{2 L_1} \pm \sqrt{\frac{R_1^2}{4 L_1^2} - \frac{1}{L_1 C_1}} \quad \text{and} \quad p_{3,4} = -\frac{R_3}{2 L_2} \pm \sqrt{\frac{R_3^2}{4 L_2^2} - \frac{1}{L_2 C_2}}. \quad (3.12, 3.13)$$

Substituting in the actual component values from the 25 Hz SA circuit model into eqs. 3.12 and 3.13 then gives: $p_{1,2}$ = -13.2 $\pm$ 389.2i and $p_{3,4}$ = -52.1 $\pm$ 706.1i.

Recognizing that the imaginary coefficient of each pole is its angular frequency, the linear frequency is calculated with f = $|\omega|/2\pi$. The results are f_1 = 61.9 Hz for the first stage and f_2 = 112.7 Hz for the second stage. Figure 3.7 is the pole-zero plot in the s (complex frequency) plane showing the locations of the poles and zeros for Stages 1 and 2. Note that all four of the poles are located in the left half plane of the plot (Re(s) < 0), indicating that the SA circuit model is stable. Also, the poles are all relatively close to the imaginary axis. The closer the poles are to this axis, the slower is the transient decay rate of the circuit [37].

The pole-zero results above are obtained for each SA circuit stage independently (i.e., not taking into account the interaction between successive SA circuit stages). In order to calculate the resonant frequencies (poles) for the overall circuit model, the overall transfer function, eq. 3.9, is solved numerically following substitution of the component values shown in Figure A.1. This is performed over the frequency of 0.1 to 200.0 Hz with a resolution of 0.02 Hz. The gain results, plotted in Figure 3.8 along with those from the SPICE theoretical analysis for the inductor based SA circuit model, reveal that the first pole is located at 62.0 Hz and the second at 111.7 Hz.
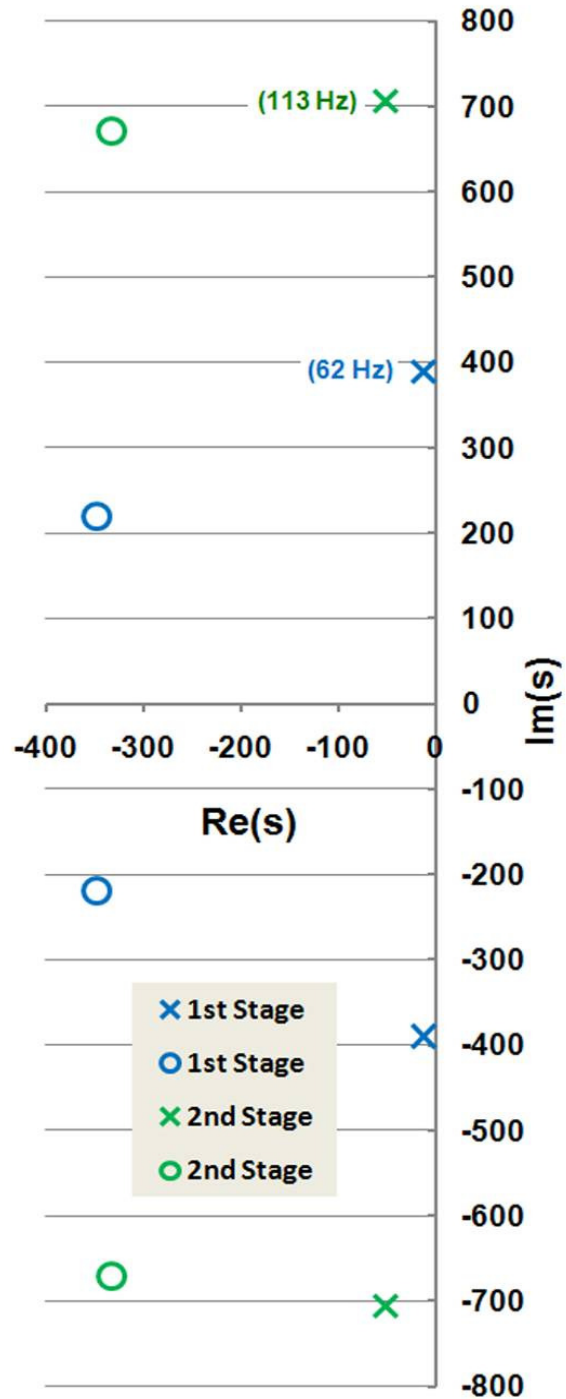
Figure 3.7: Pole-zero plot

These match precisely with the SPICE results. Note that the multiplication of the separate stages results in a slight shift ("pull") of the second pole toward the first pole (by about 1 Hz) as compared to the separate poles solution for the second stage.

Figure 3.9 compares the respective phase vs. frequency responses, which also overlap almost exactly as is the case for the signal advance results shown in Figure 3.10.
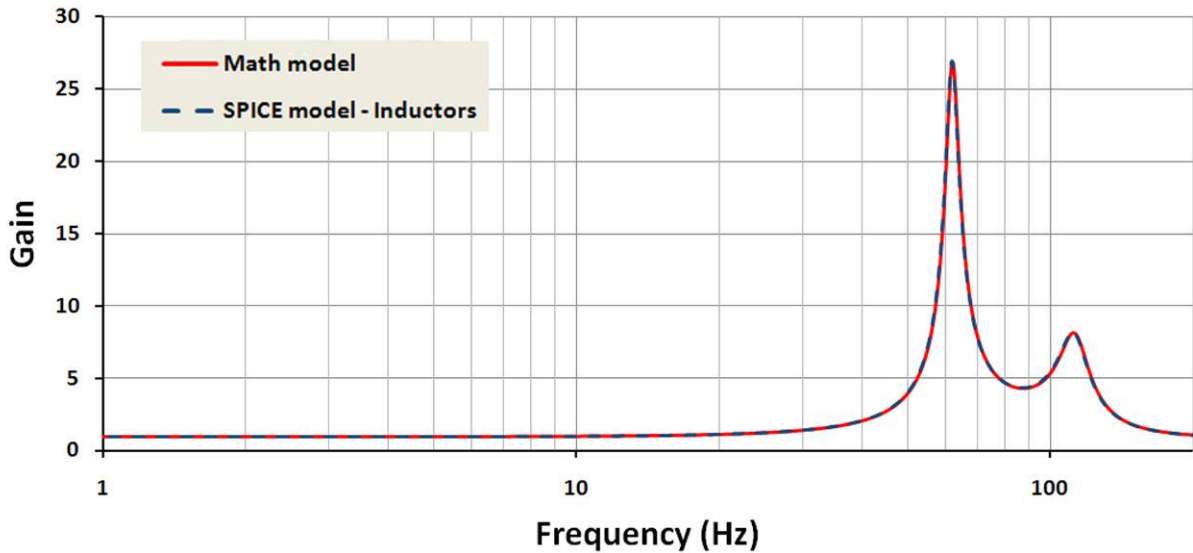
Figure 3.8: Gain vs. frequency (semi-log plot) for the mathematical model and SPICE inductor-based SA circuit model.
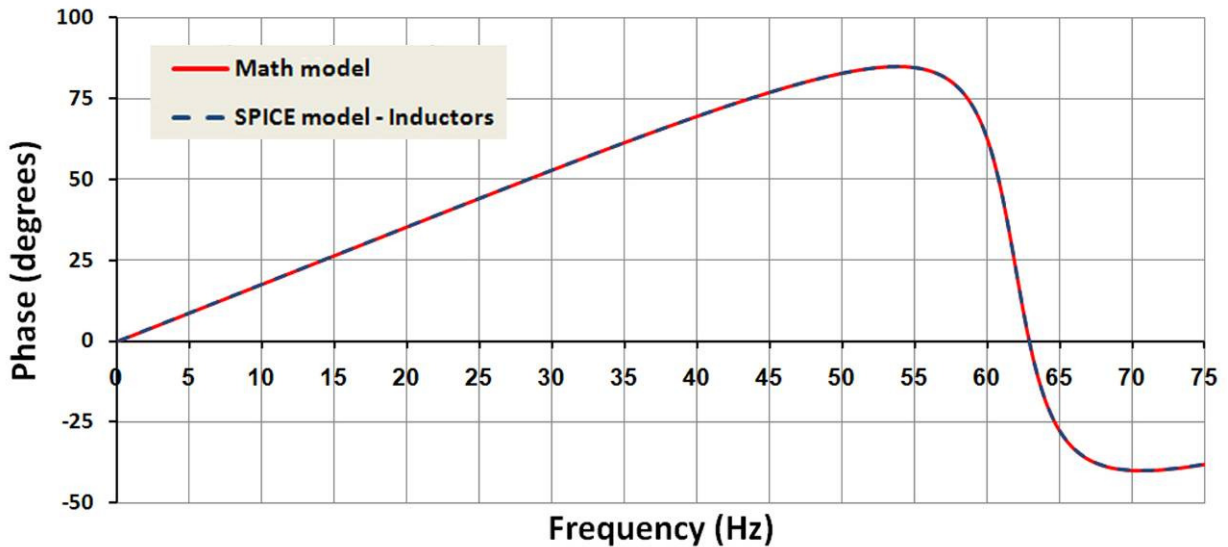
Figure 3.9: Phase vs. frequency (linear plot) for the mathematical model and SPICE inductor-based SA circuit model.
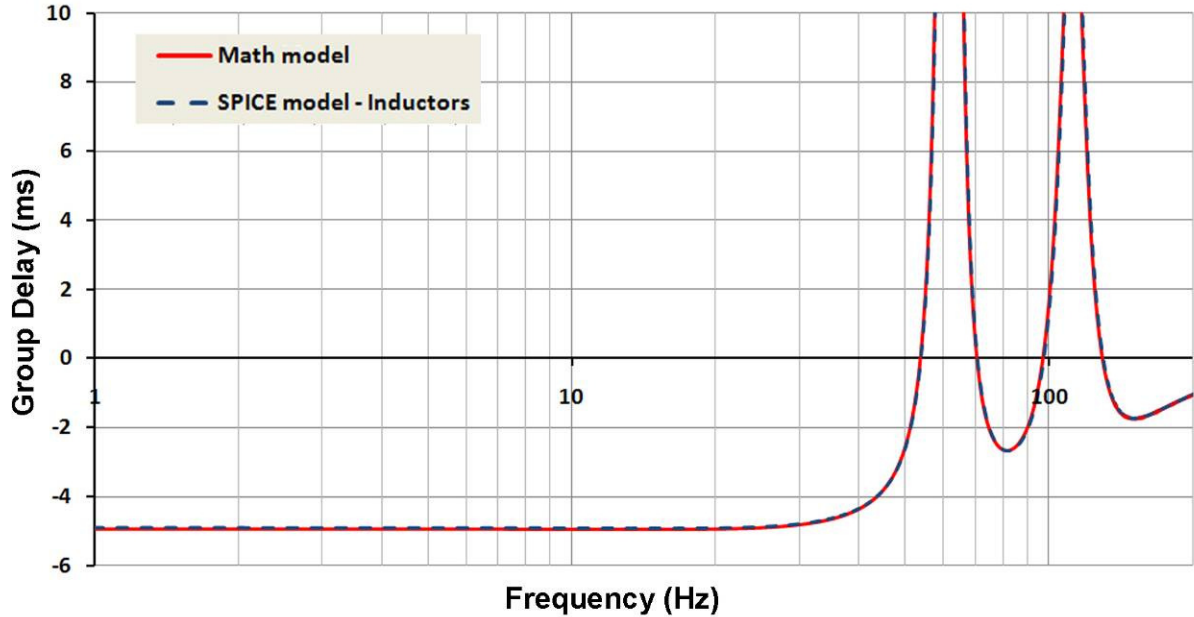
Figure 3.10: Group delay vs. frequency (semi-log plot) for the mathematical model and SPICE inductor-based SA circuit model.

Transient Response

Given the complex conjugate pole pair in the left half of the s plane for each stage (i.e., a second-order underdamped system as shown in Figure 3.7, their corresponding impulse response functions, determined by inverse Laplace transformation, are exponentially decaying sinusoids that may be represented as [37]:

$$Ae^{-\sigma t}\cos(\omega t + \varphi), \tag{3.14}$$

in which the oscillation frequency is ω, the rate of decay is σ, A is the amplitude and φ is the phase angle.

For the first circuit stage, the (complex conjugate) poles are $-13.2 \pm 389.2i$, thus the time constant is given by $\tau_1 = 1/|\sigma| = 1/13.2$ s or 75.0 ms. Similarly, for the second stage, the (complex conjugate) poles are $-52.1 \pm 706.1i$, and the time constant $\tau_2 = 1/52.1$ s or 19.2 ms.

A transient introduced into a stable system, such as the SA circuit model, will decay to 1% of its initial amplitude value in approximately five times the time constant [38]. This value would be 375 ms for the first stage and about 96 ms for the second. Based on these results and the significantly larger gain at the 62 Hz pole (Figure 3.3), the transient response or settling time of the overall SA circuit is $\geq$ 375 ms (corresponding to the longer settling time of the first two stages).

The implications of this for the SA circuit are that once "turned on" it should be allowed to run with input for at least 375 ms before the circuit output is used for any analytical purpose (to be conservative, wait at least 500 ms). In situations where the circuit input is controlled in such a way that $x(t) = 0.0$ for $t = 0$ (as is the case in this study) there is no transient input that can affect the circuit. Here, this condition is satisfied by always applying a window function to $x(t)$. Furthermore, recall that the SA circuit requires a band-limited input signal. For applications in which intermittent signal noise or other artifacts outside the signal bandwidth exist, the transient response determines the time required for an artifact to decay, at which point it would not affect the detected signal in any substantial or significant manner.

Gyrator Circuitry

In order to produce the desired temporal advance, the value of the inductive component for the first pole is set to over 100 H(enrys). This value of inductance would require a very large coil and would be impractical in a physical microelectronic circuit such as the one proposed. In most circuits, physical inductors typically have values measured in milli-Henrys (mH) or micro-Henries (μH). Therefore, in order to develop a physically realizable circuit, the inductors were replaced by gyrator circuits (see Appendix A, Figure A.2). Gyrators use capacitors, resistors and operational amplifiers to simulate large inductive impedances [7,8]. The gyrator circuitry used is an ungrounded design in which the equivalent inductive reactance for the first pole of the SA circuit model is provided by the following equation that estimates the absolute magnitude of the simulated inductance.

$$L_5 \cong C_5(R_{11}R_{15}/R_{14})R_9 \tag{3.7}$$

Following the implementation of this gyrator circuitry to simulate the large inductors in the SPICE design, the modified SA circuit model performance was confirmed using the SPICE theoretical analysis. The resultant gain and phase response data were used to compare the circuit responses for the inductor and gyrator-based SA circuit models using SPICE. Figure 3.11 shows the almost exact overlap of the gain vs. frequency response of the inductor-based and gyrator solutions, as well as for the mathematical results (frequency resolution of 0.02 Hz). Comparing inductors to gyrators, Figure 3.12 shows similar overlapping results for phase vs. frequency, and Figure 3.13 illustrates the signal advance vs. frequency. It is clear that these results are completely consistent with each other.
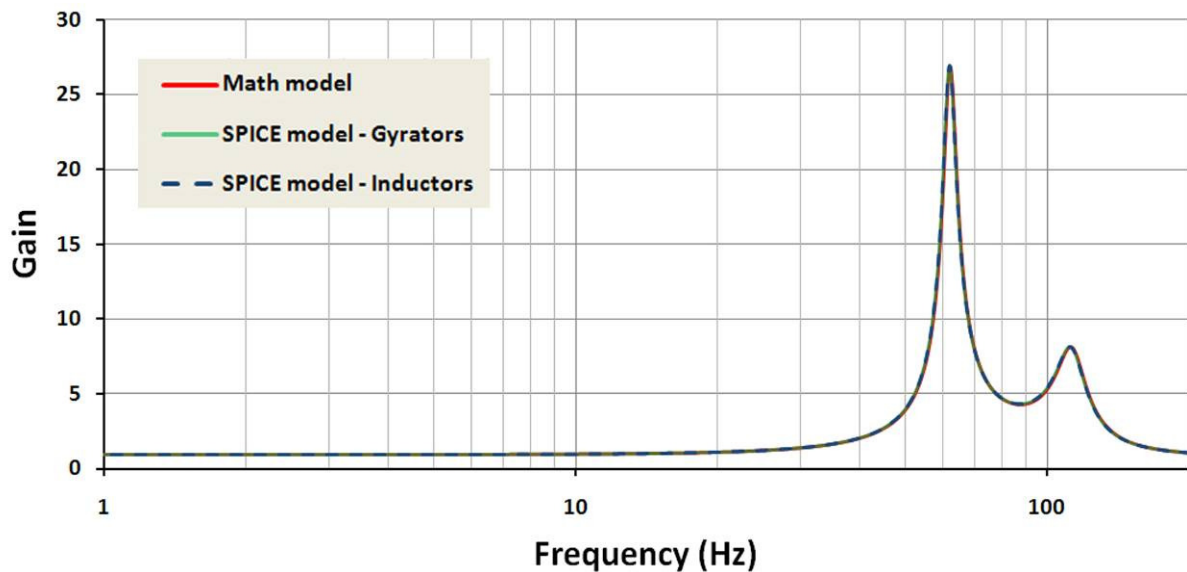
Figure 3.11: Gain vs. frequency (semi-log plot) for the mathematical model and the SPICE inductor and gyrator based SA circuit models.

While the theoretical gain, phase and group delay responses, shown in Figures 3.11 through 3.13, are observed to be essentially equivalent, the performance of the two circuit models was also compared empirically by applying sine burst test signals to both the inductor and gyrator based SA circuit models. The results obtained for both the inductor and gyrator-based SA circuit models with application of a 10 Hz sine burst test signal also confirm their equivalence (Figure 3.14).

42
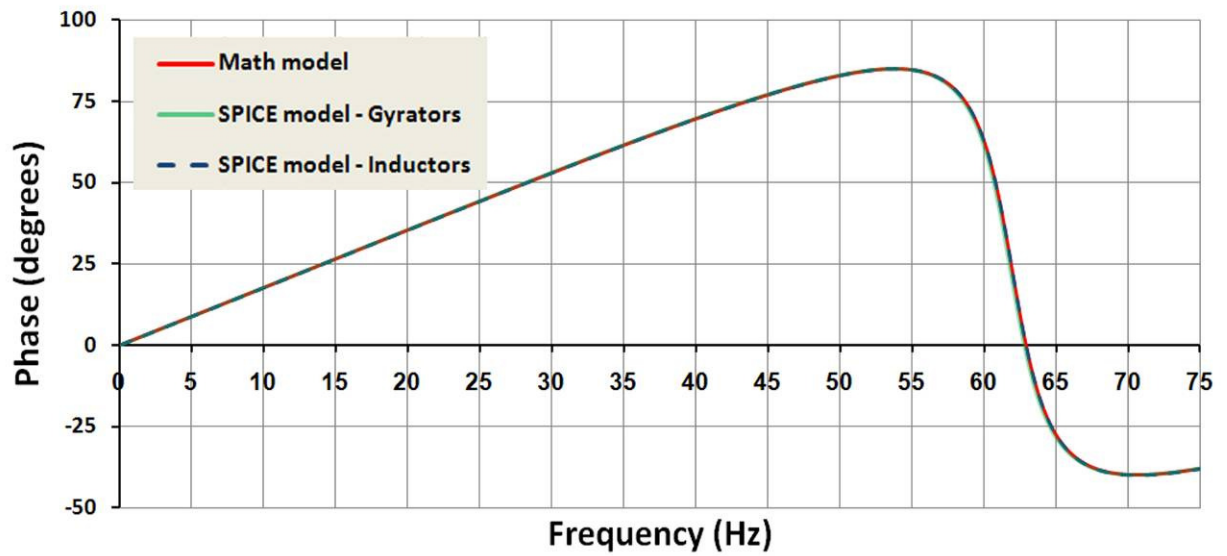
Figure 3.12: Phase vs. frequency (linear-linear plot) for the mathematical model and the SPICE inductor and gyrator based SA circuit models.
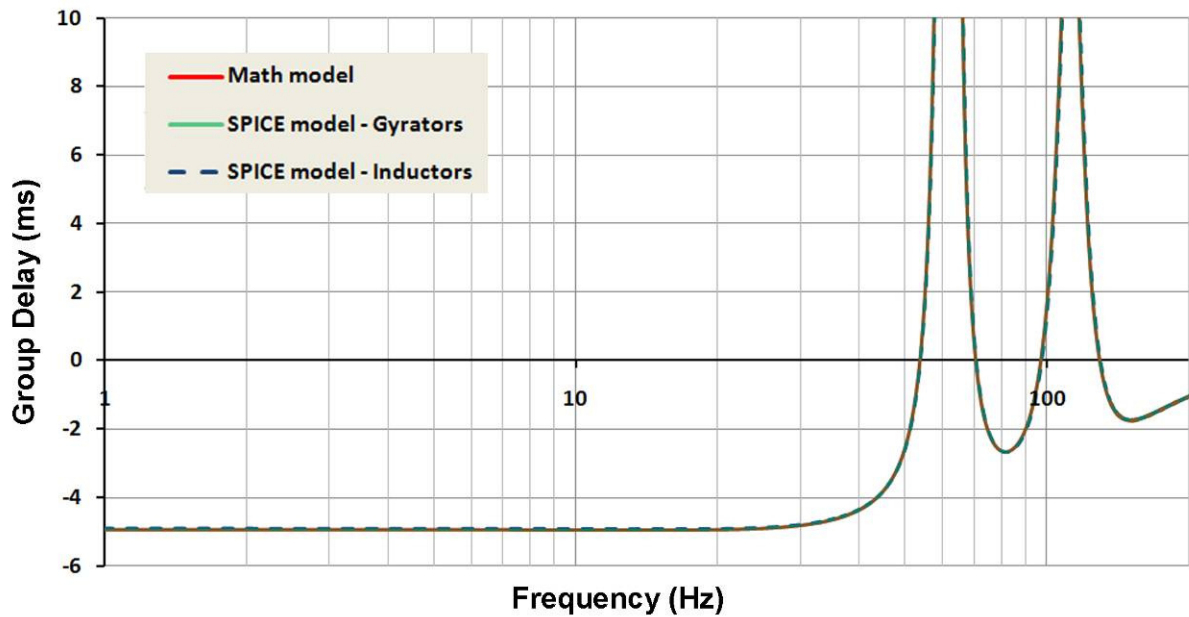
Figure 3.13: Group delay vs. frequency (semi-log plot) for the mathematical model and the SPICE inductor and gyrator based SA circuit models.

43
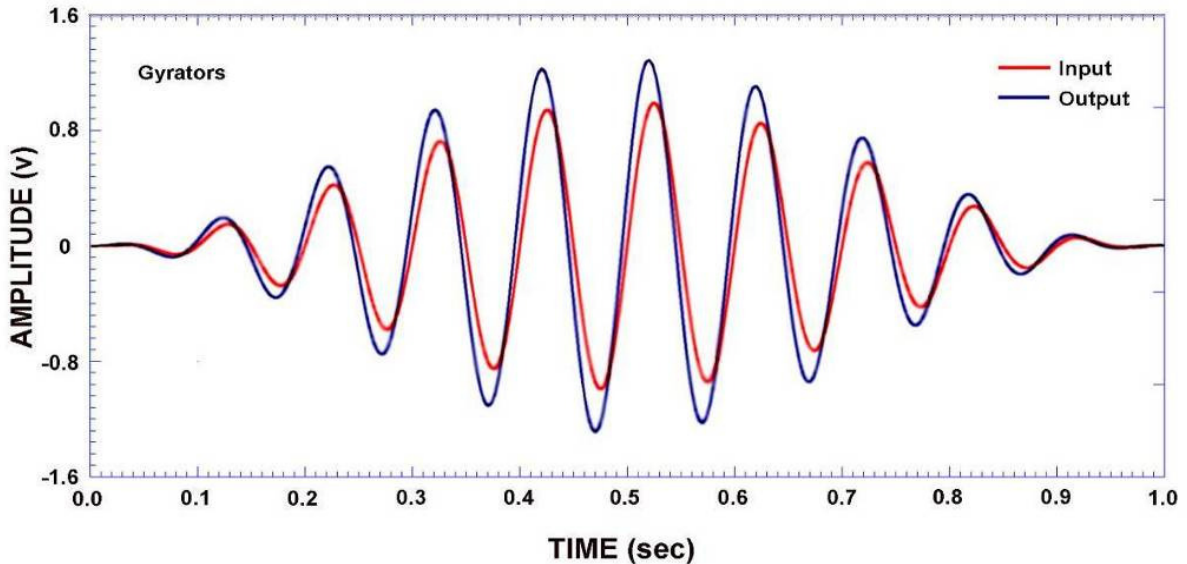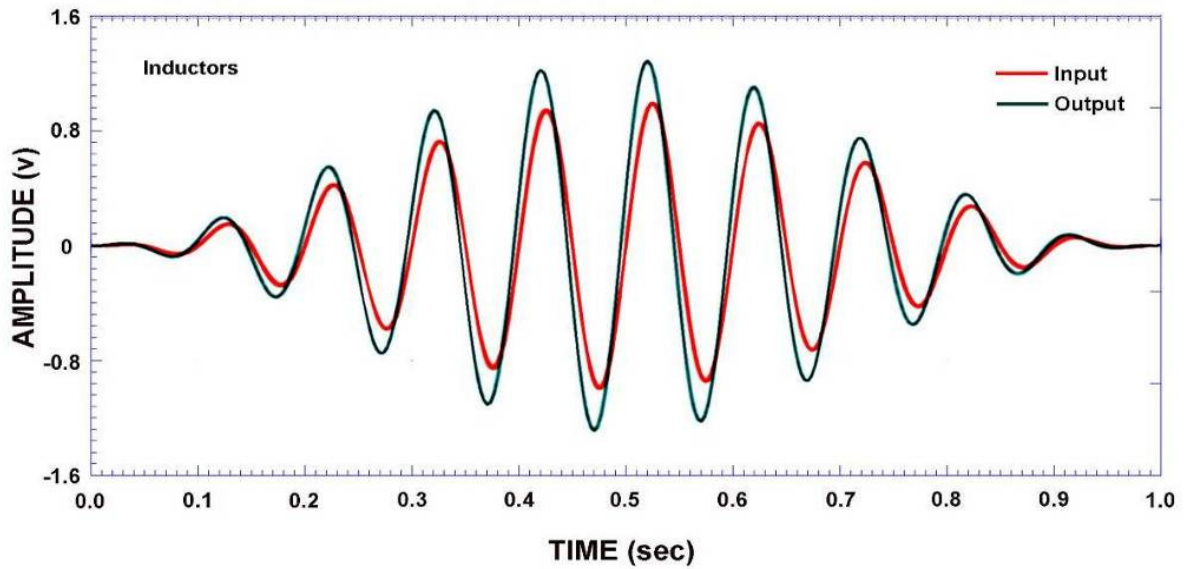
**Figure 3.14: Sine burst (10 Hz) input/output plots for the inductor
and gyrator based SA circuit models.**

The SPICE schematic (including the gyrator circuits) for the SA circuit model used in this study is provided in Appendix A, Figures A.2, A.3 and A.4. Note the voltage divider applied to the circuit following the second stage, which reduces the overall circuit gain to approximately unity. The associated SPICE net-lists and command sequences for both the theoretical AC analyses and transient analyses (for the application of time-domain test signals) are also provided in Appendix A. In the remainder of this study, for all the SPICE empirical results, the gyrator based SA circuit model is used.

Initial Input Test Signals

The SA circuit model performance was subsequently tested using Gaussian pulses and single frequency sinusoid test signals. In order to apply the time-domain test signals to the SA circuit model, the SPICE transient analysis function is applied. The transient analysis makes use of the nonlinear device characteristics and produces circuit output signals as a function of time. This analysis requires as well, the application of the digitized input signals over a user-specified time period followed by analysis of the sampled output signals.

Gaussian pulse and single frequency sine wave input signals with known temporal and spectral characteristics were constructed as input test signals for preliminary performance testing. The constructed test signals were then applied as inputs to the SA circuit model to determine empirically the actual SA circuit model performance.

The Gaussian pulses and sinusoidal test signals were generated in Microsoft Excel [39] (using the NORMDIST() and SIN() functions). These functions produced a sampled series of amplitude measures (y coordinate) as a function of time (x coordinate). The projected temporal advance was 5 ms and the coefficient of variation was expected to be less than 5%, or 250 μs. Thus, in order to accurately capture activity in this very short time period, all waveforms were ultimately sampled with a 100 μs resolution (sampling frequency of 10^4/s), which far exceeds the Nyquist criterion (sampling frequency must be at least twice the highest frequency of a signal [40]). Furthermore, using a high sampling rate avoids the generation of any output artifact resulting from discontinuities in the input test signal (discussed further in the results section below).

A Gaussian window was applied to all non-Gaussian input test signals used in the study. For the single frequency sine wave inputs, the normal distribution function was used to generate a Gaussian function equivalent to ten cycles of the sinusoid. For example, for a 1 Hz sinusoid, the Gaussian window has a 10 s duration; at 20 Hz the Gaussian window duration is 500 ms. To apply the Gaussian window, the sinusoid is multiplied by the Gaussian function (amplitude range from 0 to 1). Application of the Gaussian window functions as a low-pass filter, eliminating the introduction of high frequency spectral

components that would generate artifact in the output due to the nonlinear gain and group delay responses at the circuit resonant frequencies (poles). The resulting digitally sampled signals were then formatted for use in the SPICE arbitrary waveform generator function for application to the SA circuit.

Initial Circuit Model Performance Testing

The initial signal advance circuit testing used Gaussian pulse inputs with pulse widths ranging from 20 to 500 ms (equivalent to one half of the period of 1 to 25 Hz). During initial testing the waveform temporal advance obtained was determined by comparing the time of the appearance of the pulse peak of the output waveform relative to that of the input pulse peak. In addition, the gain was determined by comparing amplitudes of the input and output peaks. On confirming a waveform advance of approximately 5.0 ms using Gaussian pulse inputs, the circuit model was then tested using single frequency sinusoids selected from the spectral range 1 to 25 Hz.

Sinusoids were generated in Microsoft Excel. The period is the inverse of the frequency, thus for a 10 Hz signal the period is 100 ms. To produce a signal with a 100 μs sampling rate, the period required 1000 samples. Each sinusoid was then Gaussian windowed (Figure 3.15) to eliminate "edge effects" - the introduction of high frequency spectral components due to an abrupt non-zero beginning or end of the signal. Gaussian windowed inputs were used in the majority of the NGD studies cited here due to their rapid spectral roll-off and mathematical simplicity of analysis.
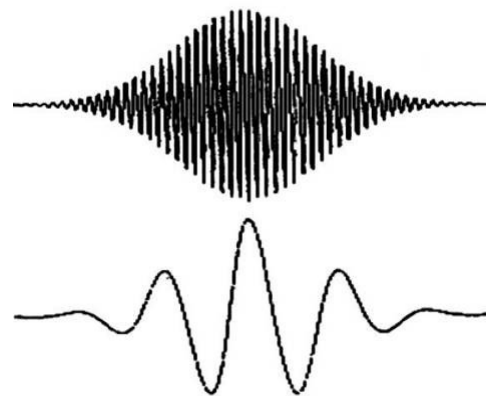
Figure 3.15: Gaussian windowed sinusoids.

SA circuit model performance in terms of waveform advance and gain were initially determined by comparing the peaks of the input and output Gaussian pulses. Similarly, the peaks and zero-crossings of the input and output sinusoids were averaged to determine the

46

advance and gain. It was important to confirm that the advance obtained is not equal to the period or half-period of any input signal as the advance would then be indeterminate. The likelihood of this occurrence is low, as the shortest period was 40 ms, while the projected advance is 5 ms or one eighth of the shortest period to be tested. Also, given the oscillatory nature of the SA circuits at frequencies above the design maximum, initial testing was used to confirm that for the input test signals 1) the slope of the Gaussian window was sufficiently low, and 2) the resolution of the input waveforms was sufficiently high so as to avoid introducing spectral artifacts that might result in high frequency oscillations in the outputs. Results are included that show the negative effects related to improper, or the completely absent, Gaussian windowing and insufficient sampling rate of the input test signals.

The initial testing was used to confirm the performance of the SA circuit model with regard to the duration and constancy of the temporal advance achieved (5 ms) and gain constancy. Furthermore, the adequacy of the input test signals in terms of resolution and windowing were assessed. Observed deficiencies prompted refinements of the SA circuit design as well as test signal refinements. These were followed by retesting.

Initial Circuit Model Test Results

After reviewing the theoretical performance of the SA circuit model utilizing gyrators, circuit simulation using input test signals was required to determine the actual circuit model performance. Initial attempts to use the available signal generator and a standard sine wave resulted in output signals containing transient oscillations in the 60 to 65 Hz range due to the resonance associated with the first pole in the SA circuit. Figure 3.16 shows the output resulting from the application of a 2.5 Hz sinusoidal input in which the transient higher frequency oscillation "died out"
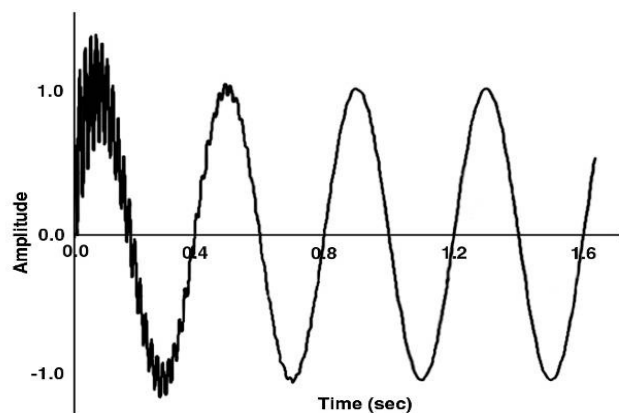
Figure 3.16: Advanced 2.5 Hz sinewave with transient decaying oscillation.

47

prior to the start of the third cycle (by about 500 ms, not inconsistent with the results of the theoretical transient decay rate of ≥ 375 ms). This oscillation results from the abrupt beginning of the input signal that contains spectral content above 25 Hz, specifically in the 60-65 Hz range. This result underscores the need to window each of the input test signals (excluding the Gaussian pulse inputs).

The limited selection of "built-in" waveform generators as well as the results obtained above made it necessary to construct piecewise linear approximations of the Gaussian pulse and single frequency sine wave test signals. In constructing the piecewise linear approximations, it was found that a sufficiently high sampling rate was required in order to avoid the introduction of any signal discontinuities that might result in artifact contamination reflected in the circuit model's temporally advanced output.

Figure 3.17 shows the results obtained when a piecewise linear approximation of a Gaussian pulse with an insufficient sampling rate (signal resolution) was used as input. While the output was temporally advanced relative to the input, the low sampling rate yielded noticeable discontinuities in the input signal, resulting in the production of a sawtooth-like artifact.
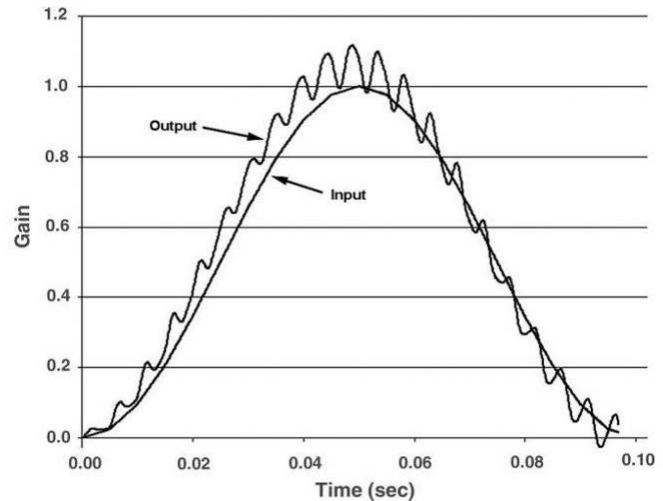
Figure 3.17: Results from a Gaussian pulse with inadequate sampling rate.

On completing the generation of the test signals, specifically Gaussian pulses and Gaussian-windowed sine waves (sine bursts), the test signals were applied as inputs to the SA circuit model and results similar to those shown in Figure 3.18 were obtained. The initial set of Gaussian pulse and sine bursts test signals had maximum (peak) amplitudes of approximately 2 V. The initial results exhibited a peak-to-peak gain of about 1.3 and temporal advance of about 5 ms.

Unlike the results obtained using Gaussian pulse inputs, the temporally advanced outputs from the sine burst test signals exhibited distortion in the wave shape at the output peak (Figure 3.19).

48
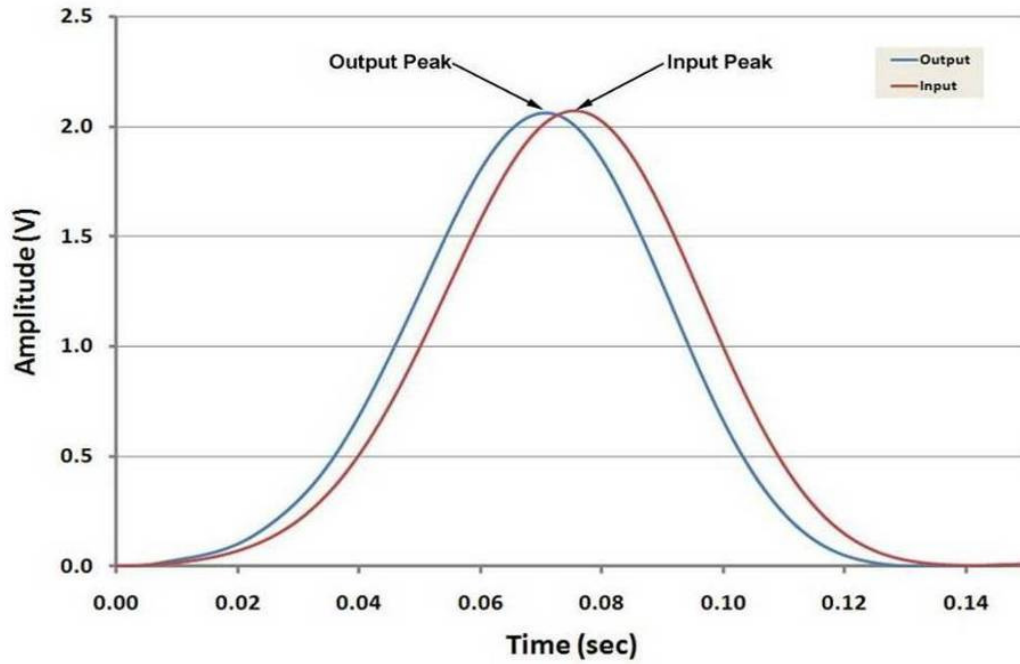
Figure 3.18: Example of the Gaussian pulse results.
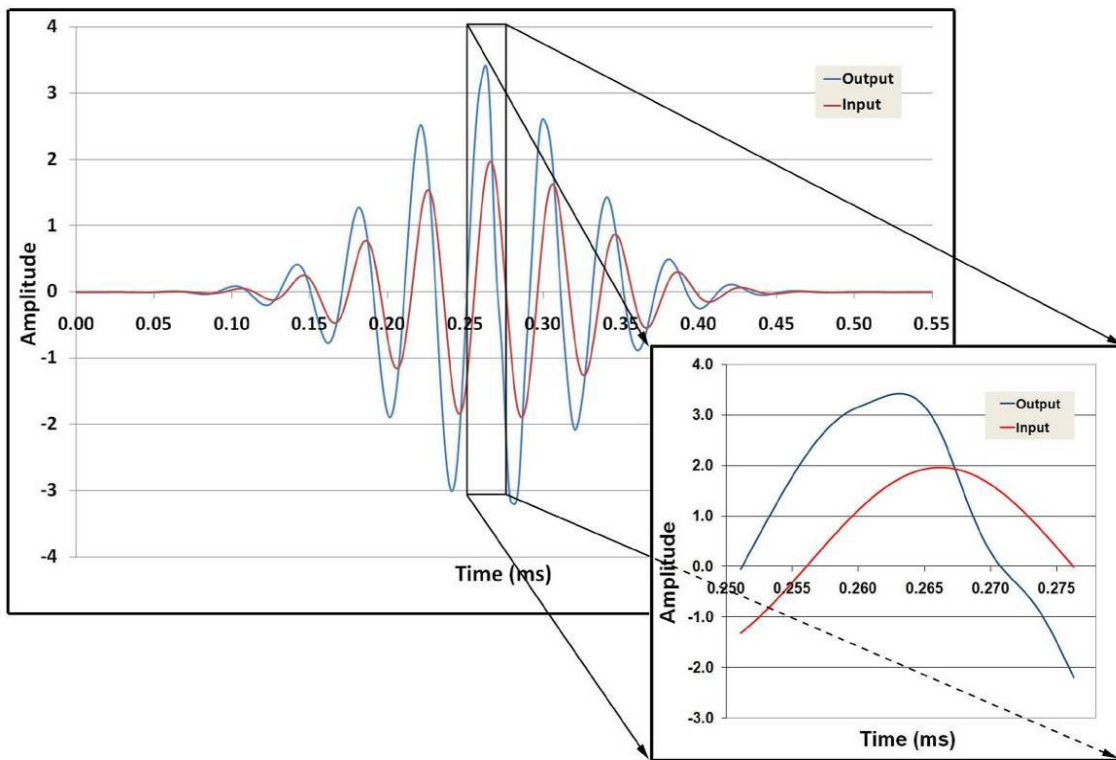
Figure 3.19: Peak distortion in the peak of the advanced sine burst output

These results prompted an adjustment in the overall gain of the SA circuit model to unity (for a mid-range Gaussian pulse input test signal) which also served to simplify the subsequent gain analyses and reduced the output to a maximum of 2 V (peak-to-peak), thereby eliminating shape distortion of the output peaks. No such peak distortion was exhibited in the inductor-based SA circuit model suggesting that the distortion is related to the voltage "headroom" requirements of the gyrator circuit.

As with the Gaussian pulse test signals, for the single frequency sine wave test signals (sine bursts), the advance and gain were determined by comparing the time of occurrence and amplitude of the peaks of the temporally advanced output with their respective inputs.

In addition, the sine bursts also have two zero-crossings occurring in every cycle (Figure 3.20). This provides an additional method to determine the temporal advance obtained by the SA circuit model.
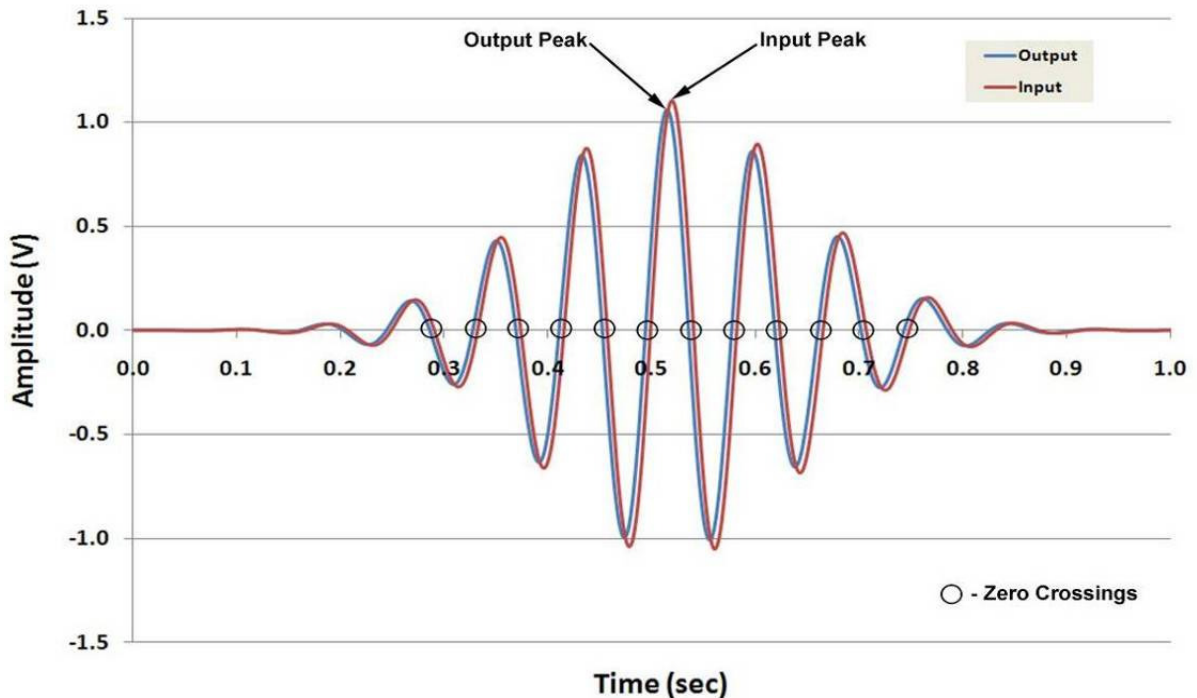
Figure 3.20: Example of the sine burst results

Thus, in addition to using the difference in the time of occurrence of the signal peaks, the difference in the time of occurrence of the zero-crossings of the temporally advanced outputs and the corresponding inputs was also calculated and averaged. The means, standard deviations and coefficients of variations were determined from these data.

Table 3.1 summarizes the results obtained for the Gaussian pulse and sine burst test signals (detailed results are provided in Appendix A, Table A.2 and A.3).

Table 3.1: Initial SA circuit model test signal results.

Statistic	Gaussian Pulses		Sine Bursts		
	Peak Advance	Peak Gain	Peak Advance	Zero-Crossing Advance	Peak Gain
Mean	4.847 ms	1.02	4.880 ms	4.882 ms	0.997
Std Dev	0.00924 ms	0.0471	0.0332 ms	0.000123 ms	0.0856
C_v	1.91%	4.60%	6.80%	4.60%	8.59%

Chapter IV

Constructed Test Signal

Methods and Results

Constructed Test Signals

The initial testing described in the previous chapter provided evidence indicating that the SA circuit model produced a temporal advance of approximately 5 ms and unity gain that are relatively constant over the design spectral range of 1 to 25 Hz. The relative constancy of these results supports the hypothesis that an SA circuit model could be developed that would minimally distort the temporally advanced output signals relative to their respective inputs over the design frequency range.

The initial results also established and subsequently confirmed the requirements for, and adequacy of the piecewise linear approximations of, the continuous test signals, as no additional signal artifacts appear to have been introduced that would result in the occurrence of high frequency oscillations in the temporally advanced output.

This chapter describes the thorough and meticulous testing of the SA circuit model using a range of constructed test signals including Gaussian pulses, single frequency

sinusoids (described in Chapter III) and waveforms consisting of three superposed single frequency sine waves. The signal detection temporal advance and gain produced by the SA circuit model was rigorously examined by comparing the circuit outputs with their corresponding inputs. Circuit distortion is quantified using both time and frequency domain analyses. The results obtained provide the necessary foundation for applying SA to human ECGs (Chapter V).

Gaussian Pulses

The first set of input test signals consists of twenty-five Gaussian pulses with half amplitude pulse widths ranging from 20 ms to 500 ms. These pulse widths are equivalent to one half of the periods of 1 to 25 Hz sinusoids. As described in Chapter III, the signals were generated using Excel. The constructed digital representation of each of the twenty five test signals were then imported into the SPICE program's arbitrary waveform generator for application to the SA circuit model (for example, Figure 3.13).

Single Frequency Sinusoids (Sine Bursts)

Following testing with Gaussian pulse inputs, the circuits were tested with twenty-five, single frequency sinusoids from 1 to 25 Hz. As described previously, the Gaussian-windowed sinusoids (sine bursts) were imported into SPICE for application to the SA circuit. Confirmation was required to show that the duration of the temporal advance obtained was not equivalent to one or one half period of a test signal frequency, specifically not equal to one or one half of one period of the input sinusoid, Shifting a pure sinewave by 2π or 360° is the same as a zero phase shift and shifting by π or 180° is the same as inverting the signal. The probability of this occurrence is quite low as the maximum test signal frequency is 25 Hz. Thus, the shortest one half period was 20 ms, while the projected temporal advance was 5 ms (see sample Figure 3.15).

Tri-Frequency Test Signals

A signal is composed of an infinite sum of sinusoids of varying frequencies and amplitudes according to the principle of Fourier decomposition (Figure 4.1). Further, the response (output) of any linear system is the sum of the responses of the system to each input [12].

Having confirmed the results obtained from the application of simple sinusoids to the SA circuit model, twenty-five input test signals were constructed by

Figure 4.1: Fast Fourier transform.
*Copyright 1994 Agilent Technologies, Inc. Reproduced with permission.

linearly superposing (adding) three randomly selected single frequency sinusoids in the range of 1 to 25 Hz (Figure 4.2). Thus, these test signals, composed of known spectral components, were of increased spectral complexity relative to both the Gaussian pulses and the single burst test signals.

Figure 4.2: Superposition.
*Copyright 1994 Agilent Technologies, Inc. Reproduced with permission.

To construct the tri-frequency input signals, integer frequencies were randomly selected (using the random number function in Excel) from each of the following ranges: 1 to 8 Hz, 9 to 16 Hz, and 17 to 25 Hz. In addition, each of the three spectral components was scaled by one of three randomly selected factors (0.2, 0.3 and 0.45) in order to ensure that their linear combination did not exceed the maximum amplitude threshold, in the event that the amplitude peaks or troughs were coincident. The randomly selected frequency and attenuation factors were then generated in Excel (see Tables B.1 and B.2 in Appendix B).

Sinusoids from each of the three frequency ranges listed above were used to insure that any advance obtained was constant for a waveform consisting of spectral content spanning the 1 to 25 Hz frequency range. The randomly selected single frequency sinusoids were scaled in Excel by multiplying the single frequency sinusoids by the randomly selected attenuation factor. The three scaled single frequency sinusoids were then superposed (time sample by time sample) and the overall duration of the input signal was set to twenty seconds. A Gaussian taper was then applied over the first and last 2 seconds of the signal. The first half of the taper (0 to 2 s) was applied by multiplying the tri-frequency composite test signal by the individual values for the first half of the normal distribution. The second half of the normal distribution (2 to 4 s) was similarly applied to the last 2 s of the test signal. The middle 16 s (steady-state portion) of the test signal was multiplied by one.

Figure 4.3 shows an example of a tri-frequency test signal consisting of super-imposed 3, 12, and 21 Hz sinusoids. Figure 4.4 is an enlargement of a small portion (2 to 3 s) of the tri-frequency test signal example. The constructed tri-frequency signals were then imported into SPICE for application to the SA circuit model.

Based on initial testing results, it was anticipated that the duration of the waveform advance is such that the actual advance obtained would not be affected by anti-aliasing and it was confirmed that the advance obtained was not equivalent to one or one half of one period of any of the selected sinusoids (i.e. exhibits a 360° or 180° phase shift).
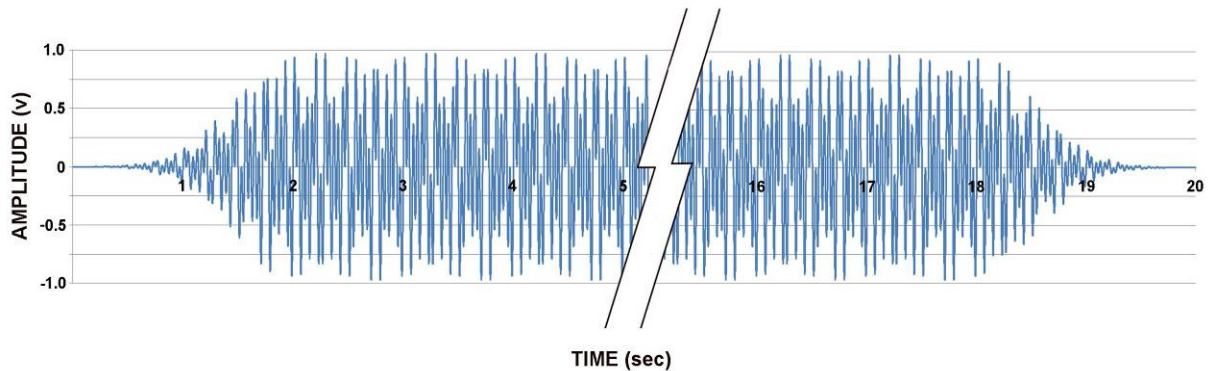
Figure 4.3: Tri-frequency test signal
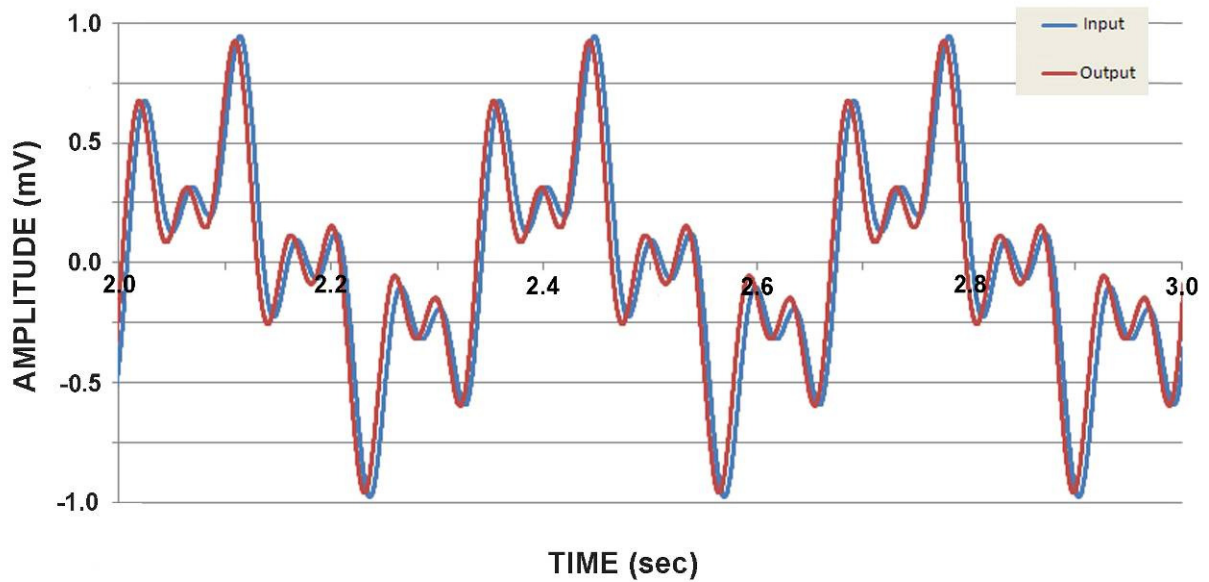
Figure 4.4: Enlarged region of the tri-frequency test signal.

Time Domain Analyses

Temporal Advance

Using SPICE, the three sets of 25 test signals were applied to the SA circuit model. The input and resulting output data were then exported into text files in three columns of 1) time, 2) input signal and 3) output signal. The resulting text file for each of the three types of signals was then imported into an Excel spreadsheet for later analyses and data plotting.

During initial circuit testing (Chapter III) the temporal advance achieved was estimated by comparing the times of occurrence of the input and output peak(s) and, in the case of the sine bursts, by additionally comparing the time of occurrence when the output signals crossed the *x* axis (zero-crossings) with their respective input zero-crossings. However, the output peaks as well as the zero-crossings were subject to variation due to output signal distortion, including signal skew and output noise, which increased the variability of the results. Therefore, cross-correlation analysis was used in order to minimize these sources of error variance.

The cross-correlation function R determines the linear relationship between two waveforms as one of them is shifted in time relative to the other [31]. Correlations (Pearson r) were calculated at each time point as the temporally advanced output was shifted with respect to the input. The time shift (or lag) associated with the maximum correlation is equal to the temporal advance imparted by the SA circuit. Cross-correlation provides a more objective measure of the advance obtained by taking into account the shape of the entire waveform and thus is less affected by various forms of output signal distortion.

The sampling rate used was 10^4 samples/s, which well exceeds the Nyquist criterion [40], and is more than sufficient resolution for the projected temporal advance of 5 ms. Let x_t denote the tth sample of the input, and y_t denote the tth sample of the output. The cross-correlation between x and y is:

$$R(i) = \sum_{t=i+1 \text{ to } t} (x_{t-l} - \mu(x))(y_{t-1} - \mu(y))/(\sigma(x)\sigma(y)), \quad i = \pm 1, \pm 2, \ldots, \pm 1500, \qquad (4.1)$$

where t is the number of data points per waveform, i is the lag index, $\mu( )$ and $\sigma( )$ are the mean and standard deviation of the respective signals. $R(i)$ yields values between -1.0 and +1.0. For a temporal advance of 5 ms, the maximum correlation is expected to appear at a lag of 500 which is equal to the projected advance divided by the sampling resolution, or 5.0 ms/10.0 μs (example in Figure 4.5). This method was used to verify the duration of the advance obtained.
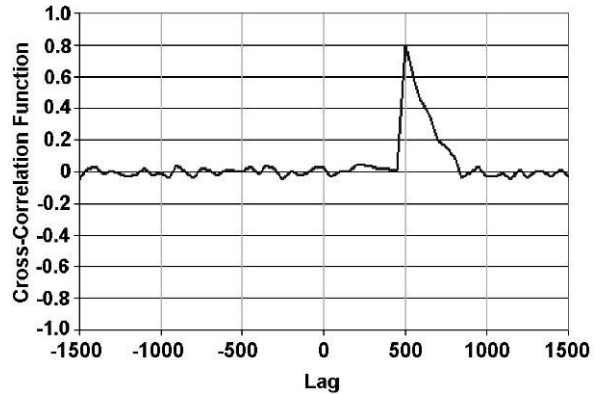
Figure 4.5: Cross-correlation vs. lag.

Cubic spline interpolation was used to provide a more precise estimate of the temporal advance by upsampling the results. This increased the *apparent* resolution of the cross-correlation (without adding any new information) [49]. Using interpolation to find the maximum correlation reduced sampling variability in the temporal advance determination resulting from the reduction in roundoff errors.

The maximum cross-correlation in the time domain (used to determine the temporal advance achieved) corresponds to the Pearson r between input and output signals calculated in the frequency domain, which is independent of time shifts (described further in the section on Frequency Domain Analyses, below). As such, to confirm the validity of the use of cubic spline interpolation, the resultant maximum cross-correlations were later compared to the correlations obtained in the frequency domain analyses. In each case the interpolated maximum cross-correlation more closely approximated the correlation obtained in the frequency domain than did the maximum cross-correlation obtained without first interpolating. This confirms the increased accuracy of the maximum cross-correlation obtained following interpolation.

Gain

The gain of the circuit model was assessed in a manner analogous to the rigorous determination of the signal detection temporal advance. In the initial testing (Chapter III), the amplitudes at the signal peaks were compared to provide an approximate gain assessment. However, the peak amplitudes could also have been affected by signal distortion. An alternative method would be to calculate the gain by taking the ratio of the average amplitude of the output waveform relative to the corresponding input over the entire waveform. While applicable to Gaussian pulse signals, the average of symmetric signals such as the sinusoids or the tri-frequency signals would approach zero.

Thus, the SA circuit gain was determined by calculating the Root Mean Square (RMS) ratio of the advanced output relative to the input signal. The RMS ratio (unlike the peak or average ratios) provides consistent results for a broad range of test signal types. For each set of twenty-five test signals (Gaussian pulses, single frequency sinusoids and triple-frequency signals), the mean (μ) and standard deviation (σ) for both the temporal advance and gain were calculated and used to determine the coefficient of variation:

$$C_V = \sigma/\mu. \qquad (4.2)$$

Temporal Advance and Gain Results

For each set of constructed test signals, the mean, standard deviation and coefficient of variation for the temporal advance was calculated. Additionally, the maximum cross-correlation between the temporally advanced output signal and the corresponding input signal is provided. The results for the Gaussian pulse, sine burst and triple-frequency test signals are summarized in Table 4.1 (and detailed results are provided in Tables B.3, B.4 and B.5 in Appendix B). The temporal advances as a function of frequency for the Gaussian pulse and sinusoidal signals are plotted in Figures 4.6 and 4.7 respectively.

Table 4.1: Constructed test signal temporal advance results.

Statistic	Gaussian Pulse		Sine Burst		Tri-frequency	
	Temporal Advance (ms)	Maximum Cross-Correlation	Temporal Advance (ms)	Maximum Cross-Correlation	Temporal Advance (ms)	Maximum Cross-Correlation
Mean	4.909	0.998968	4.869	0.999756	4.942	0.997750
Std Dev	0.0047	0.001295	0.0077	0.000336	0.0002	0.001374
C_v	0.96%		1.59%		0.05%	
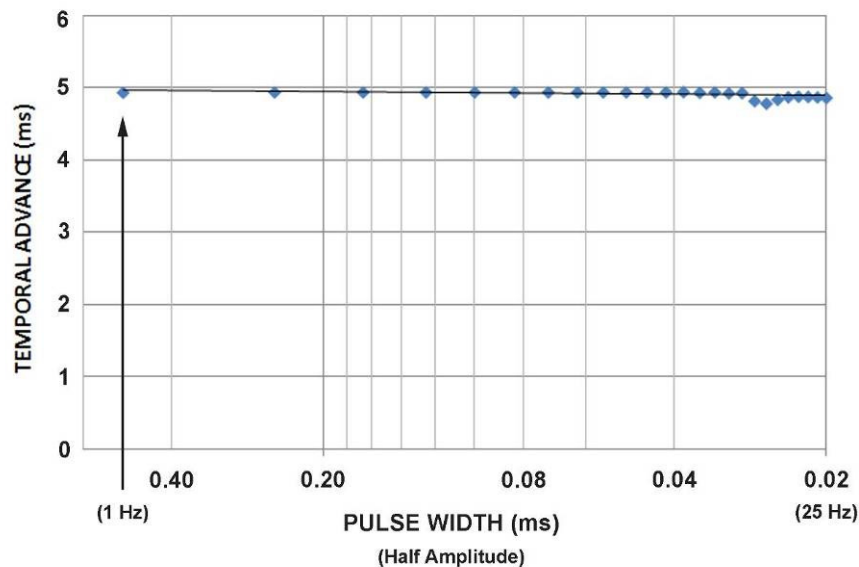
Figure 4.6: Gaussian pulse temporal advance vs. frequency.
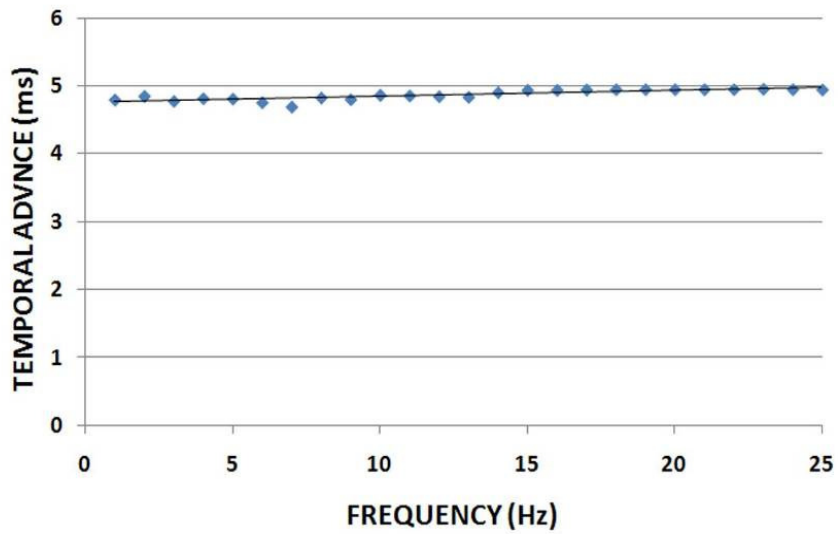
Figure 4.7: Sine burst temporal advance vs. frequency.

Figure 4.8 is a graph of the empirical Gaussian pulse and sine burst results overlaid with the theoretical results obtained from the SPICE AC analysis. Note the close match between the empirical and theoretical results as shown.
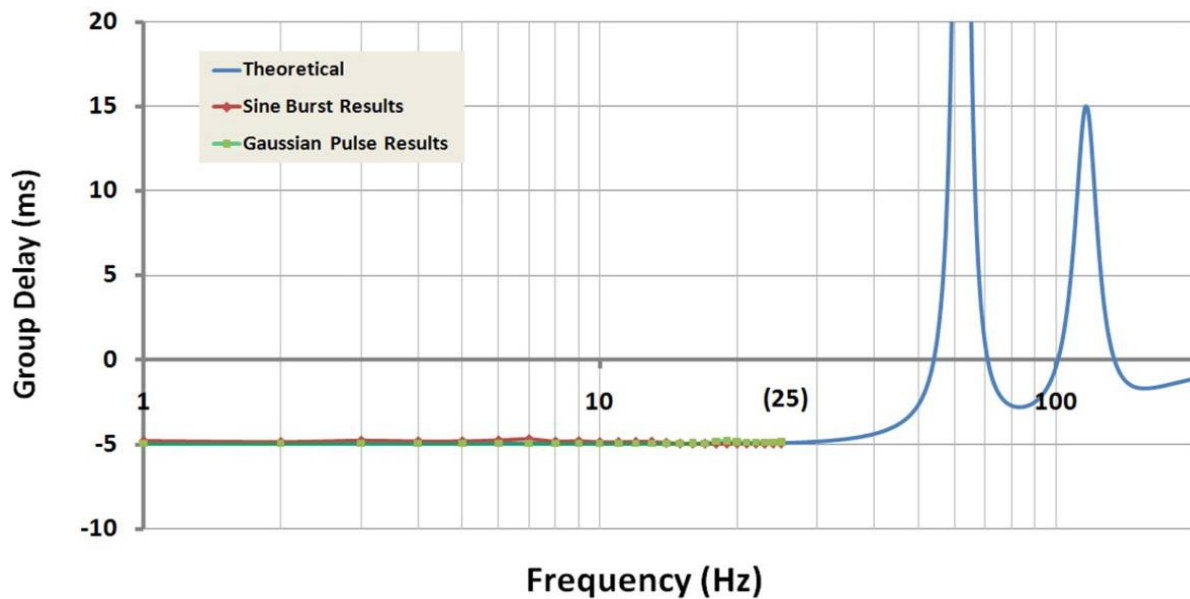
Figure 4.8: Plot of temporal advance vs. frequency for the Gaussian pulse and sine burst results compared to the theoretical results.

For each set of test signals, the mean, standard deviation and coefficient of variation for the gain were also calculated. The results for the Gaussian pulse and sine burst test

signals are summarized in Table 4.2 (and detailed results are provided in Tables B.3, B.4 and B.5 in Appendix B).

Table 4.2: Constructed test signal gain results.

GAIN			
Statistic	Gaussian Pulse	Sine Burst	Tri-Frequency
Mean	1.00	0.997	1.0018
Std Dev	0.0267	0.0866	0.03316
C_v	2.67%	8.68%	3.31%

A graph of the gain relative to frequency for the Gaussian pulse and sine burst test signals is shown in Figure 4.9. Note that below about 15 Hz the gain is a little less than 1.0 and above 15 Hz it is slightly greater than 1.0; the circuit gain response is not uniform across the frequency range of study (1 to 25 Hz). The sine burst results exhibit a wider range of gains (0.91 to 1.18) than do the Gaussian pulses (0.97 to 1.05).
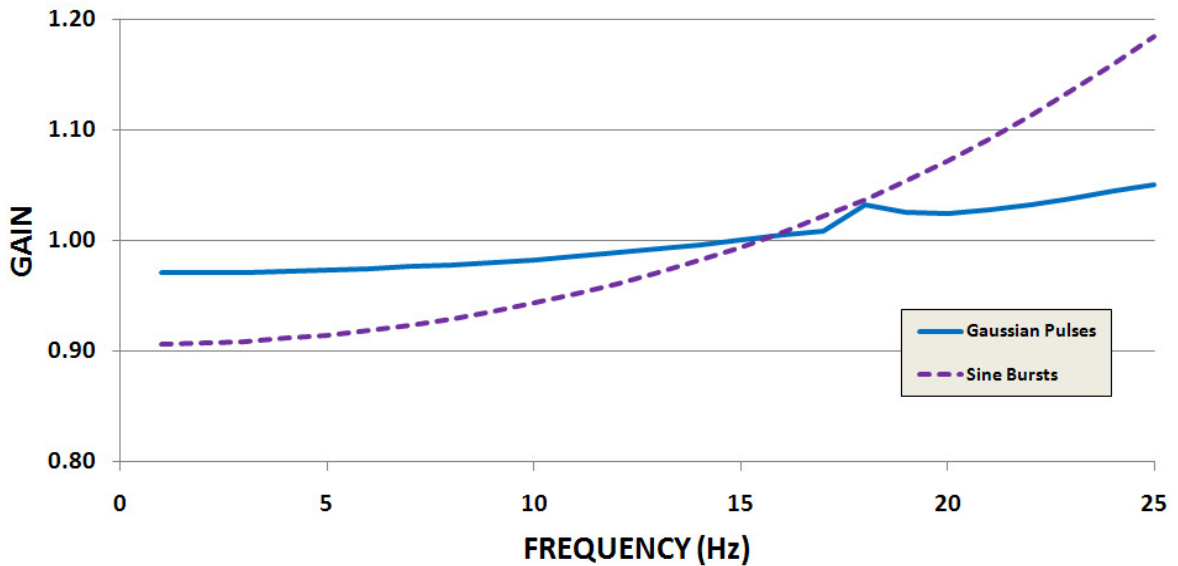
Figure 4.9: Gain vs. frequency for the Gaussian pulse and sine bursts test signals.

Had the results exceeded the hypothesized variability in terms of either the temporal advance or gain over the 1 to 25 Hz frequency range, a polynomial decomposition would have been used to more accurately determine the functional relationship (linear, quadratic

or higher order) between the signal advance and frequency. The results of these analyses confirmed that for Gaussian pulse, sine burst and tri-frequency test signals, the SA circuit produces a temporal advance of 5 ms $\pm$ 5% or greater with a coefficient of variation of less than 5%, and gain of 1.0 $\pm$ 10% with a C_v of less than 10%. These results support the rejection of the null hypotheses.

In addition, the correlation results (all greater than 0.997) indicate a high degree of morphological similarity between the input and output signals strongly suggesting that the circuit model produces minimal signal distortion. Although the circuit gain as a function of frequency is not constant (and slightly nonlinear), the deviation from slope zero linearity is sufficiently small so as to not invalidate the use of correlation as an acceptable measure of waveform shape similarity.

Frequency Domain Analyses

The experiments and analyses described in the previous sections determined the signal detection temporal advance achieved for the various input test signals using the cross-correlation function in the time domain. The constancy of the gain and temporal advance were determined by comparing the temporally advanced output waveforms to their respective inputs in the time domain. In addition, the correlation analyses provided an indication of the morphological similarity between the circuit model input and output signals. In this section the input-output signal correlations in the frequency domain are examined as a cross-check against the time domain results.

Frequency Transformation

In addition to determining the relationship between the waveform advance and frequency (which should exhibit limited variation in the spectral range from 1 to 25 Hz), the data collected were used to quantify the output waveform distortion (relative to the input). Output signal distortion includes changes in amplitude (i.e., gain distortion) as well as pulse shape or width that might cause spectral shifts or generation by the circuit of additional

(harmonic) frequencies. A visual comparison of the input and output spectral distributions revealed no evidence of either spectral shifts or additional spectral components in the output. The only changes in spectral distribution observed were variations in amplitude at various frequencies. The observed gain distortion is related to differential changes in spectral magnitude or power of the circuit output as a function of frequency. A constant scale change in spectral magnitude or power across all frequencies is not considered to be a source of distortion (and would not yield a difference in the correlation between the input and output signal spectra) [50,51].

Quantification and characterization of any resultant distortion required analyses in the frequency domain. The input and temporally advanced output waveforms were appropriately transformed to the frequency domain using the Fast Fourier Transform (FFT) [41]. Symbolically,

$$F[x(t)] \; = \; X(\omega), \tag{4.3}$$

where F[.] represents the Fourier transformation operator, $x(t)$ represents the circuit input signal and $X(\omega)$ is its Fourier transform – a complex signal in the frequency domain. Taking the absolute value of X ($|X|$) yields the so-called magnitude spectrum of the signal $x(t)$. In the follow-up, the gain as a function of frequency (Hz) was examined:

$$G(f) = |Y(f)|/|X(f)|, \tag{4.4}$$

where $|Y(f)|$ is the magnitude spectrum of the circuit model output signal $y(t)$.

Prior to applying the FFT, the time domain results were zero-padded (i.e., zeroes are added to the end) to increase the number of time domain data points to a power of 2 [41]. While there is a Fourier analysis function available in Excel, it has an upper limit of 4096 data points, which would significantly limit the frequency resolution of the result. Thus, after zero-padding the time domain results, FFT's were performed in SPICE, which does not have the same limitations with regard to the number of data points.

The circuit input and respective output magnitude spectra were then exported into text files each containing three columns of 1) frequency, 2) input signal magnitude spectrum, and 3) output signal magnitude spectrum. These data were then imported into

Excel for subsequent analyses and the respective magnitude spectra were plotted as a function of frequency.

Figures 4.10, 4.11 and 4.12 are example graphs of the spectra of the input and temporally advanced output for the Gaussian pulse, sine burst and tri-frequency test signals. The insets show the respective time domain signals.
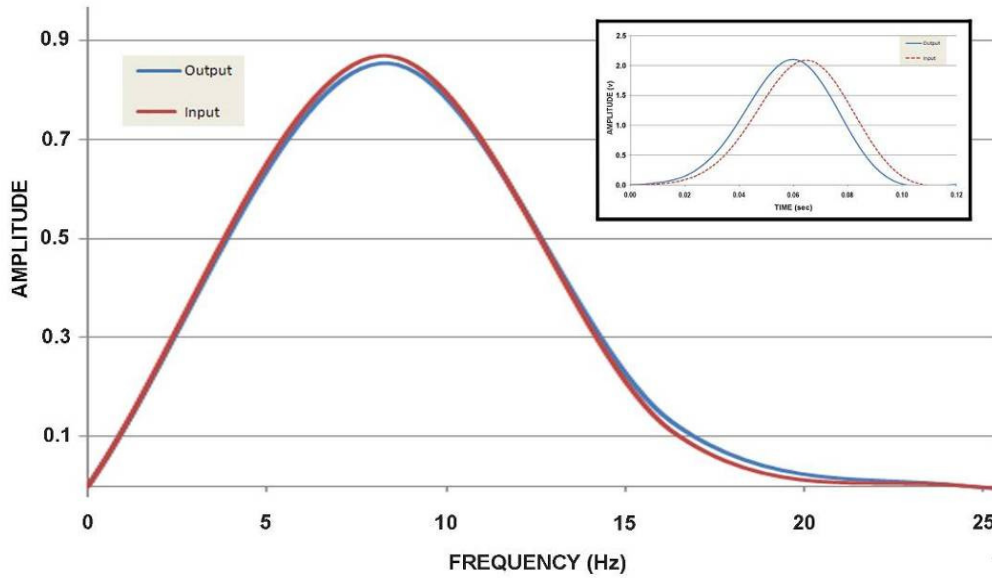
Figure 4.10: Spectral distribution - Gaussian pulse (40 ms at half amplitude).
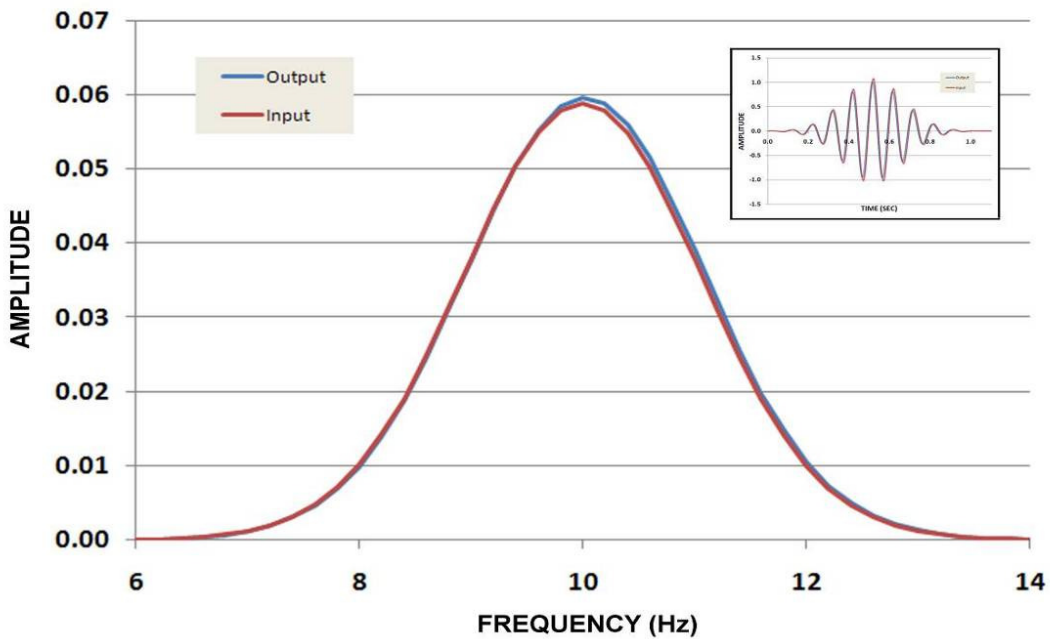
Figure 4.11: Spectral distribution - 10 Hz sine burst.
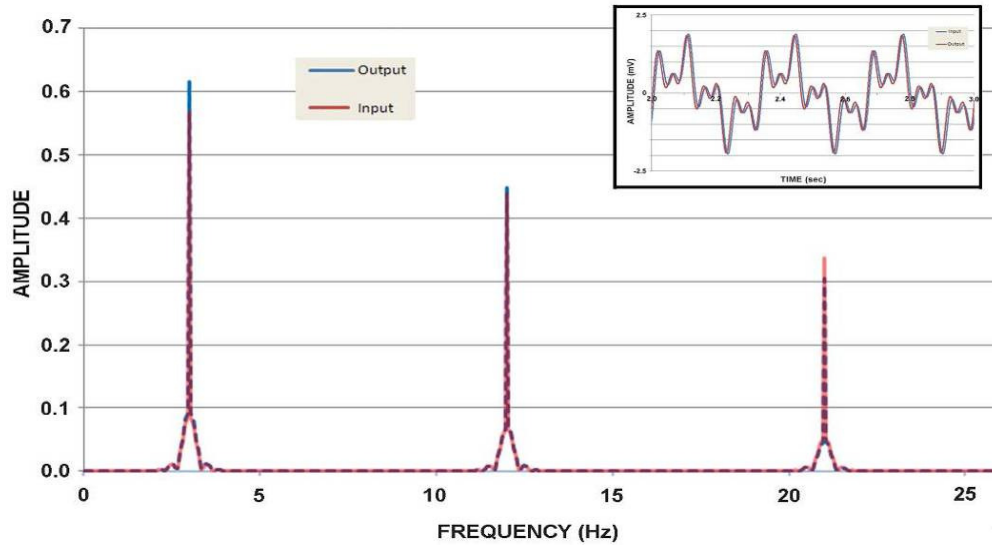
Figure 4.12: Spectral distribution - tri-Frequency test signal.

Tri-frequency Test Signal Gain

Changes in gain with respect to frequency are reflected in an increase or decrease in the magnitude at those frequencies. For the Gaussian pulse and single frequency sinusoidal input signals, the gain was calculated directly in the time domain. Changes in gain may also be determined from the spectra as these are reflected as changes in magnitude with respect to frequency. Thus, from the spectra, gain as a function of frequency was determined by taking the ratio of the output and corresponding input at each frequency of the spectral distribution. This also provided a cross-check of the gain results obtained from the time domain analyses for Gaussian pulse and single frequency sinusoidal signals. Thus the gain as a function of frequency could be determined in the frequency domain for the tri-frequency test signals - a result not obtainable via time domain analyses. The gain relative to frequency ranged from 0.958 at 1.0 Hz to 1.097 at 25 Hz. The detailed results for the tri-frequency gain as a function of frequency are provided in Table B.6 in Appendix B.

As in the time domain analyses, the results are plotted over the frequency range. These results provide additional support for the rejection of the null hypotheses. Figure 4.13 is a graph of the gain relative to frequency for the Gaussian pulse and sine burst and the tri-frequency test signals.

65
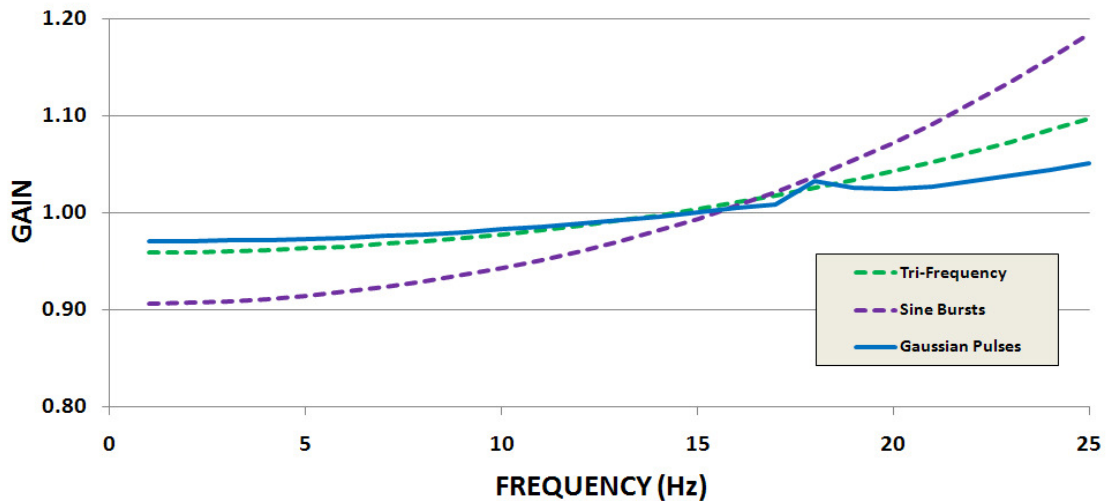
**Figure 4.13: Gain vs. frequency for the Gaussian pulse, sine burst
and tri-frequency test signals.**

Frequency Domain Correlations

The temporal advance of the output pulse relative to the input does not affect the magnitude spectra as the frequency domain representation of the signal contains no temporal information. Thus, the correlation between the spectra of the input signal and the temporally advanced output should approximate the maximum cross-correlation obtained from the time domain analyses. These results are summarized in Table 4.3 for the Gaussian pulse, sine burst and tri-frequency test signals respectively (and detailed results are provided in Tables B.2, B.4 and B.5 in Appendix B).

Table 4.3: Constructed test signal correlation results.

Statistic	Maximum Cross-Correlation (Time Domain)			Correlation (Frequency Domain)		
	Gaussian Pulse	Sine Burst	Tri-Frequency	Gaussian Pulse	Sine Burst	Tri-Frequency
Mean	0.998968	0.999756	0.997750	0.999163	0.999866	0.997750
Std Dev	0.001295	0.000336	0.001374	0.001824	0.000125	0.001374

Note the closeness of the results for the Gaussian pulses and sine bursts and the virtual equality of the results from the tri-frequency test signals.

Output Distortion

In the majority of the cited NGD studies, temporally advanced output waveforms exhibit significant waveform distortions observed in the frequency domain. These were examined in detail with the SA circuit model.

Figure 2.10 of the Preliminary Results (Chapter II) shows the actual oscilloscope traces of the input and advanced output pulse for the early SA physical circuit. The distortion in the shape of the output relative to the symmetric input pulse is readily observed. Specifically, the output pulse is narrowed and slightly skewed with respect to its corresponding input. In the frequency domain, pulse narrowing results in a phase shift to a higher frequency and the skewing of the pulse results in the introduction of higher frequency components in the output waveform that are not present in the input waveform. Given the constancy of both the gain and group delay of the spectral range of interest of the SA circuit model under investigation, these types of distortion were not expected to be present and in fact were not evident based on visual inspections of the input/output spectral distributions.

The distortion ratio (DR) [44] is determined in the frequency domain by 1) subtracting the spectral magnitude of the input from the corresponding spectral magnitude of the advanced output at each frequency, 2) the differences are squared and then summed over all the frequencies of interest, 3) the result is then divided by the sum of the squares of the input signal magnitude over all frequencies, and 4) finally, the square root of the result is taken, giving a root mean square ratio. In equation form:

$$DR = [\; \textstyle\sum_f (Y(f) - X(f))^2 \,/\, \sum_f X(f)^2 \;]^{1/2}, \qquad\qquad (4.5)$$

where the summations are over the frequency range of interest.

The distortion ratio is also determined in the time domain over the entire waveform(s) in a similar manner (replace $X(f)$ by $x(t)$, $Y(f)$ by $y(t)$, and f by t in eq. 4.5). In the time domain, however two additional steps are required. The output waveform must be shifted back in time relative to the input in order to align the input and output signals. Having shifted the output, the beginning of the input waveform and the end of the output

waveform will no longer have corresponding amplitudes from which a difference can be obtained. Thus the beginning and end portions, respectively, of the input and output waveforms must be truncated by a time period equivalent to the temporal advance.

As this measure is related to signal energy or power, calculating the distortion ratio over the entire waveform in the time domain, and from its frequency representation over the waveform's spectral range, should yield comparable results since the differences in signal energy or power are unaffected by Fourier (linear) transformation [32].

The distortion ratio results are summarized in Table 4.4 (and detailed results for each of the test signals are provided in Table B.7, Appendix B).

Table 4.4: Tri-frequency test signal distortion ratios (%).

Statistic	Time Domain	Frequency Domain
Mean	7.09	7.08
Std Dev	0.02495	0.02497

From the results of the gain analyses and the theoretical gain response of the SA circuit model, it is evident that variation in gain accounts for the majority of the overall output distortion. Further, the distortion attributable to gain rises considerably for spectral content above 25 Hz. In electrocardiology, a number of pathologies are reflected in deviations from the normal ECG timing rather than deviations in ECG amplitudes.

The R-R interval determines the heart rate and is used to diagnose various arrhythmias including bradycardia and tachycardia [195]. A decrease in R-R interval variability, indicative of autonomic dysfunction (i.e., low parasympathetic activity), often precedes atrial fibrillation and is associated with an increased risk of primary heart attack and sudden cardiac death [196-198].

The P-R interval is associated with the time required for atrial depolarization and the subsequent initiation of ventricular depolarization. A prolonged P-R interval (in excess of 0.2 s) indicates an atrioventricular block [195,199].

A prolonged QT interval (that corresponds to ventricular repolarization time) is associated with polymorphic ventricular tachycardia (*torsade de pointe*) and sudden cardiac death [195,199]. Thus, there is an interest in quantifying the morphological dissimilarity between the input and output waveforms, which is, for the most part, less related to differences in the gain.

With the exception of gain differences, the distortions impact the correlation between the spectral content of the advanced output signals and their corresponding inputs. Specifically, if output signal distortion only results from a scalar (constant with respect to frequency) change in gain relative to the input, then the correlation between the input and output signals will be uniquely 1.0 indicating that the two signals are a perfect morphological (waveform shape) match.

The Pearson r (linear correlation) provides a measure of the morphological similarity between the advanced output spectrum and its corresponding input spectrum while correcting for the overall scale amplitude difference between the two signals [45-49}. Waveform dissimilarity in the time or frequency domain may therefore be defined as the difference between perfect correlation (1.0) and the maximum cross-correlation (r_{MAX}) in the time domain, or as 1.0 minus the correlation between the input and output magnitude spectra (r_{MSP}) in the frequency domain.

Thus, for the Gaussian pulses, sine bursts and tri-frequency test signals, waveform dissimilarity was determined from the input/output correlations. The summary of these results is shown in Table 4.5.

Table 4.5: Input/output waveform dissimilarity (%) for the constructed test signals.

Statistic	Waveform Dissimilarity (100 * (1.0 - r_{MSP}))		
	Gaussian Pulse	**Sine Burst**	**Tri Frequency**
Mean	0.10	0.02	0.23
Std Dev	0.13	0.03	0.14

In summary, the mean distortion ratio is under 10% for each of the constructed test signals. In addition, waveform dissimilarity is less than 0.3% for all constructed signals. These results support the rejection of the null hypotheses.

Chapter V

Application to ECG Signals

In the previous experiments, the SA circuit model was developed and rigorously tested with three types of constructed input signals. The gain and signal detection temporal advance were analyzed to confirm the SA circuit model performance and the concomitant waveform output signal distortion was estimated. The goal of this research is to determine the effects of temporally advancing ECG signal detection using the SA circuit model. The key objectives of the investigation are to determine the constancy in terms of the gain and temporal advance achieved and to characterize any resulting distortion. To maximize the signal resolution, the ECG is segmented into individual heartbeats. The ECG waveforms from the five subjects used here are wideband: they are neither low-pass nor notch filtered to remove 60 Hz line noise.

Of the five sets of unfiltered ECG recordings, two of the subjects were recorded at a sampling rate of 1 kHz [42] and three of the subjects [43] were recorded at a sampling rate of 200 Hz. Thus the majority of the analyses were limited to a frequency range of 0.5 to 100 Hz based on the Nyquist criterion (one half of 200 Hz). Twenty individual ECG heartbeat waveforms from each of five subjects were used. These include ECG waveforms of three subjects exhibiting a normal sinus rhythm and two subjects exhibiting tachycardia. Thus, a total of one hundred individual heartbeats are temporally advanced. This was deemed to be an adequate sample based on means, standard deviations and group differences determined in the previous experiments using the constructed test signals.

ECG Signals – Individual Heartbeats

Each of the five subject's ECG recordings was reviewed using AAELVIEW signal analysis and measurement software [42]. A series of twenty consecutive sinus rhythms (i.e., individual heartbeats) was extracted from each subject's ECG. These data files were imported into Excel in separate columns of time and amplitude values and then plotted.

The ECG recordings were segmented based on the R-R interval of consecutive heartbeats. Specifically, the point of segmentation was chosen to be the midpoint between successive R-waves. This segmentation point was between the end of the U-wave and the beginning of the subsequent P-wave of each heartbeat. Using this approach, twenty contiguous ECG segments each centered roughly near the peak of the R-wave of the QRS complex were extracted per subject.

The average amplitude of each ECG segment was calculated and subtracted from each signal to eliminate the DC offset. Each segment was then Gaussian tapered at each end to eliminate high frequency ringing artifact at the beginning and end of each waveform. Application of the Gaussian taper to the ECGs was similar to its application to the tri-frequency test signals, except that the duration of the taper was 50 ms applied to the beginning and end of each ECG segment.

Figure 5.1 shows an ECG segment (individual heartbeat) in which the DC offset was not subtracted. This ECG is from lead III (LA(-) to LF(+)). The subject has coronary artery disease and has had a previous myocardial infarction. The overall ECG also displayed short periods of ventricular tachycardia, atrial and ventricular premature depolarization, and right bundle branch pattern. Notice the slight negative DC offset at the beginning of the signal (circled) as well as the oscillatory artifact in the output. The abrupt, non-zero signal start introduces an impulse artifact that contains high frequency content in which frequencies between 60-65 Hz were amplified over five-fold. This had a significant effect on the output signal QRS peak.

The individual heartbeat signals were imported into SPICE for application to the SA circuit model. The time domain results obtained from the SPICE circuit simulation were

then imported into Excel in three columns of 1) time, 2) input signal amplitude values and 3) output signal amplitude values. The two signals were plotted and the spreadsheet was retained (saved) for subsequent analyses (Figure 5.2). Note the reduction in the advanced output artifact for the same ECG signal used in Figure 5.1.
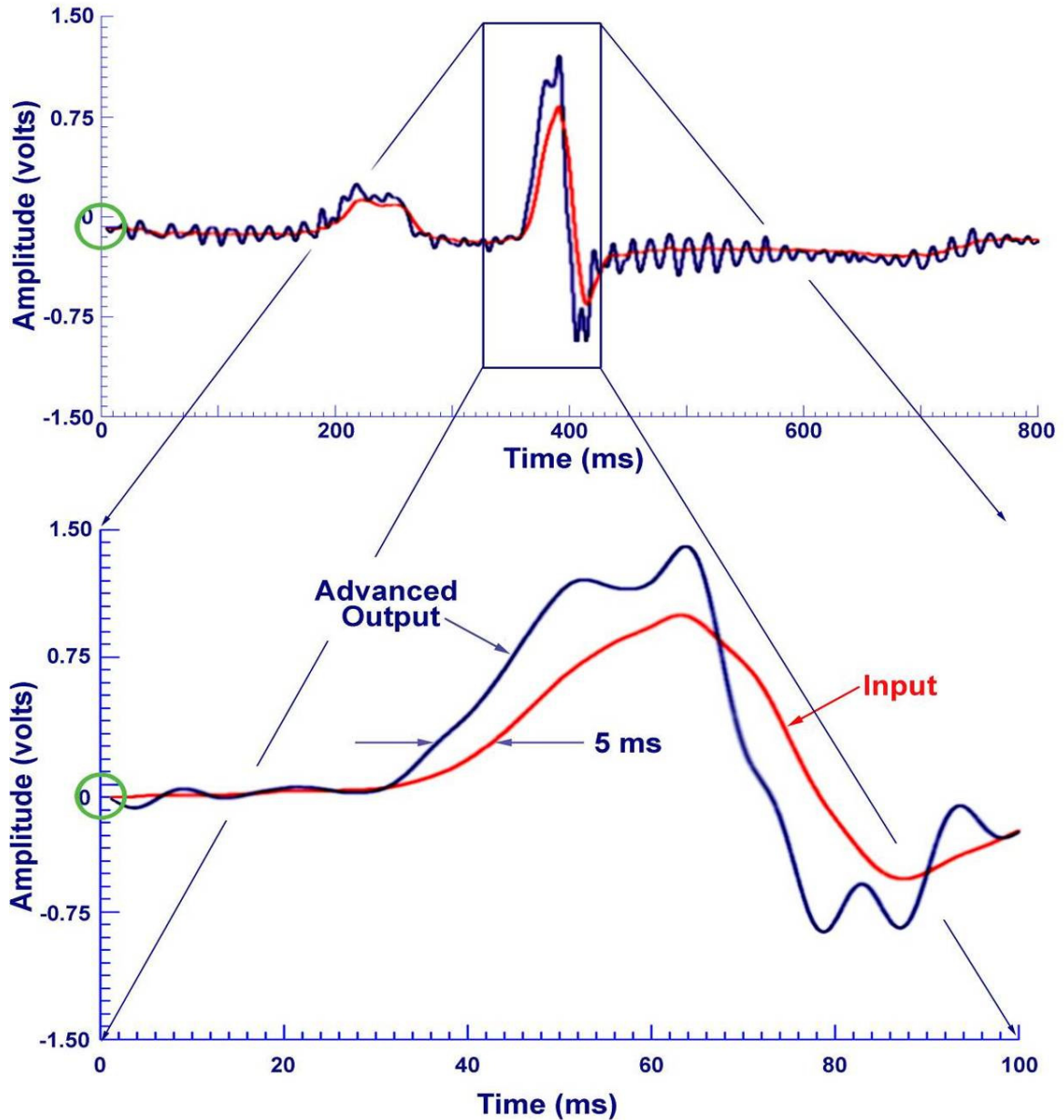
Figure 5.1: Human heartbeat - input and temporally advanced output with artifact (lead III: LA(-) to LF(+)).
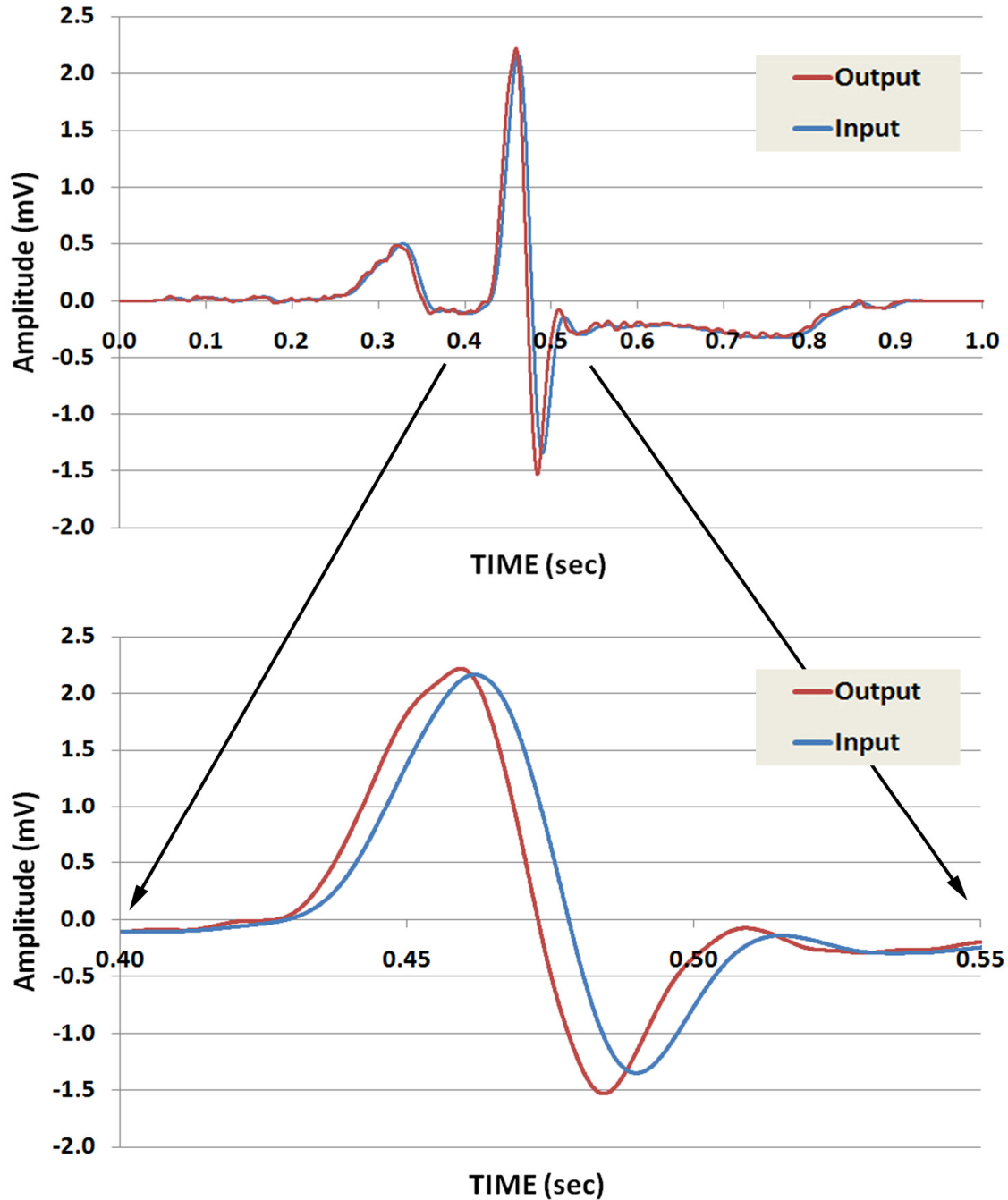
Figure 5.2: Human heartbeat - input and temporally advanced output (lead III: LA(-) to LF(+)).

A short series of heart beats was also applied to the SA circuit model to confirm the ability to temporally advance the detection of a continuous ECG signal. Figure 5.3 shows the results for four consecutive heartbeats. Note that the signal advance achieved is fairly constant from the first heartbeat to the last.
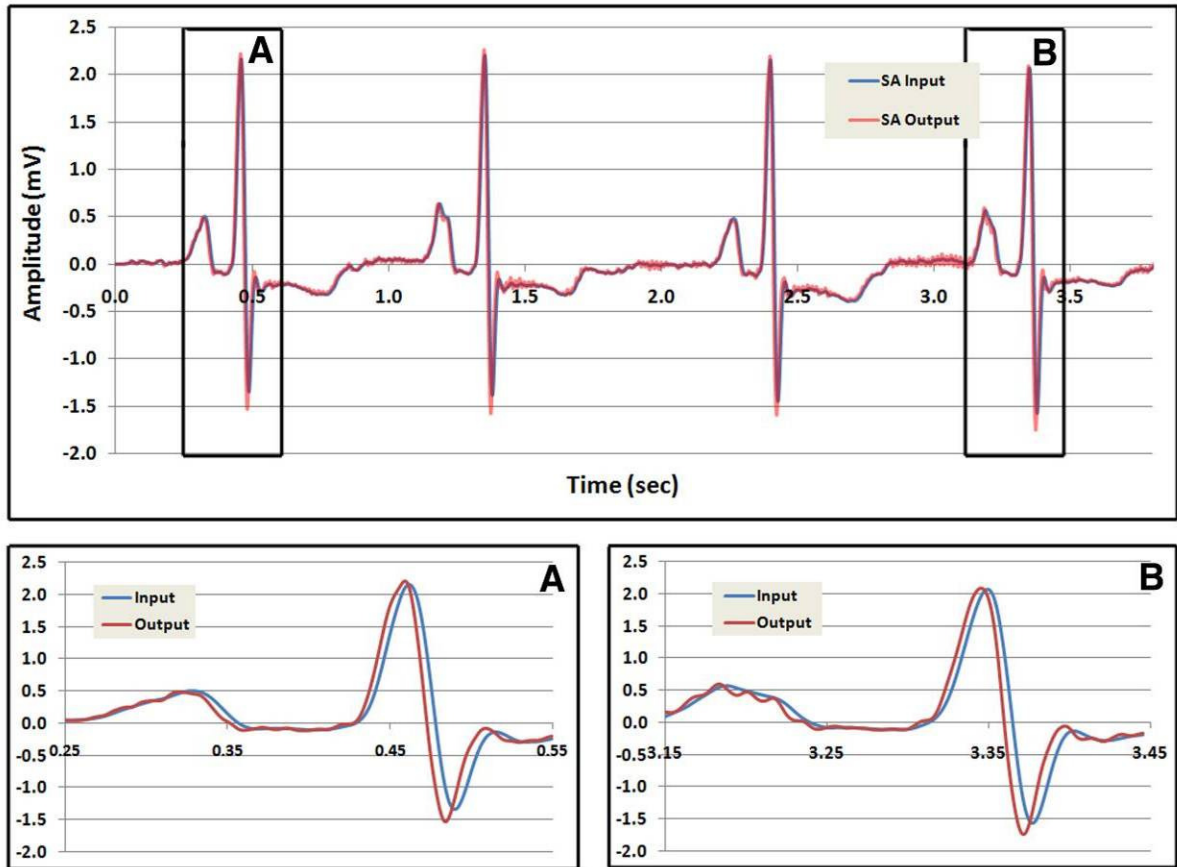
Figure 5.3: Temporally advanced detection of four consecutive heartbeats.

Temporal Advance/Gain Analyses and Results

The duration of the waveform advance achieved was quantified by using a cross-correlation to find the time lag associated with the maximum correlation between the input and temporally advanced output [31]. In addition, the overall gain of the output relative to the input was determined using the same analytic methods described in the Time Domain Analyses section of Chapter 4. The mean, standard deviation and coefficient of variation were determined for each subject. The individual overall gains (based on the RMS amplitude ratio) ranged from a low of 0.959 to a high of 1.047. The results obtained from the application of the ECG test signals to the SA circuit model are summarized in Table 5.1 (See Tables C.1 to C.5 in Appendix C for detailed results for each subject). These results support the rejection of the null hypotheses.

Table 5.1: Averaged ECG temporal advance/gain results.

Subject	Statistic	Advance (ms)	Correlations		Gain
			Time (max)	Frequency	
RJ	Mean	4.940	0.996806	0.996846	1.018
	Std Dev	1.053E-15	0.000159	0.000141	0.0018
	C_v	2.131E-16			0.18%
EG	Mean	4.897	0.995036	0.992851	1.018
	Std Dev	0.0744	0.002043	0.003281	0.0131
	C_v	0.0152			1.29%
VS	Mean	4.940	0.997810	0.997736	0.993
	Std Dev	8.899E-16	0.000216	0.000235	0.00198
	C_v	1.801E-16			0.20%
MH	Mean	4.937	0.996783	0.996825	0.995
	Std Dev	0.00251	0.000184	0.000180	0.00213
	C_v	0.00051			0.21%
MJ	Mean	4.935	0.998473	0.998578	0.964
	Std Dev	0.00197	0.000482	0.000435	0.00380
	C_v:	0.00040			0.39%
Overall	Mean	4.930 (ms)	0.997	0.997	0.997
	Std Dev	0.0366	0.0015	0.0025	0.0046
	C_v	0.74%			0.45%

As described previously, the time domain results (input/output amplitude vs. time) are first zero-padded as needed. The FFT is appropriately applied to the ECG individual heartbeat results using SPICE. The raw magnitude spectrum is computed from the FFT results, and then exported into Excel in three columns of 1) frequency, 2) input signal magnitude spectrum and 3) output signal magnitude spectrum. The results are plotted and saved for subsequent analyses (Figure 5.4).
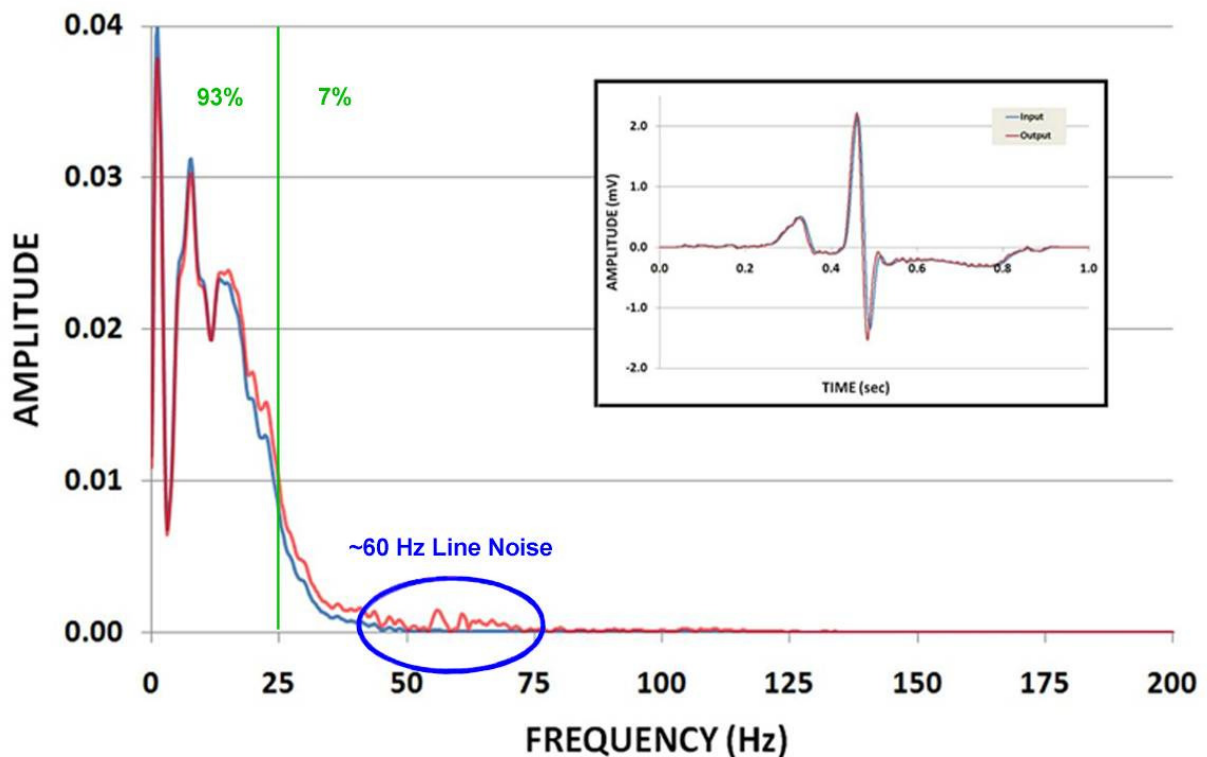
Figure 5.4: Spectral distribution of an individual heartbeat ECG

Note the elevated noise level in the spectral distribution of the temporally advanced output in the 60-65 Hz range resulting from the differentially large amplification in that range. Recall that the ECG recordings used for this study were completely unfiltered. In a typical clinical setting, the ECG recordings are low-pass and notch filtered around 60 Hz to eliminate these artifacts.

The gain as a function of frequency was derived from the spectral distribution of the inputs and their corresponding outputs. The average gain relative to frequency over the spectral range from 0.5 to 25 Hz is plotted for each of the five subjects in Figure 5.5. In addition, the Pearson *r wa*s computed from the spectral distributions using the methods described previously.

Figure 5.6 is a graph of the gain as a function of frequency for the averaged ECG results and the constructed test signals over the same spectral range.
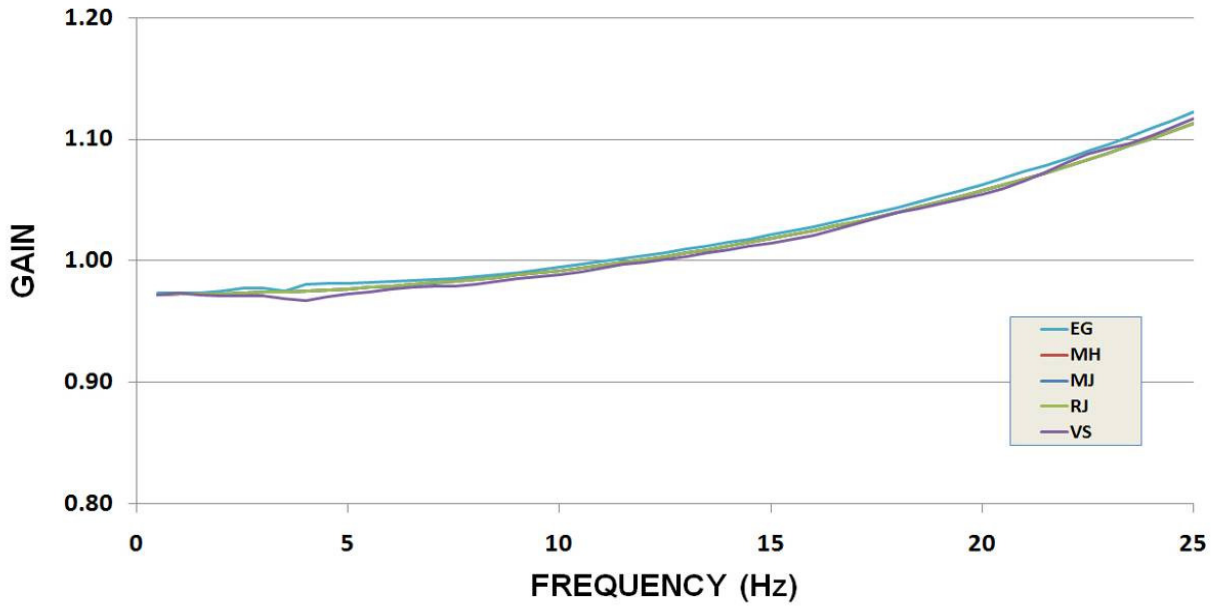
Figure 5.5: Average gain vs. frequency for each subject.
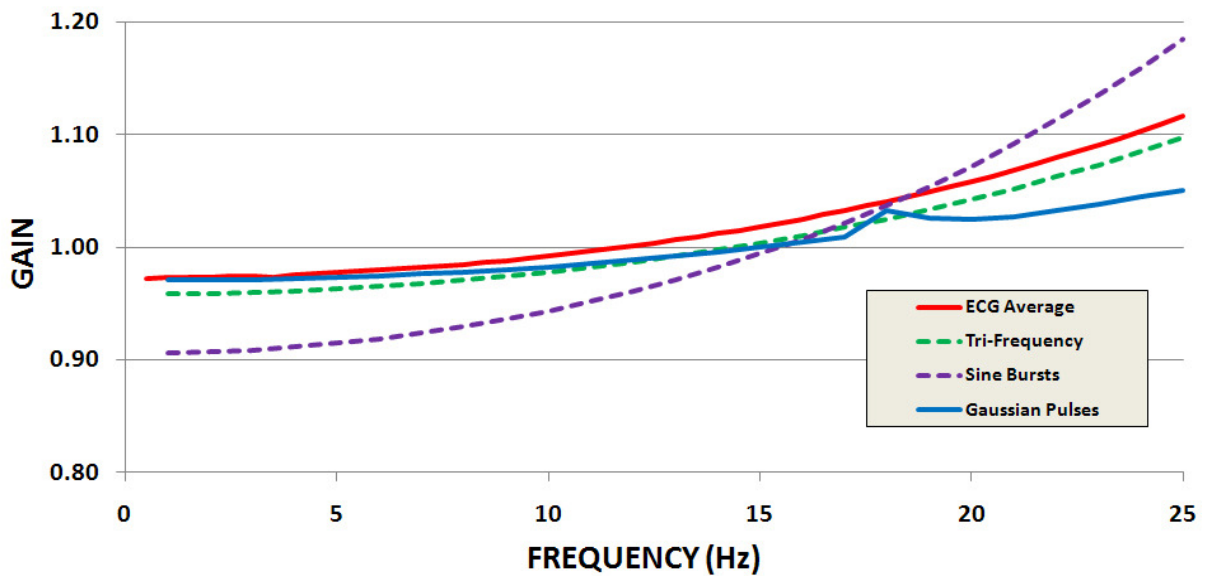
Figure 5.6: Gain vs. frequency for the ECG's and constructed test signals.

Unlike the constructed test signals, the ECG signals contain spectral content well above 25 Hz. Figure 5.7 is a graph comparing the empirical gain vs. frequency against the theoretical gain curve from the AC analysis up to 200 Hz.

Recall that three of the ECG recordings were sampled at 200 Hz, while two were sampled at 1,000 Hz. Thus, per the Nyquist criterion, the analysis of the spectral data results was limited to 100 Hz for three of the ECG datasets. Therefore the empirical gain response shown in red was derived from 100 individual heartbeats (5 subjects - 20 signals each) whereas the gain response shown in green, from 40 individual heartbeats (2 subjects - 20 signals each). There is a close match between the theoretical curve and the two empirical curves. Note the significantly reduced gain around the pole frequency locations of the empirical results. Had the data been filtered, as is the usual clinical practice, there would likely have been very little spectral content around the SA circuit model poles.
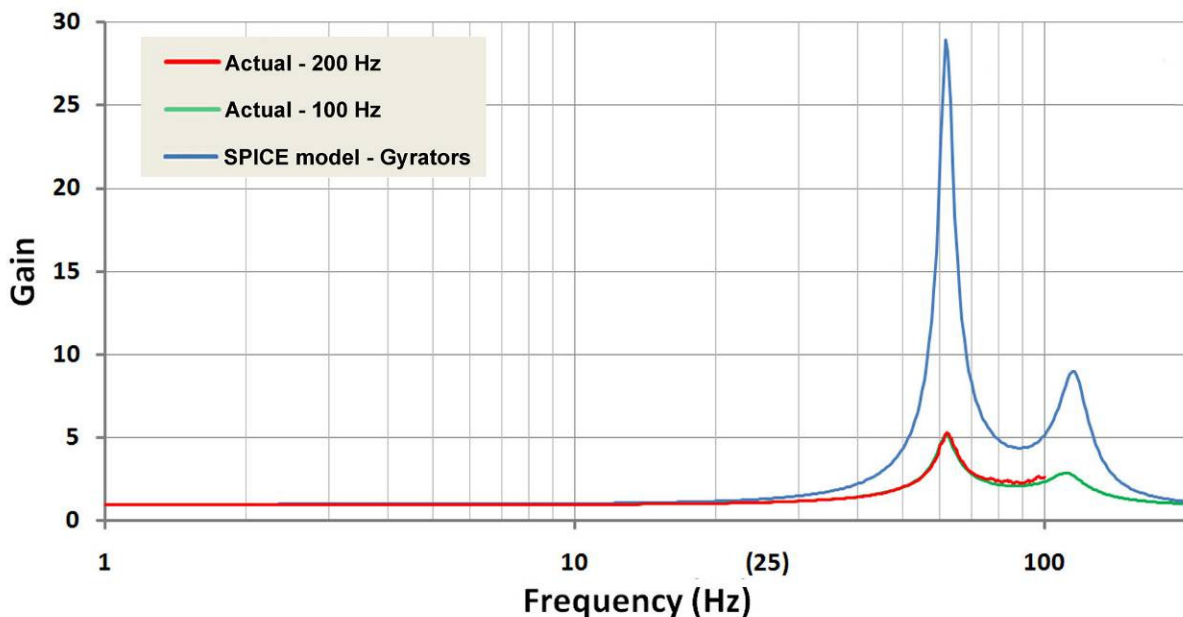
Figure 5.7: Gain vs. frequency for the ECG signals compared to the SPICE gyrator based SA circuit model analysis.

Distortion Analyses

Overall Distortion

For the ECG signals, the distortion ratio calculations (defined in the last chapter) were made for the following frequency ranges: 0.5 to 25 Hz, 25 to 200 Hz, 25 to 100 Hz

and 0.5 to 200 Hz. Note that the ECG recordings from two of the five subjects extend to 200 Hz (1,000 Hz sampling rate), the remaining three go only to 100 Hz (200 Hz sampling rate). The results are summarized in Table 5.2 (and detailed results per subject are provided in Tables C.6 to C.10, Appendix C). Note the closeness between the mean distortion ratios (DR) measured in the time domain for each subject and averaged over subjects (mean 7.90 ± 0.70) and those of the frequency domain (0.5 to 100 Hz: mean 7.81 ± 0.66).

Regarding the time domain measure of the distortion ratio, the output is first shifted to align with the input (the time points of each wave must be aligned prior to computing the DR. As a result, both the output and input waveforms must be truncated by approximately 5 ms. In the frequency domain, however, the entire signal can be used to compute the input and output magnitude spectra. Therefore, of necessity, the signals used to compute the distortion ratio in both domains are slightly different, which accounts for a portion of the difference in their respective mean distortion ratio results. The remaining very small difference between the two distortion ratio measures can be attributed to round-off error.

Table 5.2: Distortion ratios over various frequency ranges (%).

Subject	Statistic	Time	0.5 to 100 Hz	0.5 to 25 Hz	25 to 100 Hz	25 to 200 Hz
RJ	Mean	8.29	8.21	6.39	40.50	40.61
	Std Dev	0.23	0.21	0.10	1.46	1.44
EG	Mean	10.07	9.87	6.48	60.83	63.41
	Std Dev	2.16	2.02	0.65	14.07	17.88
MH	Mean	6.77	6.65	5.16	63.12	
	Std Dev	0.40	0.35	0.08	5.03	
MJ	Mean	7.98	7.94	5.84	48.18	
	Std Dev	0.23	0.23	0.06	3.16	
VS	Mean	6.38	6.36	5.38	73.46	
	Std Dev	0.48	0.47	0.19	9.58	
Overall	**Mean**	**7.90**	**7.81**	**5.85**	**57.22**	**52.01**
	Std Dev	**1.46**	**1.40**	**0.59**	**12.97**	**16.12**

These results (Table 5.2) show that the majority of the overall distortion occurs in the spectral range of 0.5 to 25 Hz. The ECG test signals used in this study had not been (pre)filtered, thus they contain spectral content above 25 Hz. In clinical practice, this spectral content would normally be reduced or eliminated through first filtering the acquired ECGs. The input signals were analyzed to determine the relative distribution of spectral content above and below 25 Hz. The average results over all of the subjects showed that spectral content below 25 Hz accounts for 93.2% of the total amount, while 6.8% comes from spectral content above 25 Hz. (detailed results on a per subject basis are provided in Tables C.11 and C.12 in Appendix C). Thus, given the overall distortion results, less than 7% of the ECG signal's total spectral content accounts for the difference between the overall distortion ratio and that in the 0.5 to 25 Hz range. The distortion results taken together support the rejection of the null hypotheses.

Input/Output Waveform Dissimilarity

Correlation may be used as a measure of the morphological similarity between two waveforms [44-49]. Additionally, as stated by Semmlow [50], "in correlation the coefficients are normalized to fall between zero and one. This makes the correlation coefficients insensitive to variations in the gain … or of the scaling of the variables." Based on the use of correlation coefficients as a measure of waveform similarity, its complement, dissimilarity, is naturally defined as the difference between perfect correlation (1.0) and that between the input and its respective output magnitude spectra (r_{MSP}). It therefore provides a relative measure of the morphological *dissimilarity* between the waveforms that is not affected by the gain variation [50,51]. The results of the waveform dissimilarity (WD) analysis, summarized in Table 5.3, support the rejection of the null hypotheses (detailed results are provided in Table C.13 in Appendix C).

Table 5.3: ECG input/output waveform dissimilarity for each subject (%).

Statistic	Waveform Dissimilarity ($100 * (1.0 - r_{MSP})$)				
	RJ	EG	VS	MH	MJ
Mean	0.32	0.46	0.23	0.30	0.10
Std Dev	0.0143	0.1488	0.0962	0.0185	0.0314

Input/Output Variability

To determine the increase in the variability of the ECG output signals relative to their corresponding inputs, three output waveform parameters were selected. The first two were the time of occurrence (time) and amplitude at the peak of the QRS complex of the ECG (circled in Figure 5.8). Given the rapid change in slope at this point of the ECG, it should exhibit the most variation in both time and amplitude making these parameters very sensitive to distortion. The last parameter was the RMS value for each waveform used previously to determine gain. This value provides an indicator that is less sensitive to distortion as it is averaged over all of the time points in the signal.

The QRS peak time and amplitude and the RMS value of each ECG input and corresponding output (20 per subject) were measured. The mean and standard deviation for each parameter were calculated for each subject's ECG signals. The F-test was then used to compare the variance of each input parameter to that of the respective output parameter (F in this case is equal to the ratio of output to input

Figure 5.8: Human ECG QRS peak.

variance with 19 degrees of freedom). In addition, the correlations between the inputs and advanced outputs were determined for each subject. The results are summarized in Table 5.4 (and detailed individual results are provided in Tables C.14 to C.18 in Appendix C).

If the F-test results in a significance level of $p < 0.05$, then the data support the assertion that there is a statistically significant difference in the variability of the circuit output parameter relative to its input parameter. For only one subject (EG), one of the F test results ($p < 0.0015$) indicates that the variability of the QRS peak amplitude of the output is significantly different from that of the input. For all of the other subjects the F test results indicate no significant circuit input-output differences in variability of the QRS peak amplitudes. For the other two parameters, time of occurrence of the QRS peak and the RMS amplitude, there is no indication of significant variability difference in the output relative to the input.

In order to obtain a statistical result for all five subjects, Fischer's method for combining F-tests [52], is used to compute the overall significance level:

$$P = -2 \ln(\pi_i p_i),$$ (5.1)

where the p_i are the individual (5) subject's F-test p values (and π_i signifies multiplication of the p_i altogether). The overall significance level is then determined using a Chi-square test with 2N (in this case, 10) degrees of freedom. The resulting overall $p <$ results are as follows: QRS peak amplitude: 0.1545; QRS peak time: 1.0; RMS amplitude: 0.9728. Thus, there is no indication of significant variability difference in the output parameters relative to their respective input parameters across all subject-sets. In addition, the correlations between all subjects' input and output parameters ranged from 0.91 and 1.00. These results support the rejection of the null hypotheses.

Interbeat Variability

A series of eight consecutive heartbeats was selected from each subject's ECG recordings in which there appeared visually to be little fluctuation. The cross-correlation was found between each of the eight consecutive heartbeats providing twenty-eight interbeat cross-correlations for each of five subjects. The maximum correlations were then averaged to determine the interbeat variability of each subject's sinus rhythms. Table 5.6 provides a summary of the parameters measured. This interbeat variability provides a physiological reference for the correlations between the ECG input and output signals (n-20) from the circuit model.

Table 5.5 also includes the p level of statistical difference between each subject's interbeat correlation and their respective circuit input-output correlation in both the time and frequency domains. In each subject's case, comparing interbeat correlation and time domain circuit input-output correlation, the difference is statistically significant at the 0.05 level as shown. These results suggest that no significant additional variability is introduced by the SA circuit model, beyond each subject's natural interbeat ECG variability.

Table 5.4: Statistical comparison of the three variability parameters of ECG signals.

Subject	Statistic	INPUT				OUTPUT		
		Peak Ampl. (mV)	Peak Time (ms)	RMS (mV)		Peak Ampl. (mv)	Peak Time (ms)	RMS (mV)
EG	Mean	2.2510	0.5585	2.366		2.3557	0.5564	2.409
	Std Dev	0.0934	0.0572	0.0777		0.2021	0.0577	0.0969
	* $p <$	0.0015	0.9743	0.3438				
	Pearson r	0.9151	0.9998	0.9560				
RJ	Mean	1.6161	0.3025	2.214		1.6861	0.2977	2.254
	Std Dev	0.0534	0.0191	0.0759		0.0543	0.0191	0.0785
	* $p <$	0.9449	0.9990	0.8814				
	Pearson r	0.9678	0.9999	0.9988				
MH	Mean	0.5634	0.2818	0.972		0.5736	0.2770	0.9672
	Std Dev	0.0306	0.0437	0.0514		0.0316	0.0439	0.050
	* $p <$	0.8993	0.9827	0.9369				
	Pearson r	0.9898	0.9999	0.9993				
MJ	Mean	0.5088	0.2564	1.412		0.5100	0.2528	1.361
	Std Dev	0.0830	0.0332	0.2336		0.0739	0.0334	0.2198
	* $p <$	0.6161	0.9830	0.7924				
	Pearson r	0.9973	1.0000	1.0000				
VS:	Mean:	1.5081	0.4140	1.686		1.5833	0.4089	1.673
	Std Dev	0.0518	0.0670	0.0715		0.0509	0.0670	0.0683
	* $p <$	0.9395	0.9985	0.8453				
	Pearson r	0.9802	1.0000	0.9994				
Overall	** $p <$	0.1545	1.0000	0.9728				

* from the F test for variance differences.

** combined result from the Chi-square test (using Fischer's method)

Table 5.5: ECG interbeat vs. input/output correlations.

Subject:	Statistic	Correlations		
		Interbeat	Time (max)	Frequency
RJ:	Mean	0.99057	0.99681	0.99685
	Std Dev	0.006148	0.00016	0.00014
	* p <		0.0418	0.0401
EG	Mean	0.985771	0.99504	0.99285
	Std Dev	0.010799	0.00204	0.00328
	* p <		0.0465	0.1357
VS	Mean	0.993167	0.99781	0.99774
	Std Dev	0.004248	0.00022	0.00024
	* p <		0.0351	0.0392
MH	Mean	0.984707	0.99678	0.99683
	Std Dev	0.007494	0.00018	0.00018
	* p <		0.0064	0.0060
MJ	Mean	0.974946	0.99847	0.99858
	Std Dev	0.021486	0.00048	0.00044
	* p <		0.0000	0.0000
Overall	Mean	0.986	0.997	0.997
	Std Dev	0.0100	0.00062	0.00086

* Tested using Fischer's conversion of each correlation to a z-score and standard error calculated as square root of [(1/(28-3) + 1/(20-3))].

Chapter VI

Conclusions and Discussion

Overall Results

This investigation had three major objectives to be met in testing the hypothesis that ECG waveform detection (specifically, individual heartbeats) could be temporally advanced by approximately 5 ms using a single-stage SA circuit model and that the output distortion would be limited to ten percent or less.

In order to test the main hypotheses, the following performance goals were established for the SA circuit model:

1) Temporal advance of ECG waveforms by 5 ms ($\pm$ 5% or 0.25 ms) with a coefficient of variation (C_v) of less than 5%,

2) Mean gain of 1.0 $\pm$ 5% with a C_v of less than 10%,

3) Total output distortion of less than 10%,

4) A statistically insignificant increase in variance (based on the F-test comparing multiple input and output ECG waveform features),

5) Input/output waveform dissimilarity of less than 1%.

The first research objective was the development of an SA circuit model designed to operate over the frequency range of 1 to 25 Hz. The circuit model developed by the investigator for this study combined several features from two previously developed circuit models that operated over the 0.5 to 500 Hz and 0.5 to 100 Hz frequency ranges (described in Preliminary Results, Chapter II), circuits described in the cited literature [3-5] (also discussed in Chapter II) and cascaded physical circuitry developed "in-house."

The SPICE AC analyses confirmed the theoretical performance of the SA circuit model design. Test signals (Gaussian pulses and single frequency sinusoids) of known spectral content were constructed and applied to the SPICE circuit simulation to confirm that the circuit model performed adequately in terms of the gain and temporal advance. In addition, the procedures for generation of the test signal construction were validated.

The second research objective was the rigorous testing of the circuit model using three different types of test signals of known spectral content. The data analyses, performed in both the time and frequency domains, yielded results in terms of the temporal advance achieved, the gain and output distortion. For all three types of test signals, over the design frequency range (1 to 25 Hz) the temporal advance achieved was 4.9 ms with (overall) C_v of less than 2%. The gain averaged 1.0 with a C_v of less than 9%. The total distortion ratio was less than 7% and the input/output waveform dissimilarity was less than 0.3%.

These results provide strong evidence supporting the rejection of the null hypotheses of this study. In addition, the outcomes provide bases for the analyses and interpretation of the ECG test results.

For the third research objective, ECG test signals from five subjects, three exhibiting normal cardiac rhythms and two exhibiting tachycardia, were prepared and applied to the SA circuit model. The time and frequency domain analyses used for the second research objective were applied to the ECG signal data.

The overall results obtained in this study are summarized as follows:

- Temporal advance: 4.93 ms and C_v of less than 1% (Figure 6.1).
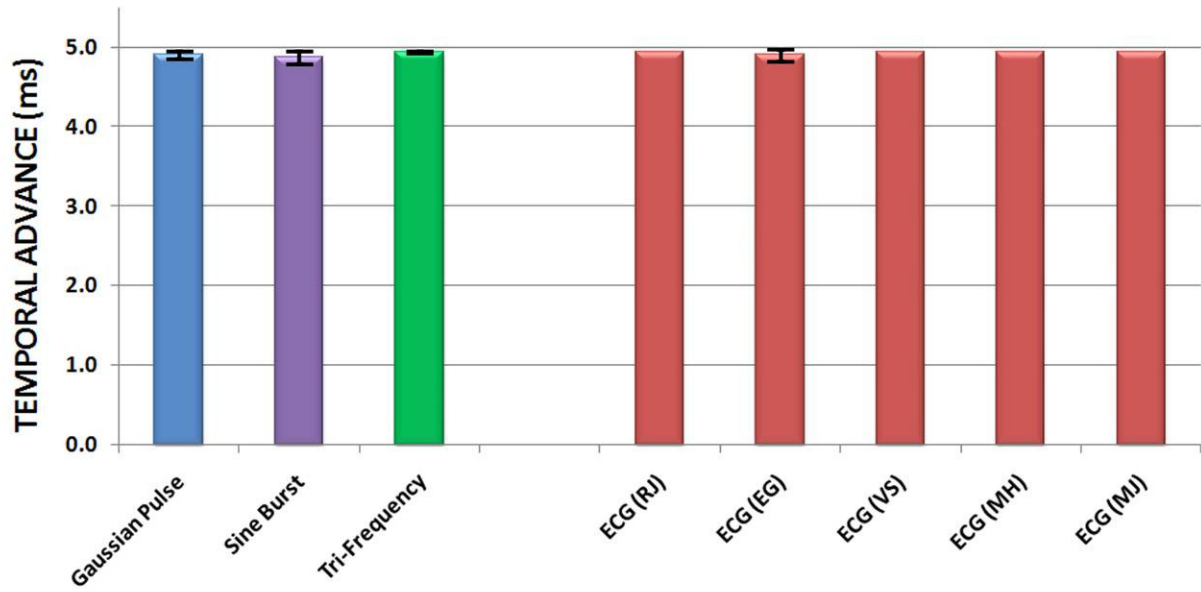
Figure 6.1: Overall temporal advance results.

- Gain: 0.997 and C_v of less than 0.5% (Figure 6.2).
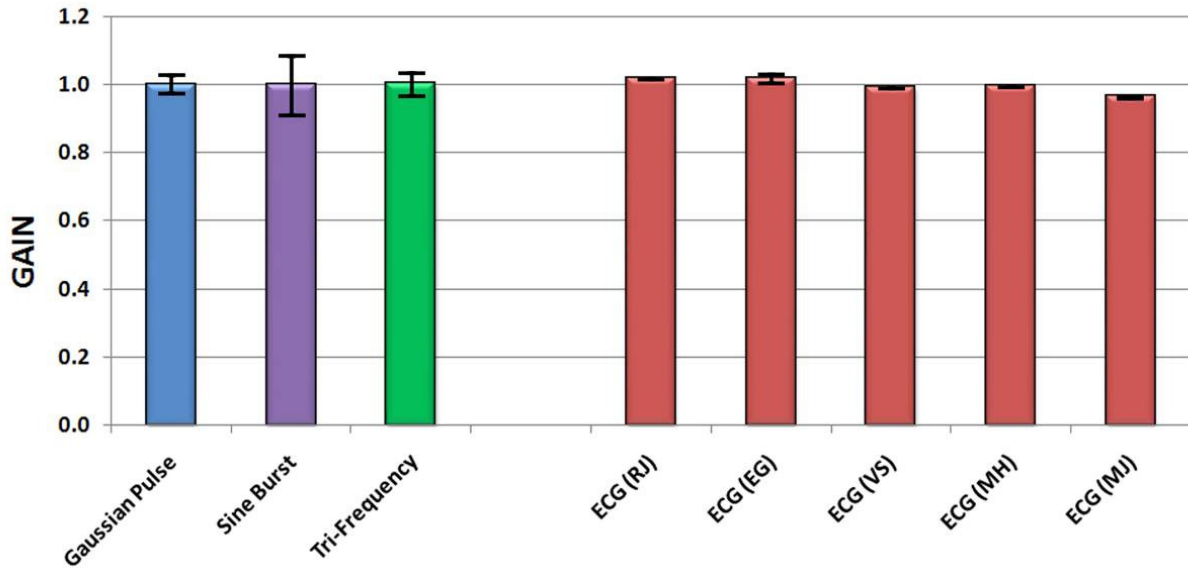
Figure 6.2: Overall gain results.

- For the ECG and tri-frequency test signals the mean distortion ratio is less than 8%. Over the frequency range of 0.5 to 25 Hz, it is less than 6% (Figure 6.3).
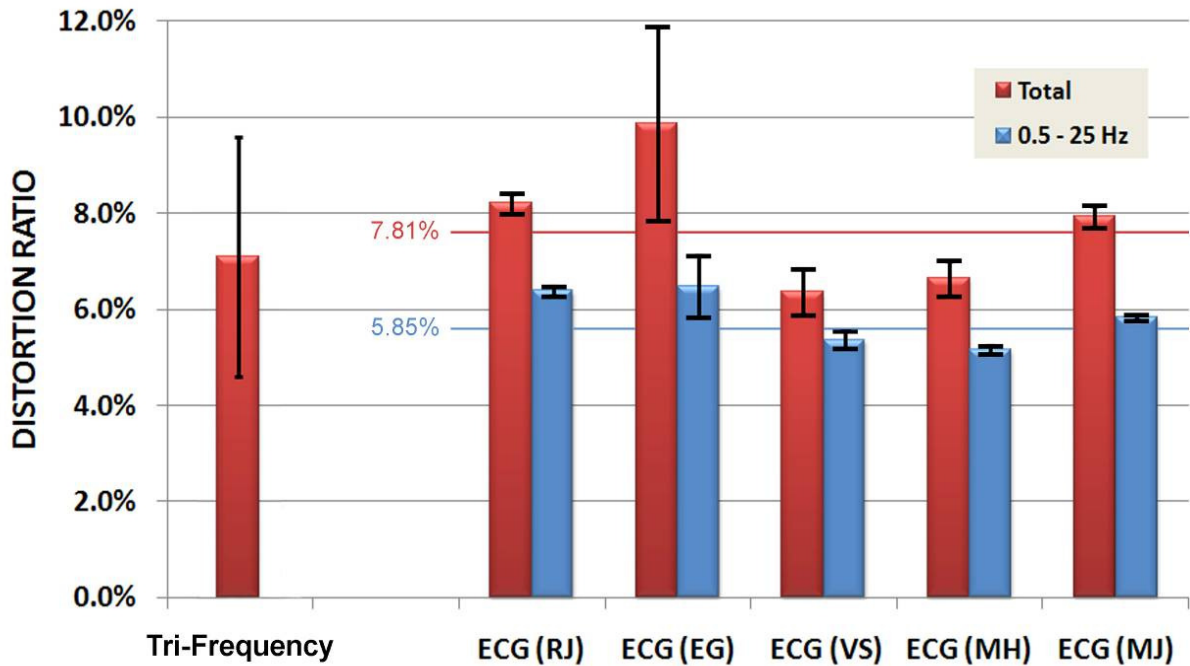
Figure 6.3: Input/output distortion ratios

- Based on the Chi-square test applied to the overall ECG results, the variance between the three input and output parameters was found not to be statistically different.

- The mean input/output waveform dissimilarity is less than 0.3% (Figure 6.4).

Further, the correlations between input and output parameters averaged 0.997.

For the time of occurrence of the QRS peak parameter, the F-test was also applied following the subtraction of the individual temporal advances from the output. While the results were essentially the same, the study goal was to determine the overall effect on variability which necessarily includes variability associated with the temporal advance of the signal and thus the adjustment was ultimately not used.
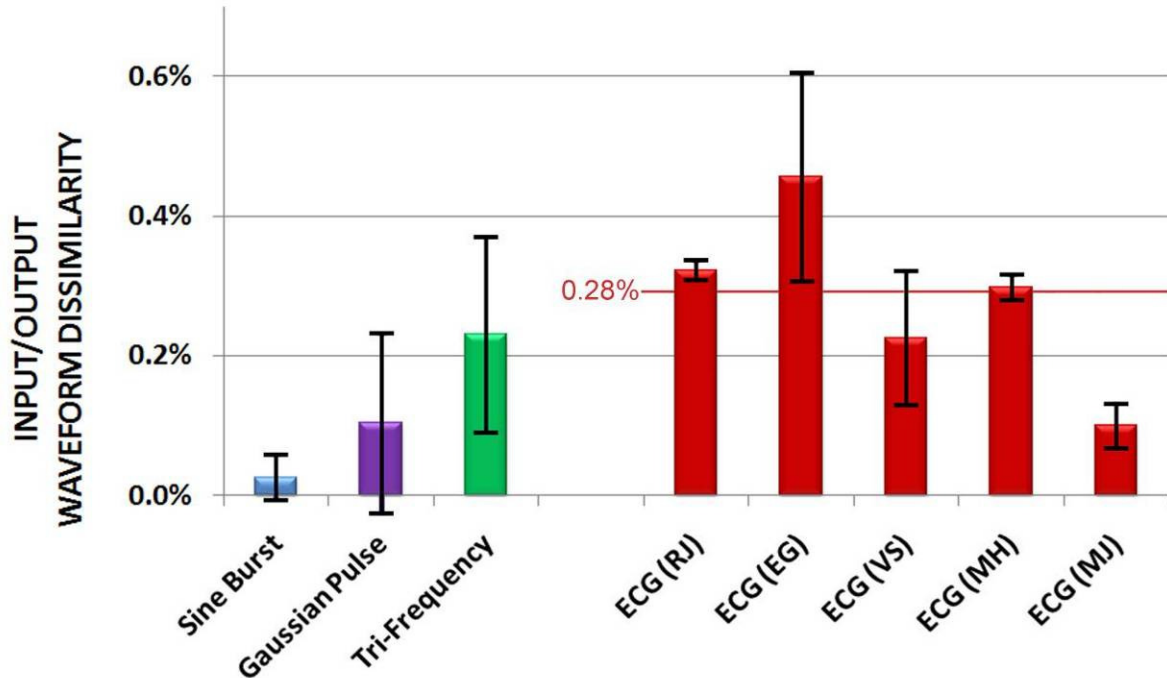
Figure 6.4: Input/output waveform dissimilarity.

In a separate analysis, the input/output correlations were compared to correlations between successive heartbeats in each subject's ECG recording. The mean interbeat correlation over all subjects was 0.986 with a standard deviation of 0.01, whereas the mean circuit model input/output correlation was 0.997, with a standard deviation of less than 0.001 (see Table 5.6). Thus, the variability resulting from the application of ECG signals to the SA circuit model is much less than among successive heartbeats in each subject's ECG recording. Also, the significance level (p) of the difference between each subject's interbeat correlations and the respective SA circuit input/output correlations suggests no additional variability was introduced by the SA circuit model beyond that attributable to each subject's natural beat-to-beat variability.

On the basis of the above results, the null hypotheses of this study are not supported. The SA circuit model provides a signal detection temporal advance of approximately 5 ms with fairly constant gain close to 1.0, with total distortion under 10% and with input/output waveform dissimilarity under 1%.

Example Applications

To date, no published studies have been found in which the ability to temporally advance electrophysiological signals has been demonstrated. The results described here enable a range of possibilities, all of which will require further investigation. Seven potential applications for signal advance technology are described. For some of these applications, it may be five to ten years before the utility will be realized; for others the benefit might well be more immediate. This list is intended to highlight the range of possibilities and is by no means exhaustive.

Electrocardiology

In 2004, there were roughly 2.4 million patients with pacemakers and 460,000 with implantable cardioverter-defibrillators (ICD's). These numbers were expected to increase at an annual rate of 5% and 14-22% respectively [59] to over 3 million and 1 million by 2010.

The earliest pacemakers stimulated at a constant rate without adjusting for varying physiological demands. They could thus potentially pace during a naturally occurring T wave, which could cause tachycardia or fibrillation. Integrated circuits were added to sense atrial/ventricular signals and provide programmable functionality in "demand" type pacemakers. Later improvements, including microprocessor use, allowed for dual-lead placement, sensing and stimulation [61,62]. More recent advances include the development of cardiac resynchronization therapy (CRT) [63-65], implantable cardioverter defibrillators (ICD) [66-68], and improved rate-response (i.e., adaptive) pacing algorithms as well as other improvements related to enhanced pacing [61,62,69]. Recent investigations have focused on the application of pacing technology in the management of cardiac tachycardia and fibrillation [70-74].

Early detection and intervention are crucial as anti-tachycardia therapies are most effective the earlier the delivery following onset [76,77]. Ventricular fibrillation, a critical arrhythmia that can quickly lead to sudden cardiac death, "… begins as a coarse, irregular deflection on the ECG, then degenerates to a fine, irregular pattern, and eventually

becomes asystole. The probability of successful defibrillation decreases as the VF (ventricular fibrillation) waveform becomes smoother with time." [78,79]. However, the detection and discrimination of cardiac arrhythmias in the cardiac signal are often confounded by the overlap of signals from multiple sources which have precipitated the development of numerous detection algorithms attuned to particular types of arrhythmias.

For example, spectral ECG analysis is used to analyze F-waves (superposed on the QRST waveform) to distinguish atrial flutter from atrial fibrillation [80]. In the case of ventricular arrhythmias, early repolarization (which generates the T-wave in a normal sinus rhythm), indicative of ventricular tachycardia overlaps the ST segment of the QRST manifesting as an increased amplitude. [81]. Variations in R-R intervals, indicative of high ventricular rates may overlap supraventricular tachycardia [82].

Discriminating atrial fibrillation/tachycardia that precipitates a rapid ventricular response from true ventricular tachycardia/fibrillation is difficult [82]. A saw-tooth pattern in the ECG, indicating atrial flutter, may overlap with ventricular repolarization, confounding correct diagnosis [83]. Discrimination of ventricular fibrillation from other arrhythmias given the very short time available for intervention to avoid lethal consequences is of particular interest [78,81]. Thus, several detection methods are being investigated that will provide real-time feature extraction/classification to distinguish between supraventricular and ventricular arrhythmias [84-87].

Several of the methods used to reveal these "masked" anomalies include both time-domain and spectrotemporal analysis of ECG's in which several cardiac signals are averaged to reduce signal interference and reveal slight variations in the QRST complex [88,89]. Another method involves subtracting a template QRST complex from the ECG followed by spectral analysis to detect fibrillation waves. [80,91]. Spectral analyses are employed in these methods to distinguish the unique frequency content of various cardiac arrhythmias [92].

The application of SA circuitry to ECG detection and analysis may provide a viable mechanism to temporally advance cardiac waveform detection. However, regarding cardiac pacing (the original target application), ECG detection algorithms require acquisition of at least a few consecutive heartbeats to determine their timing characteristics before initiating

a response [69,71]. As such, the temporally advanced detection of each beat would be of little benefit.

For ICD's, "much of the progress in ICD detection algorithms in the past 15 years has been in the development of supraventricular tachycardia discrimination algorithms to reduce the number of inappropriate therapies delivered by ICDs." [82]. SA technology may provide a mechanism to temporally separate various components of the ECG based on the spectral content by advancing some components while delaying others. The spectral content of normal cardiac rhythms, for which the SA circuit used in this study was designed, contains harmonics up to about 25 Hz [53].

The rapid irregular heart rates associated with atrial fibrillation (and connected with increased risk of heart failure, stroke and death) are typically 350 to 400 beats-per-minute [74] - well under 10 Hz. As such, a longer duration of ECG detection temporal advance (10 ms or more) might be obtained for SA circuitry designed to detect fibrillation waveforms.

Further, supraventricular tachyarrhythmia is typically masked by the much larger amplitude ventricular QRST complex.

Differential SA technology, using multiple spectrally tuned bands of single-stage SA circuits in parallel (Figure 2.7), has the potential to temporally shift overlapping ECG components thereby unmasking the supraventricular tachyarrhythmia waveforms, such as atrial fibrillation, from the QRST complex in real time while avoiding the delays associated with the use of band-stop filter banks.

Hue-Teh Shih, M.D., Director of the Center for Cardiac Arrhythmias, Houston, Texas expressed his expert opinion stating: "Signal Advance technology … can revolutionize the non-pharmacological treatment of cardiac arrhythmias and epilepsy" [60].

Artifact Detection and Correction

The use of SA technology in artifact detection and correction potentially applies to a wide range of electrophysiological signals including electrocardiography (ECG) and

electroencephalography (EEG). For the purpose of this discussion, the focus will be on EEG signals but its application is analogous to other bioelectric signals such as magneto-encephalography (MEG), electromyography (EMG) and tracking of eye movements (electro-oculography – EOG).

Sources of non-brain EEG artifacts include eye blinks/movements (EOG), muscle activity (EMG), cardiac pulses (ECG), AC power (line noise), skin/perspiration, respiration, electrodes and more recently, artifacts induced by functional MRI [93-95]. The spectral content of some of these artifacts (e.g. EOG and line noise) are limited to narrow frequency bands that may not significantly overlap with the EEG signals of interest. In addition, some artifacts (e.g. ECG, EOG) have large amplitudes relative to the EEG or are spatially localized (e.g. EOG) [96,97]. These unique artifact characteristics facilitate artifact removal using band-pass filtering or weighted subtraction of the artifact from the EEG signals using various statistical regression techniques [96-102].

Functional magnetic resonance imaging (fMRI) artifacts, including ballisto-cardiac and large gradient artifacts, have proven to be more challenging given the unique environment of high magnetic field MRI [103-107]. Myogenic artifacts (e.g. EMG) contain spectral content that overlaps with that of the EEG making EMG detection and removal more difficult [96-98].

The strategies employed to separate these overlapping signals involve different types of multivariate analyses for wave or source separation (often referred to as blind source separation [108]) to automatically remove non-brain electromagnetic signals that are assumed to be linearly superimposed on the actual brain signals. The methods used to separate and classify relevant features from detected signals include such methods as principal components analysis [94,105-107], independent components analysis [93,97,99,101,109], maximum signal fraction [94], canonical correlation [94,102,111,112], time-frequency representations [99,109,113,114], factor analyses [115], neural networks [116,117], support vector machines [118,119], method of delays [94,120], and others. A number of these analyses operate in the frequency domain on narrow spectral bands as "…some EEG artifacts … are more easily identifiable in the frequency domain" [97,110,121-125]. Performance improvements have been demonstrated through the use of various combinations of these techniques [94,104,106].

Beyond automated artifact correction, there is a need for online (real time) artifact correction for use in responsive applications such as neurofeedback/neurotherapy, brain-computer/neural interfaces, seizure warning/suppression systems and electrocardiology applications. Thus, much of the current research focus is on reducing the computational load of these techniques in order to shorten the processing time [94,97,101,102,104,105, 108-110,120,124,125].

While discussion of these artifact correction techniques is well beyond the scope of the present study, the following observations are consistent with potential SA applications:

1. Artifacts overlap or mask the true bioelectric signal requiring separation.
2. A number of these analyses operate in the frequency domain over narrow spectral bands.
3. Much of the current research focus is on reducing the computational load of these techniques in order to reduce processing time.

For online real-time applications, temporally advanced signal detection could potentially offset signal processing delays. Further, SA technology using multiple spectrally tuned bands of single-stage SA circuits in parallel (see Figure 2.7), has the potential to temporally shift overlapping signal components (artifacts/noise) differentially to allow unmasking of bioelectric signal components of interest, which would, facilitate artifact detection/correction.

Epileptic Seizure Detection/Suppression

It is estimated that epilepsy affects roughly 1% of the U.S. population or over 3 million individuals. Of those affected, 25% (about 750,000 people) do not respond well to drug therapy, thus suffering disabling side effects [126]. Alternatives to long-term pharmaceutical treatment strategies are therefore needed.

Studies of the pathophysiology of seizures have provided a number of operational theories. A recent study using the WAG/Rij strain of rats, a validated animal model for absence seizures [127] in which the location of the seizure onset is well defined, provides

strong evidence that the seizure activity begins focally and takes approximately 500 ms to become generalized [128]. These findings support the speculation that rapid detection of initial seizure onset at this central focus could facilitate intervention.

Epileptiform signals are distinguishable from normal EEG signals based on their wave-shapes. Signals indicative of epileptiform activity include impulses called spikes (20 to 70 ms) and sharp waves (70 to 200 ms) which are twice the amplitude of background activity, and slow waves (low frequency, amplitude > 100 µV, duration: > 200 ms). In addition, various high frequency oscillations have been associated with localized epileptogenic pathologies.

A number of these characteristic indicators of epileptiform activity can be detected in the EEG prior to clinical manifestation. Much like the detection of artifacts, considerable progress has been made not only in the automated detection of such activity in the EEG but also the development of closed-loop "on-demand" seizure therapies with first-generation, "intelligent" seizure-treatment devices in clinical trials [129]. These therapies are highly dependent on the performance of automatic seizure detection algorithms to distinguish epileptiform activity in order to control the delivery of an appropriate therapy.

These algorithms have been developed using combinations of methodologies based on spatiotemporal and spectral analyses, artificial neural networks, morphological filters to extract specific EEG waveform features (both linear and nonlinear), wavelet analyses, as well as chaos and fractal analyses [130-137]. Furthermore, a number of the methodologies demonstrated improved performance when more individualized or patient specific approaches were employed [138-141]. Several algorithms have yielded excellent results with regard to sensitivity and specificity but have detection rates ranging from 30 seconds to fewer than 2 seconds. While these detection delays are significant, a number of these methods are still considered predictive since seizure detection in the EEG typically precedes clinical manifestation.

The performance features that are most critical to success in this area of research include high sensitivity, high specificity, and rapid or early detection [142-147]. Earlier seizure detection of (and response to) initiation of paroxysmal oscillations is believed to

enhance intervention efficacy providing a rationale for investigating the applicability of SA technology to improve detection performance.

Neurofeedback

In EEG biofeedback or neurofeedback, an individual's brainwaves are detected and displayed in some manner to provide feedback regarding the brain activity. Typically, the time domain EEG signals are then divided into spectral bands either by applying a fast Fourier transform (FFT) or by using a bank of narrow band filters. The traditional frequency bands are termed delta (1 to 4 Hz), theta (4 to 8 Hz), alpha (8 to 13 Hz), beta (13 to 38 Hz) [148] and gamma (38 to 42 Hz). The reported upper beta boundary and gamma range boundaries vary among investigators [149-151].

Brain activity at various frequencies correlates with various states of awareness, arousal, attention, relaxation, etc. For example an individual who is drowsy may exhibit increased delta activity, and inattention/day-dreaming is associated with increased theta. Calm, relaxed wakefulness (with eyes closed) is typically associated with alpha whereas EEG activity in the 16-20 Hz range of beta is related to thinking/problem solving. Excessive beta activity however, is associated with anxiety or stress [148,149].

It is speculated that gamma activity is associated with integrating neural signal activity from disparate brain regions (in the late 70's and 80's much research was done on 40 Hz brain rhythms associated with a state of "focused arousal"). Beyond the correlations between frequency and behavioral/clinical symptoms, there are also spatial correlations. In other words, anomalous signals from specific brain regions are also associated with particular clinical behaviors or manifestations [152,154].

In addition to oscillations in various frequency bands, there are other EEG components indicative of specific brain activities that are targeted by various neural training protocols. These patterns include slow cortical potentials (SCPs) related to increasing attention/focus and mental preparation, and event related potentials (ERPs) indicative of developmental effects [149,151].

Spectral EEG abnormalities are considered either hypo- or hyper-functional or both depending on the frequency and associated brain regions involved. For example, patients with attention deficit disorder (ADD) and attention deficit with hyperactivity (ADHD) tend to exhibit higher than normal levels of slow wave activity (theta) in the pre-frontal and frontal regions of the brain as well as reduced alpha/beta levels [149,151,153,155]. These individuals have difficulty with impulsive behavior, attention, emotions, concentration and memory [155,156]. Significant improvements in these areas have been achieved through the use of neurofeedback training to assist the subject in shifting brain wave activity to a more normal pattern (e.g., reducing the slow wave activity and increasing alpha/beta activity) [157-161].

While the application of neurofeedback to ADD/ADHD has been the most extensively studied, a partial list of other clinical applications includes epilepsy [162-165], recovery from brain injury/stroke [166-169], alcoholism [170-172], drug abuse [173-176], post-traumatic stress, anxiety, sleep and obsessive compulsive disorder [187-189], depression [148,153,179,180], chronic fatigue syndrome, fibromyalgia [148], headaches/pain [181-184], autism [148,185,186], various tremors, cerebral palsy [148,187] dyslexia [188,189] and learning disabilities (mental retardation) [190]. In addition, neurofeedback has been reported to enhance memory and cognitive functioning [191-194] as well as improved creative/athletic performance [195-201].

Most investigators describe neurofeedback training as a form of operant conditioning [149,151,152,162,166,202-205]. When desirable changes in brain activity are obtained, a positive reward is provided, whereas undesirable changes result in either a negative reward or the positive reward is withheld - usually under the guidance of a neurotherapist or trainer [206]. It is this feedback and associated rewards or reinforcements that provide the mechanism by which the individual learns to change his/her brain waves.

Advances in electronics and signal processing technology continue to improve the performance of neurofeedback systems thus reducing the inherent delay in them between brain wave detection and feedback presentation. A number of studies investigating the effects of delayed feedback on operant conditioning have concluded that increased feedback delay has a negative effect on learning [207-211]. It is believed that "Unless the (feedback) signal, like other biological signals is almost instantaneous, there is a risk it will

not be effective. …delayed feedback is unlikely to be effective when trying to facilitate change." [209].

Another author/investigator made the following statement "…delay in feedback complicates the learning process" [211]. In a personal communication, Harold L Russell, Ph.D., an experienced clinical neurotherapist and neuropsychologist/researcher offered his view that Signal Advance technology could significantly improve the precision of timing of neurofeedback stimulation thereby improving treatment efficacy, and may significantly decrease the total amount of treatment time required [212]. In short, reducing the delay between EEG signal acquisitions and feeding the processed signals back to the subject holds promise of significantly improving training speed and efficacy.

Brain-Computer/Neural Interfaces

There is great interest in the restoration and enhancement of human motor and sensory functions by interfacing prosthetic devices of various types with the nervous system. This broad research area includes both neuromuscular stimulation (e.g. functional electrical stimulation in which peripheral nerves or muscles are stimulated to approximate normal movement in paralyzed limbs) and neural signal detection (peripheral or central) [213]. Neuroprostheses are artificial replacements for missing body parts or functions that are interfaced to and controlled by the nervous system, or by signals from muscles through neural interfaces. These interfaces could also be used to control exoskeletal systems or tele-robots and may involve bi-directional communication using both detection and stimulation electrodes for closed-loop feedback control [213-215].

The electrodes used in prosthetic interfaces to detect signals from the peripheral and central nervous system as well as the signals from muscles may be invasive or non-invasive [213,216-218]. Non-invasive scalp electrodes are used to record EEGs whereas invasive electrodes could be placed directly upon the cortical surface for electrocorticography (ECoG) to acquire the local neuronal field potentials, or directly into the neurons to record single unit activity [214,217,219,220]. For peripheral interfaces, skin surface electrodes are used to stimulate or detect signals from peripheral nerves (ENG) or

muscles (EMG) in which both used to estimate various movement parameters such as force or torque [213,221].

Invasive muscle electrodes include both epimysial and intramuscular types. Invasive peripheral nerve electrodes include a variety of extraneural or intraneural electrodes [213]. Generally, the more invasive the sensor, the more specific is the measured signal content [213,214,216,217]. Generation of stimulation signals to activate paralyzed limbs is of similar complexity. For the purpose of the present study, the balance of the discussion will focus on signal detection.

Regardless of the type of sensor used or signal detected, the overall goal is to derive from the detected signals the subject's intent with regard to a control output. A number of processing steps are required to translate the detected biosignals into control signals [213,220,222-224]. The required signal processing is the same as described in previous sections discussing artifact correction, neurofeedback and seizure detection. The first step, signal pre-processing, includes signal amplification and anti-alias filtering. Subsequent processing steps include artifact correction, temporal/spectral/spatial filtering and improvement of the signal-to-noise ratio of the detected signal.

A further step is feature extraction, the process of separating a signal with specific characteristics (or features) from all of the other informational subsets of data, followed by feature reduction/classification to determine which features represent or predict the subject's actual intent [225-227]. Post-processing may then be applied to reduce prediction errors, followed by the translation of classified predictors into output signals that are used to control devices such as artificial limbs or computer cursors thus providing feedback completing the control loop [214,215,220,222].

Much of the current research targets performance improvement of algorithms used for feature extraction/classification in terms of accuracy and computational efficiency [216,226-228]. A number of the methods employed with non-invasive electrodes report average latencies or response times in the range of 200-400 ms [218, 229-231]. Response improvements in the last ten years are reflected in the reduction in the average time required to move a computer cursor across the screen and press a button (BCI system

using scalp electrodes) from 16 s reported in the year 2000 [232] to 2.4 s in 2006 [233] compared to an average response time for normal control using a mouse of just over 1 s.

This example reflects only one-dimensional control (left-right), whereas multiple dimensions of control will be required to mimic natural limb movement [220]. The use of invasive electrodes to detect cortical motor activity increased the communication rate to 6.5 bps (or approximately 150 ms) by 2006 [234]. A recent press release (RIKEN, June 29, 2009) entitled "Real-time control of wheelchairs with brain waves" reports one of the fastest closed loop response times: "commands for smooth left and right turns and forward motion of the wheelchair are processed every 125 milliseconds."

The overall problem with response time of neuroprosthetics is captured in the following excerpt from an Associated Press article (July 2007), entitled "War Fuels Prosthetics Research Blitz":

> The myoelectric Utah Arm, made by Motion Control Inc., of Salt Lake City, has circuitry that reads muscle twitches as electric signals to open and close a hook or hand attachment. But its response time, even at less than a second, is so slow that Salzman prefers an old-fashioned, "body-powered" prosthesis, controlled by a cable and rubber bands. … I don't like having to wait if I want to grab something. (Saltzman stated in discussing his neuroprosthetic arm).

Furthermore, learning to use any prosthetic system requires the same operant conditioning process used in neurofeedback. Response delays (i.e. delayed feedback) have a negative impact upon learning to use these devices, especially when there is a significant difference between normal biological response time and that of the prosthetic device.

While processing speed of electronic devices will continue to improve, increasingly sophisticated prostheses will demand increased computational efficiency. Until prosthetic response times are equivalent to biological response times, widespread acceptance and use of neuroprostheses will be hindered. On the other hand, offsetting these delays will increase and facilitate the adoption and widespread use of prosthetics by permitting faster

processing of neural signals of increasing dimensions to control ever more complex prostheses. Performance increases in the speed of signal detection, analysis and transmission could be incremental in the development of more sophisticated neuro-prosthetic devices potentially enabling higher dimensional levels of control.

The performance improvement over the last decade in the acquisition, detection and processing of these signals for use in neuroprosthetics has been over five-fold. By projecting another five-fold performance increase over the next decade, one might speculate that a significant number of practical applications of signal advance technology could emerge during this period.

Medical Imaging

In medical imaging, such as CT or MRI, motion is one of the most common causes of image artifact, degrading the quality of the acquired images. The prevention of motion artifact results in improved image quality and increased diagnostic utility. These artifacts result from voluntary motion such as overall body movement, and involuntary motion including the beating heart and breathing, as well as vascular pulsation from blood and cerebral spinal fluid flow.

In MRI and CT, the images are created by combining a number of repeated image sequences. Respiratory and cardiac cycles are periodic, thus the changes in anatomical positions of organs are cyclical. For example, the heart expands and contracts during each cardiac cycle. For a number of imaging procedures, in order to avoid motion artifacts due to heart movement, each image sequence must be captured at the same point in the cardiac cycle [235], preferably during a quiescent period when there is minimal movement. An example of such a quiescent period is diastole, when the heart is passively filling with blood [236,237]. The situation is analogous to the respiratory cycle in which organs move during each breath [236,238], when one would like to acquire data during a quiescent period at the end of expiration [239,240].

In order to synchronize successive scans, a trigger is used to initiate the scan at the correct time – referred to as gated imaging. For cardiac imaging the trigger signal is

typically based on the QRS portion of the cardiac rhythm given its easily distinguishable peak [241,242]. However, the ECG signal is often distorted due to artifacts from the imaging equipment. In the MRI environment, sources of artifact include radio-frequency interference, magnetohydrodynamic and/or gradient effects [235,241,243]. Artifact removal may require preprocessing steps, such as digital low-pass filtering (with a frequency cut-off of 25 Hz), or more sophisticated artifact correction/removal (as described previously) to be applied to the ECG, further delaying its use [241,243].

In addition, typical jitter in the ECG trigger is about 10-15 ms [243]. These delays could adversely affect image quality, especially in the case of rapid heartbeats when the quiescent period is shortened. In the case of irregular heartbeats or breathing, these trigger signals also indicate early movement and thus could prompt termination of the scan sequence to minimize unnecessary patient exposure and unusable image sequences given the greater probability of motion artifact [236].

Temporally advanced detection of these trigger signals could potentially improve image quality by reducing the time required for image acquisition, thus improving temporal resolution. Furthermore, earlier detection of movements may allow sufficient time to interrupt imaging sequences likely to contain motion artifact due to irregular cardiac or respiratory rhythms.

Radiation Therapy

The goal of radiation therapy is the delivery of radiation doses to a specific target (e.g., tumor) while avoiding the irradiation of normal tissue. This is accomplished by targeting the treatment areas from several different angles to minimize normal tissue exposure and concentrating the radiation delivery at the intersection of the various delivery trajectories. Achieving this goal is particularly challenging when the target is mobile, its position constantly changing due to cardiac and respiratory movement. Respiration can change the location of thoracic and abdominal tumors as much as 3 cm during treatment [244]. This movement clearly results in reduced treatment efficacy and increased irradiation of normal tissue [245].

Gated radiotherapy operates in a manner analogous to gated imaging, using external triggers to limit irradiation to periods when the tumor is in a specific target position, thereby reducing exposure of normal tissue [246,247]. The triggers are obtained by tracking the position of markers. These markers are either internal (implanted radio-opaque gold markers at or very near to the tumor) [244,246,248], or external (markers placed on the skin surface where their movements approximate the tumor movements) and may be used in combination [245]. Gated radiotherapy may, in addition, use respiratory gating to restrict treatment to the period of the respiratory cycle corresponding to the proper target position [240, 245,249-251].

By gating radiotherapy, smaller target volumes can be used and normal tissue toxicity can be reduced [240,245,248,251]. However, despite position tracking, there are response delays in these gating systems. For example, The Varian linac-based gating system has a response delay of 170 ms [252]. The following excerpt [246] underscores this response delay issue:

If the marker moves at a speed less than 9 mm/s, compensation for the delay between movement recognition and irradiation is not required; at higher speeds the discrepancy between the planned and actually irradiated spots exceeds 1 mm due to the time delay. This time delay is not specific to our system but rather a general problem in gated systems.

"The time delay between recognition of the marker position and the start or stop of megavoltage x-ray irradiation was 0.03 seconds. … precise and real-time target localization is crucial for gated treatment." [245].

In this application, temporally advanced signal detection could potentially improve performance by providing earlier detection of changes in the position of the radiation target thereby increasing treatment effectiveness while possibly reducing the negative side effects associated with irradiation of normal tissue.

Applications Summary

Some potential applications described include real-time artifact detection/correction, neural pacing/seizure suppression, neurofeedback/neurotherapy, brain-computer/neural interfaces and electrocardiology. Furthermore, SA technology could enhance the performance of physiologically gated diagnostic and therapeutic applications such as imaging and radiotherapy in which temporally advanced triggering could significantly improve performance in the near-term. For each of these applications, reducing response time and/or temporally separating overlapping signals could yield significant improvements in overall system performance. This may allow for more effective treatment of certain pathologies potentially opening the door to a whole new class of medical devices that respond faster than any currently available.

In general, SA technology could be applied to temporally advance 1) narrowband signals to offset delays associated with filtering, and/or 2) broadband signals (offsetting overall signal processing delays). In addition, differential SA technology using multiple spectrally tuned bands of SA circuits might be used to temporally separate overlapping signal components facilitating masked signal component separation/detection in responsive systems.

For any potential application, the signal characteristics of interest and the application requirements determine the SA circuit design-performance criteria. For example, in the case of ECG's, in implantable cardioverter/defibrillators (ICDs), the frequency range of interest is between approximately 10 and 40 Hz (the wave shape is also important regarding the feature extraction characteristics). Thus the SA circuit would be designed to provide a constant advance and gain beyond 40 Hz. Contrast this (ICD) application with ECG-gated imaging or radiation therapy in which the only requirement is the detection of the QRS peak. As such, the wave shape is not nearly as important. Some amount of signal distortion may be acceptable in order to increase the peak detection advance.

Respiration rates are typically under 60 breaths per minute (frequency rate: 1 Hz). Lung or other organ movement as a result of respiration would present a similar movement

cycle as that of the respiratory cycle. To temporally advance respiratory related signals, SA circuitry would need to be developed to advance the detection by over 500 ms. In respiratory-gated radiation therapy, SA circuitry designed for such lower cycle rates could provide a much earlier trigger to terminate irradiation due to irregular or unanticipated movement, helping to minimize damage to normal tissue.

Some electrocorticographic (ECoG) recording studies (from electrodes placed on the cortex) indicate activity of interest at around 40 Hz, whereas others target activity in the 70-150 Hz range. Thus for any ECoG application, an SA circuit would be designed accordingly, with higher frequency requirements imposing greater single stage and overall cascaded detection advance limitations as discussed previously (Chapter II, Circuit Cascading).

In neuroprosthetics, electroneurograms (ENGs) are often sampled up to 10 kHz. However, the force transients required for functional neuromuscular stimulation vary between 0 and 50 Hz. Thus SA circuitry designed to advance the detection of these force transients could be designed for the lower spectral range.

In neurofeedback, a number of systems operate on signals with spectral content from the delta to the beta range (0.5 to 30Hz), others through the gamma range and higher (typically up to about 100 Hz). For an application limited to the beta range, an SA circuit design similar to that described in this study might suffice.

In essence, the SA circuitry must be designed for the specific application and there will be trade-offs between the detection advance that may be achieved, the minimum spectral range required, and the amount of signal distortion that can be tolerated. For SA technology to be of practical use in electrophysiological applications, the overall temporal advance achieved must provide a significant offset to signal processing delay or provide a usable temporal shift for separating masked or overlapping signal components based on spectral content. For near-term applications, the temporally advanced output signal should be a high fidelity representation of the input signal in order to take advantage of detection, feature extraction and other signal processing methodologies.

Significant Improvements in SA technology performance could be accomplished by 1) cascading multiple SA circuit stages to increase the overall temporal advance achieved, 2) applying pre- and post-conditioning to reduce/eliminate signal distortion and 3) arranging parallel arrays of narrowband SA circuit cascades to meet specific spectrotemporal requirements.

Investigation Limitations

This study demonstrated the performance of a circuit model rather than an actual physical circuit. While circuit modeling is common practice in electronics development, ultimately the physical circuit must be built and tested. The SA circuit model is prone to oscillations given the resonant nature of the poles and thus is sensitive to noise in their spectral vicinity. Based on the experience obtained in constructing earlier circuits, actual SA circuit construction requires experience and attention to strategic circuit board layout, noise suppression and shielding. While the SA circuit model performed as anticipated, further refinement and testing is likely required. These revisions could include changes in the design frequency range, cascading of multiple SA circuit stages, addition of pre- and post signal conditioning stages, and expansion from a two-pole design to three or more poles to improve circuit response characteristics.

The present study focused on requirements specific to ECG signals. Other types of electrophysiological signals will certainly present different performance requirements. In terms of the study itself, additional testing should be performed to address study limitations. For example, the tri-frequency testing could be expanded to include frequencies beyond the circuit model pole frequencies. The ECG signals used were not initially low-pass filtered and thus they contained noise not normally found in clinical recordings. The additional study of low-pass and 60 Hz notch filtered ECG signals, representative of those obtained clinically, should be carried out. The effect of varying noise content could also be investigated.

The focus of this study was the effect of signal advance on individual ECG heartbeats. However, most practical clinical applications will require studies using

continuous ECG signals. Temporally advanced continuous ECG recordings could be reviewed by electrocardiologists experienced in the interpretation of ECGs to test whether or not temporal advancement of the ECG adversely affects clinical interpretation. For other types of electrophysiological signals, there is an analogous list of research possibilities.

Future Research

The goal of the present study is to demonstrate the ability of the SA circuit model to temporally advance the detection of the ECG. The following list of potential experiments (in no particular order) could build on and expand the results obtained in this study.

1. Extend the spectral range of constructed test signals - in particular, sine burst and tri-frequency signals from 25 Hz to 150 Hz to include both poles of the SA circuit model. In this way, the circuit response characteristics may be more explicitly determined across a range that includes the circuit pole frequencies.

2. Test ECG signals, typical of those obtained clinically, which have first been low-pass filtered at a frequency threshold below the first pole location, and notch (60 Hz) filtered to minimize the effect of the mains frequency. Test both single heartbeat segments as well as continuous ECG recordings.

3. Test the impact of varying levels of random noise on SA circuit model performance. In addition, vary the spectral content of the noise to characterize the relationship between the noise effects relative to frequency.

4. Develop a series of SA circuit models designed for frequency ranges above 25 Hz (e.g. 30, 40, 50 Hz, etc.) to compare/contrast changes in SA circuit response.

5. Develop an SA circuit model using more than two poles to potentially improve the duration and constancy of the signal detection temporal advance obtained.

6. Investigate the effect of shifting SA circuit model poles to change the frequencies at which the circuit resonates while maintaining a constant temporal advance with minimal additional distortion.

7. Use the temporally advanced detection of a specific component of an analog waveform to produce a trigger pulse or signal within the duration of the advance obtained, demonstrating the ability to generate an interventional signal based on the advanced detection of a specific component of an analog waveform.

8. Study the effects of SA detection on the clinical interpretation of ECG recordings. Temporally advance ECG recordings taken from multiple patient populations (e.g. normal, tachycardia and arrhythmia). The original and advanced waveforms would be randomly ordered. Experienced electrocardiographers would review all the waveforms (both original and temporally advanced) and categorize them as normal or as indicative of tachycardia or arrhythmia. *Kappa*, a measure of interclass correlation, would be used to determine the agreement between the original and temporally advanced ECG recording categorizations for each interpreter.

9. Develop and test a cascaded SA circuit model and investigate effects of cascading in terms of increased temporal advance, changes in gain and output distortion. The cascaded SA circuit model should be tested with both constructed test signals, and electrophysiological recordings.

10. Develop and test a parallel SA circuit array designed to temporally advance the detection of particular narrow spectral ranges. This could potentially be used in conjunction with a parallel filter bank to reduce delays in a responsive system. Configure different parallel paths to impart varying delays/advances over certain spectral ranges to demonstrate temporal separation of waveform components based on their spectral content.

11. Develop pre- (analog) and post- (analog or digital) filtering/signal conditioning circuit models using high-speed electronics with response times significantly less than the temporal advance obtained, to minimize or eliminate altogether high frequency output distortions. Test the filter stage response to confirm that the added delays are significantly less than the temporal advance achieved in order to be of utility (possibly even an order of magnitude or two less).

12. Build the actual physical circuitry to test its performance. Due to the oscillatory nature of the circuit, in particular to spectral content approaching the poles, this will likely require shielding and particular attention to the layout and placement of circuit traces to avoid artifacts.

13. Adapt the SA circuit model for use in other electrophysiological applications having different waveform/spectral characteristics, such as those related to the EEG for epileptic seizure detection, neurotherapeutic and/or neuroprosthetic applications.

Appendix A
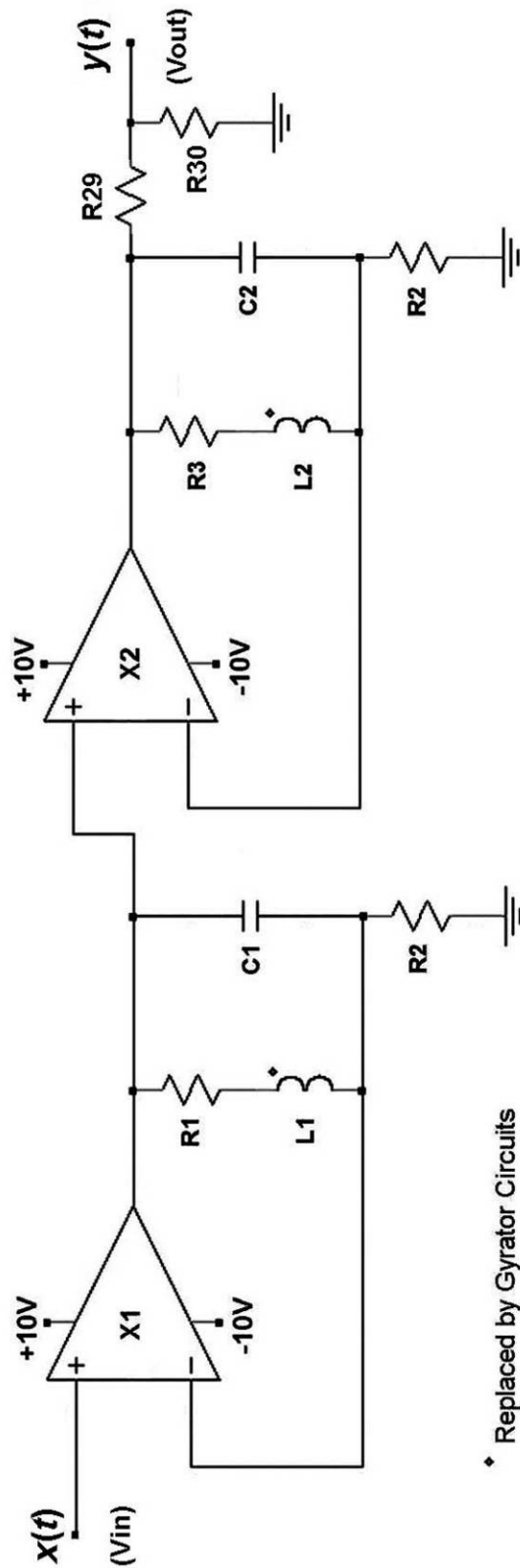
Figure A.1: Generic SA circuit model schematic.
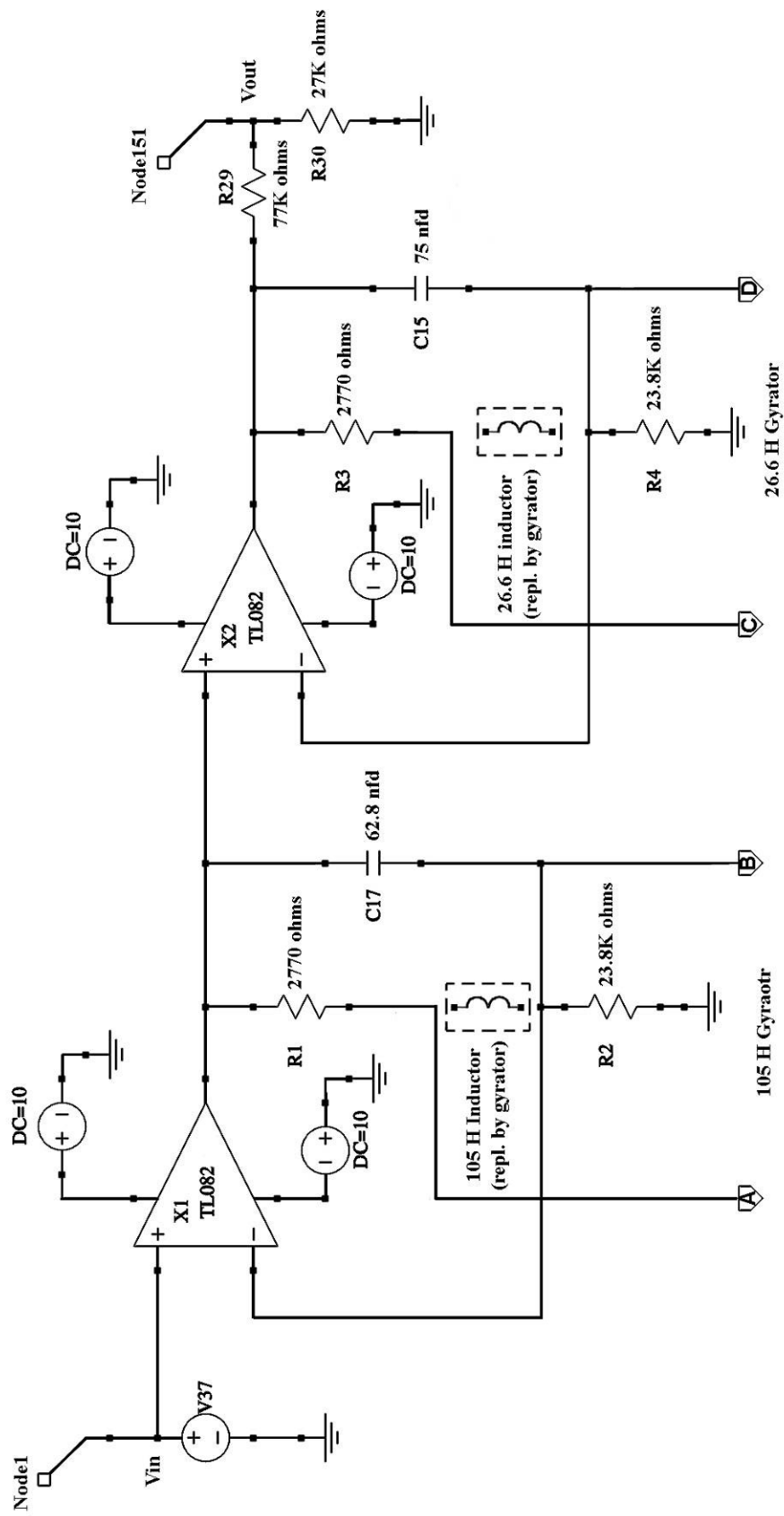
Figure A.2: SPICE 25 Hz SA circuit model schematic (1 of 3).

111
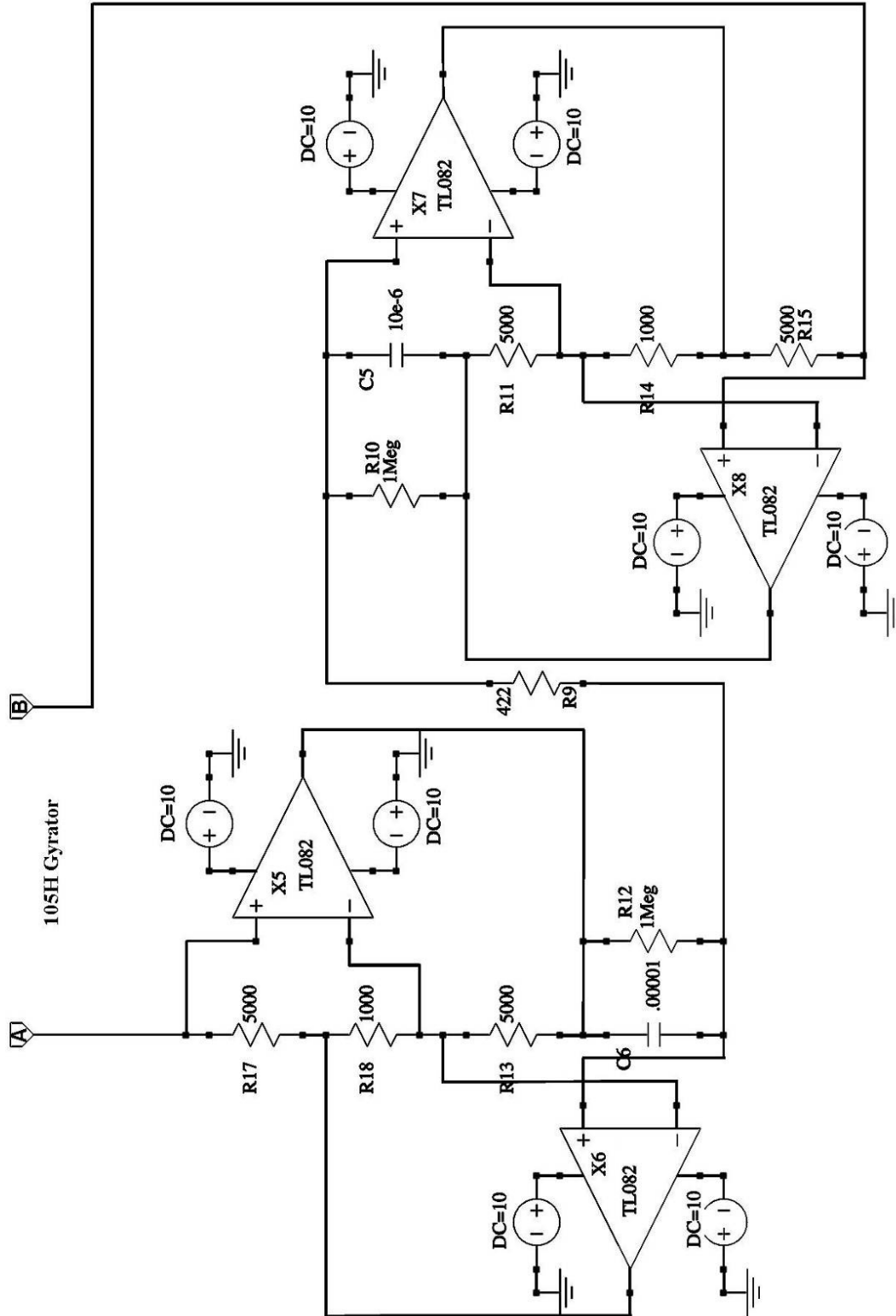
Figure A.3: SPICE 25Hz SA circuit model schematic - 105H gyrator circuit (2 of 3).
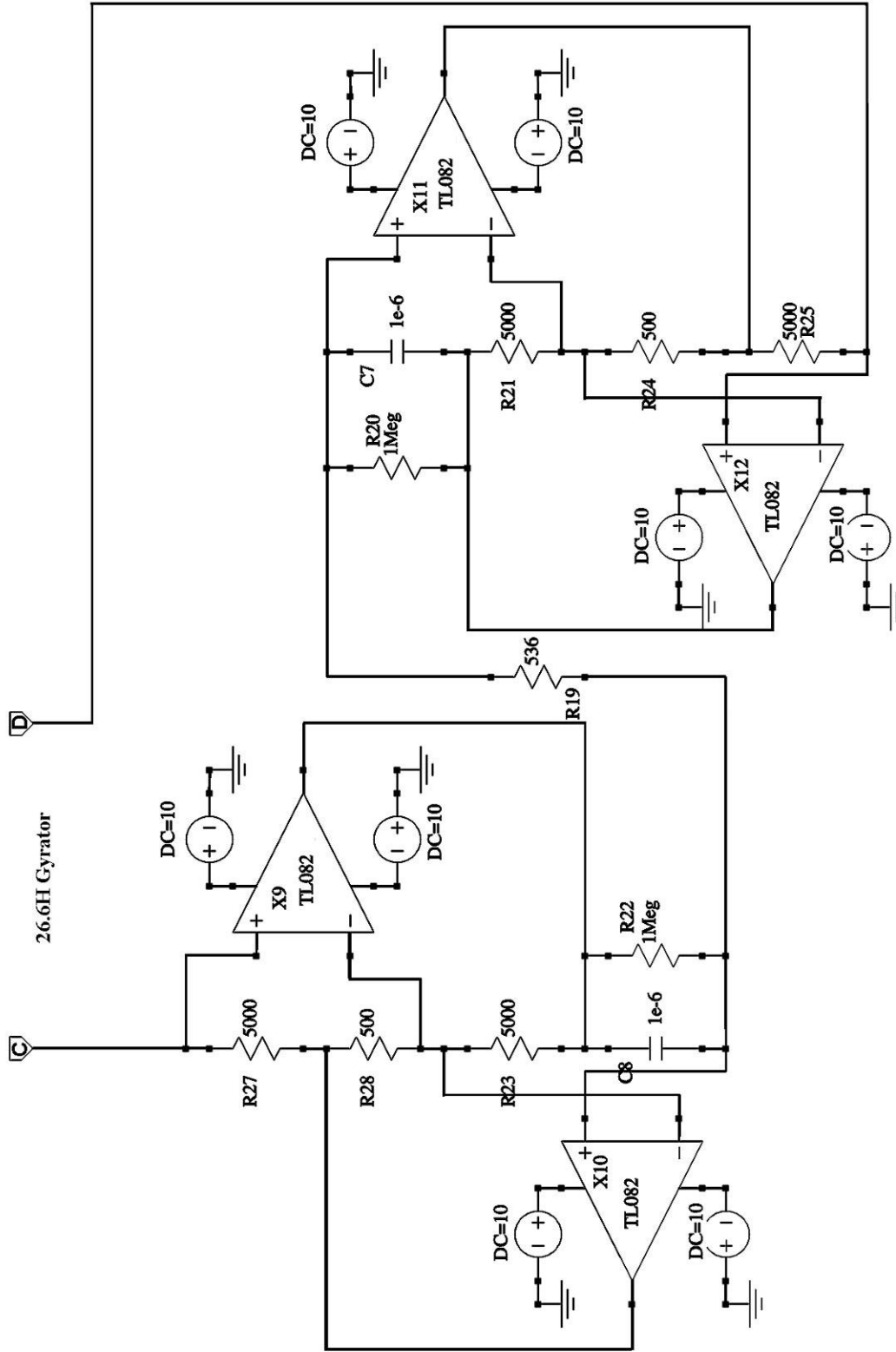
Figure A.4: SPICE 25Hz SA circuit model schematic - 26.6H gyrator circuit (3 of 3).

SPICE command sequences, net lists, libraries, etc.

AC Analysis:

```
*** N:\Res\SPICE\AC Analysis\AC-AnalysisModels.lib ***

*** Spice Control Statements Start ***

.OPTIONS TEMP=27
.OPTIONS ITL1=5K
.OPTIONS ITL2=5K
.OPTIONS ITL4=500
.OPTIONS GMIN=10p
.OPTIONS GMINSTEPS=2K
.OPTIONS SRCSTEPS=5K
.OPTIONS floatdata=1
.AC DEC 200 100m 200

*** Spice Control Statements End ***

.SUBCKT TL082/301/TI_XN _ssi_pin0 _ssi_pin1 _ssi_pin2 _ssi_pin3 _ssi_pin4
* _SS_Symbol [C:\Program
Files\AnaSoft\SuperSpice\System\AmpsAndBuffers.ssm] [OpAmp5Pin]
V_ssi_pin4 _ssi_pin4  5 0
V_ssi_pin3 _ssi_pin3  4 0
V_ssi_pin2 _ssi_pin2  3 0
V_ssi_pin1 _ssi_pin1  2 0
V_ssi_pin0 _ssi_pin0  1 0
*
*
C1   11 12 3.498E-12
C2    6  7 15.00E-12
DC    5 53 DX
DE   54  5 DX
DLP  90 91 DX
DLN  92 90 DX
DP    4  3 DX
EGND 99  0 POLY(2) (3,0) (4,0) 0 .5 .5
FB    7 99 POLY(5) VB VC VE VLP VLN 0 4.715E6 -5E6 5E6 5E6 -5E6
GA    6  0 11 12 282.8E-6
GCM   0  6 10 99 8.942E-9
ISS   3 10 DC 195.0E-6
HLIM 90  0 VLIM 1K
J1   11  2 10 JX
J2   12  1 10 JX
R2    6  9 100.0E3
RD1   4 11 3.536E3
RD2   4 12 3.536E3
RO1   8  5 150
RO2   7 99 150
RP    3  4 2.143E3
RSS  10 99 1.026E6
VB    9  0 DC 0
VC    3 53 DC 2.200
VE   54  4 DC 2.200
```

```
VLIM  7  8 DC 0
VLP  91  0 DC 25
VLN   0 92 DC 25
.MODEL DX D(IS=800.0E-18)
.MODEL JX PJF(IS=15.00E-12 BETA=270.1E-6 VTO=-1)
.ENDS


*** N:\Res\SPICE\AC Analysis\AC-Analysis.sss ***


*** Component Net List Start ***

V37 Node1 0 DC 0 AC 1 PWL
V28 Node24 0 DC 10
V27 0 Node25 DC 10
X12 Node5 Node9 Node24 Node25 Node22 TL082/301/TI_XN
V26 0 Node18 DC 10
V25 Node15 0 DC 10
X11 Node8 Node9 Node15 Node18 Node13 TL082/301/TI_XN
R28 Node12 Node40 500
R27 Node40 Node6 5K
V24 Node42 0 DC 10
V23 0 Node43 DC 10
X10 Node10 Node12 Node42 Node43 Node40 TL082/301/TI_XN
V22 0 Node35 DC 10
V21 Node32 0 DC 10
X9 Node6 Node12 Node32 Node35 Node11 TL082/301/TI_XN
R25 Node5 Node13 5K
R24 Node13 Node9 500
R23 Node11 Node12 5K
C8 Node11 Node10 1u IC=0
R22 Node10 Node11 1Meg
R21 Node9 Node22 5K
C7 Node8 Node22 1u IC=0
R20 Node22 Node8 1Meg
R19 Node10 Node8 536
V20 Node77 0 DC 10
V19 0 Node78 DC 10
X8 Node84 Node62 Node77 Node78 Node4 TL082/301/TI_XN
V18 0 Node71 DC 10
V17 Node68 0 DC 10
X7 Node7 Node62 Node68 Node71 Node66 TL082/301/TI_XN
R18 Node65 Node93 1K
R17 Node93 Node89 5K
V16 Node95 0 DC 10
V15 0 Node96 DC 10
X6 Node63 Node65 Node95 Node96 Node93 TL082/301/TI_XN
V14 0 Node88 DC 10
V13 Node85 0 DC 10
X5 Node89 Node65 Node85 Node88 Node64 TL082/301/TI_XN
R15 Node84 Node66 5K
R14 Node66 Node62 1K
R13 Node64 Node65 5K
C6 Node64 Node63 10u IC=0
R12 Node63 Node64 1Meg
R11 Node62 Node4 5K
```

```
C5 Node7 Node4 10u IC=0
R10 Node4 Node7 1Meg
R9 Node63 Node7 422
V5 Node129 0 DC 10
V4 Node122 0 DC 10
V3 0 Node121 DC 10
V2 0 Node126 DC 10
X2 Node134 Node5 Node122 Node121 Node132 TL082/301/TI_XN
X1 Node1 Node84 Node129 Node126 Node134 TL082/301/TI_XN
R1 Node89 Node134 2.77K
R2 0 Node84 23.8K
R3 Node6 Node132 2.77K
R4 0 Node5 23.8K
C15 Node132 Node5 75n IC=0
C17 Node134 Node84 62.8n IC=0
R30 0 Node151 27K
R29 Node132 Node151 77K


*** Component Net List End ***



*** Spice Library Statements Start ***


*** Spice Library Statements End ***


*** Spice Include Statements Start ***

.INCLUDE N:\Res\SPICE\AC\AC-Analysis.lib
.INCLUDE N:\Res\SPICE\AC\AC-Analysis.lib

*** Spice Include Statements End ***

.SAVE @VP(Node151) @VM(Node151)

.END

.control
set filetype=ascii
.endc
```

Transient Analysis:

*** Spice Control Statements Start ***

```
.OPTIONS TEMP=27
.OPTIONS ITL1=5K
.OPTIONS ITL2=5K
.OPTIONS ITL4=500
.OPTIONS GMIN=10p
.OPTIONS GMINSTEPS=2K
.OPTIONS SRCSTEPS=5K
.OPTIONS floatdata=1
.OP
.TRAN 500u 8 0 500u
.FOUR 1Meg V(Node151)
```

*** Spice Control Statements End ***

```
.SUBCKT TL082/301/TI_XN _ssi_pin0 _ssi_pin1 _ssi_pin2 _ssi_pin3 _ssi_pin4
* _SS_Symbol [C:\Program
Files\AnaSoft\SuperSpice\System\AmpsAndBuffers.ssm] [OpAmp5Pin]
V_ssi_pin4 _ssi_pin4  5 0
V_ssi_pin3 _ssi_pin3  4 0
V_ssi_pin2 _ssi_pin2  3 0
V_ssi_pin1 _ssi_pin1  2 0
V_ssi_pin0 _ssi_pin0  1 0
*
*
C1   11 12 3.498E-12
C2    6  7 15.00E-12
DC    5 53 DX
DE   54  5 DX
DLP  90 91 DX
DLN  92 90 DX
DP    4  3 DX
EGND 99  0 POLY(2) (3,0) (4,0) 0 .5 .5
FB    7 99 POLY(5) VB VC VE VLP VLN 0 4.715E6 -5E6 5E6 5E6 -5E6
GA    6  0 11 12 282.8E-6
GCM   0  6 10 99 8.942E-9
ISS   3 10 DC 195.0E-6
HLIM 90  0 VLIM 1K
J1   11  2 10 JX
J2   12  1 10 JX
R2    6  9 100.0E3
RD1   4 11 3.536E3
RD2   4 12 3.536E3
RO1   8  5 150
RO2   7 99 150
RP    3  4 2.143E3
RSS  10 99 1.026E6
VB    9  0 DC 0
VC    3 53 DC 2.200
VE   54  4 DC 2.200
```

```
VLIM  7  8 DC 0
VLP  91  0 DC 25
VLN   0 92 DC 25
.MODEL DX D(IS=800.0E-18)
.MODEL JX PJF(IS=15.00E-12 BETA=270.1E-6 VTO=-1)
.ENDS




*** N:\Res\SPICE\Trans\Transient.sss ***



*** Component Net List Start ***


V37 Node1 0 DC 0 AC 1 PWL
V28 Node24 0 DC 10
V27 0 Node25 DC 10
X12 Node5 Node9 Node24 Node25 Node22 TL082/301/TI_XN
V26 0 Node18 DC 10
V25 Node15 0 DC 10
X11 Node8 Node9 Node15 Node18 Node13 TL082/301/TI_XN
R28 Node12 Node40 500
R27 Node40 Node6 5K
V24 Node42 0 DC 10
V23 0 Node43 DC 10
X10 Node10 Node12 Node42 Node43 Node40 TL082/301/TI_XN
V22 0 Node35 DC 10
V21 Node32 0 DC 10
X9 Node6 Node12 Node32 Node35 Node11 TL082/301/TI_XN
R25 Node5 Node13 5K
R24 Node13 Node9 500
R23 Node11 Node12 5K
C8 Node11 Node10 1u IC=0
R22 Node10 Node11 1Meg
R21 Node9 Node22 5K
C7 Node8 Node22 1u IC=0
R20 Node22 Node8 1Meg
R19 Node10 Node8 536
V20 Node77 0 DC 10
V19 0 Node78 DC 10
X8 Node84 Node62 Node77 Node78 Node4 TL082/301/TI_XN
V18 0 Node71 DC 10
V17 Node68 0 DC 10
X7 Node7 Node62 Node68 Node71 Node66 TL082/301/TI_XN
R18 Node65 Node93 1K
R17 Node93 Node89 5K
V16 Node95 0 DC 10
V15 0 Node96 DC 10
X6 Node63 Node65 Node95 Node96 Node93 TL082/301/TI_XN
V14 0 Node88 DC 10
V13 Node85 0 DC 10
X5 Node89 Node65 Node85 Node88 Node64 TL082/301/TI_XN
R15 Node84 Node66 5K
R14 Node66 Node62 1K
R13 Node64 Node65 5K
C6 Node64 Node63 10u IC=0
R12 Node63 Node64 1Meg
```

```
R11 Node62 Node4 5K
C5 Node7 Node4 10u IC=0
R10 Node4 Node7 1Meg
R9 Node63 Node7 422
V5 Node129 0 DC 10
V4 Node122 0 DC 10
V3 0 Node121 DC 10
V2 0 Node126 DC 10
X2 Node134 Node5 Node122 Node121 Node132 TL082/301/TI_XN
X1 Node1 Node84 Node129 Node126 Node134 TL082/301/TI_XN
R1 Node89 Node134 2.77K
R2 0 Node84 23.8K
R3 Node6 Node132 2.77K
R4 0 Node5 23.8K
C15 Node132 Node5 75n IC=0
C17 Node134 Node84 62.8n IC=0
R30 0 Node151 27K
R29 Node132 Node151 77K


*** Component Net List End ***



*** Spice Libary Statements Start ***


*** Spice Libary Statements End ***



*** Spice Include  Statements Start ***

.INCLUDE N:\Res\SPICE\Trans\Transient.lib
.INCLUDE N:\Res\SPICE\Trans\TransientModels.lib

*** Spice Include  Statements End ***

.SAVE @VM(Node1) @VM(Node151)

.END

.control
set filetype=ascii
.endc



*** N:\Res\SPICE\Trans\Transient.sss ***

V37 Node1 0 DC 0 AC 1 PWL 0.00000 0.00000
+0.0000E+00 5.1413E-06
+1.0000E-03 5.6609E-06
+2.0000E-03 6.1901E-06
+3.0000E-03 6.7279E-06
+4.0000E-03 7.2734E-06
+5.0000E-03 7.8255E-06
...
```

Table A.1: Gaussian pulse initial test results.

Half Amplitude Equivalent Frequency (Hz)	Pulse Width (sec)	Peak Advance (ms)	Peak Gain
1	0.500	0.004940	0.970583
2	0.250	0.004975	0.971221
3	0.167	0.005005	0.972263
4	0.125	0.004875	0.974110
5	0.100	0.004680	0.976177
6	0.083	0.004990	0.978217
7	0.071	0.004970	0.981271
8	0.063	0.004775	0.985320
9	0.056	0.004995	0.990116
10	0.050	0.004790	0.994224
11	0.045	0.004965	0.999585
12	0.042	0.004855	1.006358
13	0.038	0.004770	1.011762
14	0.036	0.004770	1.017688
15	0.033	0.004865	1.025180
16	0.031	0.004850	1.033448
17	0.029	0.004800	1.041546
18	0.028	0.004765	1.049337
19	0.026	0.004760	1.057243
20	0.025	0.004775	1.065718
21	0.024	0.004795	1.074991
22	0.023	0.004815	1.085097
23	0.022	0.004825	1.095991
24	0.021	0.004760	1.107618
25	0.020	0.004820	1.119921
Mean		**0.004847**	**1.02**
Std Dev		**0.0000924**	**0.0471**
C_v		**1.91%**	**4.60%**

Table A.2: Sine burst initial test results.

Input (Hz)	Peak Advance (ms)	Zero-Crossing Advance (ms)	Peak Gain
1	0.003500	0.004833	0.90573019
2	0.005000	0.004818	0.90685312
3	0.005000	0.004875	0.90868589
4	0.004500	0.004778	0.91126965
5	0.005000	0.004864	0.91461614
6	0.005000	0.004769	0.91949268
7	0.005000	0.005250	0.92360561
8	0.005000	0.004955	0.93255589
9	0.005000	0.004731	0.93593073
10	0.005000	0.004955	0.95037615
11	0.005000	0.004917	0.95012127
12	0.005000	0.004885	0.96094755
13	0.005000	0.004867	0.96068351
14	0.005000	0.004962	0.98226495
15	0.005000	0.004705	0.99436925
16	0.005000	0.004731	1.00776168
17	0.005000	0.005071	1.01553379
18	0.005000	0.004857	1.03967239
19	0.004500	0.004885	1.05527022
20	0.005000	0.004833	1.06191037
21	0.005000	0.004937	1.09271784
22	0.004500	0.004857	1.11502913
23	0.005000	0.005101	1.11942156
24	0.005000	0.004833	1.16181795
25	0.005000	0.004778	1.18681622
Mean	**0.004880**	**0.004882**	**0.996538**
Std Dev	**0.000332**	**0.000123**	**0.085645**
C_v	**6.80%**	**2.53%**	**8.59%**

Appendix B

Table B.1: Triple frequency randomization table.

Range	Freq (Hz)		Selected Frequencies		
		Input Signal	**Low**	**Mid**	**High**
Low:	1				
	2				
	3	1	7	11	25
	4	2	4	13	17
	5	3	2	10	20
	6	4	1	10	18
	7	5	6	9	20
	8	6	1	15	17
		7	5	11	17
Mid:	9	8	3	11	22
	10	9	7	14	21
	11	10	3	14	22
	12	11	5	15	17
	13	12	3	12	21
	14	13	3	16	25
	15	14	8	15	21
	16	15	2	13	19
		16	1	12	21
High:	17	17	5	11	20
	18	18	2	14	22
	19	19	6	11	25
	20	20	5	14	20
	21	21	7	9	22
	22	22	3	16	20
	23	23	4	15	22
	24	24	4	13	23
	25	25	2	15	23

Table B.2: Attenuation factor randomization table.

Random Number	Signal Attenuation Factor		
	Low	Mid	High
5	0.20	0.30	0.45
4	0.30	0.20	0.45
6	0.20	0.45	0.30
6	0.20	0.45	0.30
1	0.45	0.30	0.20
5	0.20	0.30	0.45
2	0.45	0.20	0.30
2	0.45	0.20	0.30
1	0.45	0.30	0.20
1	0.45	0.30	0.20
3	0.30	0.45	0.20
1	0.45	0.30	0.20
3	0.30	0.45	0.20
4	0.30	0.20	0.45
3	0.30	0.45	0.20
5	0.20	0.30	0.45
3	0.30	0.45	0.20
3	0.30	0.45	0.20
3	0.30	0.45	0.20
6	0.20	0.45	0.30
2	0.45	0.20	0.30
2	0.45	0.20	0.30
3	0.30	0.45	0.20
2	0.45	0.20	0.30
6	0.20	0.45	0.30

Table B.3: Gaussian pulse results summary.

Half Ampl. Equiv. Freq.	Pulse Width (s)	Advance (ms)	Correlations Time	Freq.	Gain
1	0.500	4.935	0.999999	0.999999	0.9705
2	0.250	4.940	0.999999	0.999999	0.9708
3	0.167	4.940	0.999998	0.999999	0.9714
4	0.125	4.940	0.999996	0.999999	0.9722
5	0.100	4.940	0.999990	0.999999	0.9732
6	0.083	4.940	0.999980	0.999992	0.9745
7	0.071	4.940	0.999966	0.999979	0.9760
8	0.063	4.940	0.999941	0.999984	0.9779
9	0.056	4.940	0.999893	0.999953	0.9801
10	0.050	4.940	0.999841	0.999938	0.9826
11	0.045	4.940	0.999744	0.999831	0.9855
12	0.042	4.940	0.999680	0.999755	0.9886
13	0.038	4.945	0.999524	0.999646	0.9921
14	0.036	4.935	0.999442	0.999993	0.9959
15	0.033	4.941	0.999327	0.999893	1.0001
16	0.031	4.925	0.999142	0.999824	1.0044
17	0.029	4.930	0.998878	0.999779	1.0088
18	0.028	4.815	0.998956	0.999588	1.0321
19	0.026	4.780	0.998460	0.999985	1.0256
20	0.025	4.835	0.997938	0.999782	1.0246
21	0.024	4.870	0.997471	0.999191	1.0274
22	0.023	4.880	0.997077	0.998636	1.0324
23	0.022	4.875	0.996745	0.995323	1.0384
24	0.021	4.870	0.996348	0.994582	1.0445
25	0.020	4.860	0.995865	0.993435	1.0506
Mean		**4.909**	**0.998968**	**0.9991634**	**1.0000**
Std Dev		**0.0471**	**0.001295**	**0.001824**	**0.0267**
C_v		**0.96%**			**2.67%**

Table B.4: Sine burst results summary.

Input (Hz)	Advance (ms)	Correlations Time	Freq.	Gain
1	4.790	0.998798	1.000000	0.9057
2	4.845	0.999771	1.000000	0.9068
3	4.770	0.999999	0.999999	0.9086
4	4.810	0.999987	0.999990	0.9112
5	4.805	0.999996	0.999990	0.9145
6	4.750	1.000000	0.999980	0.9186
7	4.685	1.000000	0.999965	0.9235
8	4.820	0.999998	0.999942	0.9291
9	4.795	0.999998	0.999913	0.9356
10	4.860	0.999992	0.999877	0.9430
11	4.850	0.999989	0.999837	0.9513
12	4.840	0.999984	0.999795	0.9605
13	4.830	0.999978	0.999758	0.9707
14	4.900	0.999955	0.999731	0.9817
15	4.935	0.999913	0.999721	0.9939
16	4.935	0.999884	0.999736	1.0071
17	4.940	0.999838	0.999774	1.0215
18	4.945	0.999780	0.999831	1.0372
19	4.945	0.999722	0.999894	1.0540
20	4.945	0.999653	0.999946	1.0721
21	4.945	0.999570	0.999967	1.0914
22	4.945	0.999467	0.999938	1.1130
23	4.950	0.999350	0.999849	1.1354
24	4.945	0.999212	0.999702	1.1595
25	4.940	0.999056	0.999514	1.1844
Mean	**4.869**	**0.999756**	**0.999866**	**0.9972**
Std Dev	**0.0077**	**0.000336**	**0.000125**	**0.0866**
C_v	**1.59%**			**8.68%**

Table B.5: Tri-frequency results summary.

	Frequency Components			Advance (sec)	Correlations Time	Freq.	Gain
1	7	11	25	4.940	0.993788	0.993788	1.1050
2	4	13	17	4.945	0.998952	0.998952	1.0051
3	2	10	20	4.940	0.997982	0.997982	0.9933
4	1	10	18	4.940	0.998833	0.998833	0.9823
5	6	9	20	4.940	0.998500	0.998499	0.9597
6	1	15	17	4.945	0.999447	0.999447	1.0172
7	5	11	17	4.940	0.998748	0.998747	0.9675
8	3	11	22	4.945	0.995691	0.995690	0.9935
9	7	14	21	4.940	0.998308	0.998308	0.9780
10	3	14	22	4.945	0.997483	0.997478	0.9740
11	5	15	17	4.940	0.999320	0.999320	0.9934
12	3	12	21	4.940	0.997935	0.997935	0.9647
13	3	16	25	4.940	0.997308	0.997308	1.0189
14	8	15	21	4.945	0.997721	0.997720	1.0561
15	2	13	19	4.940	0.999026	0.999026	0.9814
16	1	12	21	4.945	0.997608	0.997608	1.0545
17	5	11	20	4.940	0.998794	0.998794	0.9731
18	2	14	22	4.940	0.998260	0.998259	0.9958
19	6	11	25	4.940	0.996875	0.996872	0.9845
20	5	14	20	4.945	0.998811	0.998811	1.0151
21	7	9	22	4.940	0.996252	0.996250	0.9977
22	3	16	20	4.945	0.997141	0.997141	0.9897
23	4	15	22	4.940	0.998360	0.998359	1.0044
24	4	13	23	4.945	0.995059	0.995056	1.0023
25	2	15	23	4.945	0.997555	0.997554	1.0377
Mean				**4.942**	**0.997750**	**0.997750**	**1.0018**
Std Dev				**0.002**	**0.001374**	**0.001374**	**0.03316**
C_v				**0.05%**			**3.31%**

Table B.6: Gain as a function of frequency for the tri-frequency signals.

Frequency	Gain
1	0.958
2	0.959
3	0.960
4	0.961
5	0.963
6	0.965
7	0.968
8	0.971
9	0.974
10	0.978
11	0.982
12	0.987
13	0.992
14	0.998
15	1.004
16	1.010
17	1.017
18	1.025
19	1.033
20	1.042
21	1.052
22	1.062
23	1.073
24	1.085
25	1.097
Mean	**1.005**
Std Dev	**0.04322**
C_v	**4.30%**

Table B.7: Distortion ratio (%) for the tri-frequency signals.

	Distortion Ratio	
	Time Domain	**Frequency Domain**
1	0.1574	0.1573
2	0.0464	0.0462
3	0.0638	0.0637
4	0.0512	0.0510
5	0.0672	0.0671
6	0.0379	0.0377
7	0.0591	0.0590
8	0.0928	0.0928
9	0.0617	0.0616
10	0.0748	0.0748
11	0.0375	0.0373
12	0.0724	0.0723
13	0.0766	0.0764
14	0.0894	0.0893
15	0.0476	0.0475
16	0.0897	0.0895
17	0.0555	0.0554
18	0.0591	0.0590
19	0.0800	0.0800
20	0.0516	0.0514
21	0.0866	0.0865
22	0.0760	0.0759
23	0.0577	0.0576
24	0.0996	0.0996
25	0.0807	0.0806
Mean	**0.0709**	**0.0708**
Std Dev	**0.02495**	**0.02497**

Appendix C:

Table C.1: ECG individual subject temporal advance/gain results (subject RJ).

	Advance (sec)		Correlations Time (max)	Frequency		Gain
1	4.940E-03		0.997010	0.997036		1.016757
2	4.940E-03		0.996816	0.996851		1.016618
3	4.940E-03		0.996843	0.996901		1.018724
4	4.940E-03		0.996863	0.996850		1.018238
5	4.940E-03		0.996797	0.996863		1.018410
6	4.940E-03		0.996847	0.996914		1.018950
7	4.940E-03		0.996948	0.996991		1.016277
8	4.940E-03		0.996551	0.996638		1.019390
9	4.940E-03		0.996697	0.996801		1.018474
10	4.940E-03		0.996957	0.996977		1.018226
11	4.940E-03		0.996785	0.996789		1.019213
12	4.940E-03		0.996777	0.996830		1.017414
13	4.940E-03		0.996952	0.996999		1.015790
14	4.940E-03		0.996690	0.996764		1.018094
15	4.940E-03		0.996772	0.996742		1.018991
16	4.940E-03		0.996577	0.996629		1.020117
17	4.940E-03		0.996581	0.996652		1.022305
18	4.940E-03		0.996578	0.996665		1.016995
19	4.940E-03		0.997099	0.997142		1.013752
20	4.940E-03		0.996984	0.996878		1.016576
Mean	**4.940E-03**		**0.996806**	**0.996846**		**1.02E+00**
Std Dev	**1.053E-18**		**0.000159**	**0.000141**		**1.81E-03**
C_v	**2.131E-16**					**0.18%**

Table C.2: ECG individual subject temporal advance/gain results (subject EG).

	Advance (sec)		Time (max)	Frequency		Gain
				Correlations		
1	4.940E-03		0.996759	0.996000		1.009070
2	4.940E-03		0.996262	0.994892		1.008871
3	4.935E-03		0.995773	0.994823		1.007881
4	4.735E-03		0.990778	0.988099		1.045035
5	4.935E-03		0.995433	0.993126		1.014452
6	4.935E-03		0.995560	0.994295		1.010215
7	4.935E-03		0.995580	0.993894		1.010994
8	4.895E-03		0.994530	0.992090		1.019644
9	4.930E-03		0.995155	0.992543		1.015371
10	4.940E-03		0.996821	0.996242		1.010546
11	4.940E-03		0.996545	0.995233		1.007137
12	4.920E-03		0.995024	0.993562		1.016995
13	4.740E-03		0.990741	0.986755		1.047232
14	4.920E-03		0.996096	0.986755		1.013551
15	4.920E-03		0.995886	0.994811		1.017562
16	4.935E-03		0.995527	0.993712		1.015016
17	4.935E-03		0.996789	0.996458		1.008626
18	4.720E-03		0.990145	0.986041		1.047654
19	4.940E-03		0.996484	0.994882		1.009134
20	4.850E-03		0.994826	0.992811		1.023520
Mean	**4.897E-03**		**0.995036**	**0.992851**		**1.02E+00**
Std Dev	**7.435E-05**		**0.002043**	**0.003281**		**1.31E-02**
C_v	**1.518E-2**					**1.29%**

Table C.3: ECG individual subject temporal advance/gain results (subject VS).

	Advance (sec)		Time (max)	Frequency		Gain
			Correlations			
1	4.940E-03		0.997588	0.997498		0.994115
2	4.940E-03		0.997740	0.997679		0.993488
3	4.940E-03		0.997615	0.997507		0.992754
4	4.940E-03		0.997805	0.997725		0.992032
5	4.940E-03		0.997584	0.997527		0.996060
6	4.940E-03		0.997606	0.997478		0.992724
7	4.940E-03		0.997823	0.997767		0.991812
8	4.940E-03		0.997712	0.997644		0.995889
9	4.940E-03		0.998222	0.998159		0.992502
10	4.940E-03		0.997506	0.997393		0.995934
11	4.940E-03		0.997775	0.997718		0.993632
12	4.940E-03		0.997741	0.997640		0.992080
13	4.940E-03		0.997740	0.997657		0.992863
14	4.940E-03		0.998047	0.997988		0.991658
15	4.940E-03		0.997859	0.997815		0.992212
16	4.940E-03		0.997596	0.997473		0.992083
17	4.940E-03		0.998129	0.998071		0.989812
18	4.940E-03		0.998131	0.998085		0.990806
19	4.940E-03		0.997845	0.997797		0.988819
20	4.940E-03		0.998134	0.998099		0.989667
Mean	**4.940E-03**		**0.997810**	**0.997736**		**9.93E-01**
Std Dev	**8.899E-19**		**0.000216**	**0.000235**		**1.98E-03**
C_v	**1.801E-16**					**0.20%**

Table C.4: ECG individual subject temporal advance/gain results (subject MH).

	Advance (sec)		Time (max)	Frequency		Gain
1	4.935E-03		0.996582	0.996615		0.993799
2	4.935E-03		0.996613	0.996660		0.995318
3	4.940E-03		0.996777	0.996815		0.997130
4	4.935E-03		0.996559	0.996566		0.998369
5	4.935E-03		0.996581	0.996639		0.991139
6	4.935E-03		0.996697	0.996717		0.994246
7	4.935E-03		0.996856	0.996865		0.994929
8	4.935E-03		0.996765	0.996856		0.991703
9	4.935E-03		0.996765	0.996856		0.991703
10	4.935E-03		0.996671	0.996769		0.992776
11	4.935E-03		0.996672	0.996731		0.996011
12	4.940E-03		0.996887	0.996910		0.993871
13	4.940E-03		0.997164	0.997181		0.993401
14	4.940E-03		0.997281	0.997300		0.994353
15	4.940E-03		0.996850	0.996882		0.996805
16	4.940E-03		0.996663	0.996663		0.997880
17	4.935E-03		0.996888	0.996912		0.993724
18	4.940E-03		0.996861	0.996942		0.994140
19	4.935E-03		0.996805	0.996872		0.993747
20	4.940E-03		0.996724	0.996753		0.997836
Mean	**4.937E-03**		**0.996783**	**0.996825**		**9.95E-01**
Std Dev	**2.513E-06**		**0.000184**	**0.000180**		**2.13E-03**
C_v	**5.090E-04**					**0.21%**

Table C.5: ECG individual subject temporal advance/gain results (subject MJ).

	Advance (sec)		Correlations Time (max)	Frequency		Gain
1	4.940E-03		0.999086	0.999120		0.960111
2	4.935E-03		0.999067	0.999114		0.959517
3	4.935E-03		0.999152	0.999189		0.958933
4	4.935E-03		0.999220	0.999251		0.958809
5	4.935E-03		0.999320	0.999349		0.958463
6	4.935E-03		0.999083	0.999142		0.959544
7	4.935E-03		0.998514	0.998628		0.962656
8	4.935E-03		0.998348	0.998457		0.965520
9	4.935E-03		0.998347	0.998460		0.967464
10	4.935E-03		0.998068	0.998223		0.969114
11	4.935E-03		0.998195	0.998338		0.967554
12	4.935E-03		0.998105	0.998240		0.968978
13	4.930E-03		0.998312	0.998448		0.963231
14	4.930E-03		0.998124	0.998242		0.965064
15	4.935E-03		0.998317	0.998447		0.964428
16	4.935E-03		0.998188	0.998281		0.965663
17	4.935E-03		0.998051	0.998189		0.966816
18	4.935E-03		0.997984	0.998110		0.967643
19	4.935E-03		0.997899	0.998110		0.967759
20	4.935E-03		0.998072	0.998228		0.968147
Mean	4.935E-03		0.998473	0.998578		9.64E-01
Std Dev	1.970E-06		0.000482	0.000435		3.80E-03
C_v	3.992E-04					0.39%

Table C.6: Distortion ratios (%, subject RJ).

	DR (overall)		Frequency Range (Hz)		
	Time Domain	Frequency Domain	0.5 to 25	25 to 100	25 to 200
1	7.99	7.94	6.33	38.35	38.48
2	8.24	8.17	6.33	41.08	41.18
3	8.24	8.16	6.42	39.29	39.39
4	8.26	8.21	6.35	40.67	40.78
5	8.30	8.20	6.38	40.45	40.56
6	8.25	8.15	6.53	40.11	40.30
7	8.07	7.98	6.26	40.03	40.17
8	8.62	8.50	6.48	41.23	41.32
9	8.41	8.28	6.45	40.31	40.38
10	8.11	8.05	6.39	38.70	38.79
11	8.39	8.31	6.43	39.33	39.50
12	8.29	8.21	6.34	41.42	41.50
13	8.04	7.96	6.28	40.16	40.26
14	8.44	8.31	6.38	42.16	42.26
15	8.41	8.36	6.45	41.65	41.72
16	8.62	8.53	6.48	41.54	41.67
17	8.68	8.56	6.63	40.46	40.55
18	8.52	8.41	6.33	44.13	44.17
19	7.81	7.73	6.20	37.63	37.71
20	8.15	8.13	6.26	41.36	41.48
Mean	8.29	8.21	6.39	40.50	40.61
Std Dev	0.23	0.21	0.10	1.46	1.44

Table C.7: Distortion ratios (%, subject EG).

	DR (overall)		Frequency Range (Hz)		
	Time Domain	Frequency Domain	0.5 to 25	25 to 100	25 to 200
1	8.13	8.03	6.20	46.01	46.24
2	8.73	8.60	6.25	51.04	51.27
3	9.22	9.11	6.10	58.81	58.93
4	14.47	13.94	7.74	89.54	101.71
5	9.73	9.67	6.17	59.68	59.75
6	9.50	9.36	6.11	60.27	60.39
7	9.51	9.38	6.19	58.88	59.05
8	10.74	10.53	6.53	65.76	69.67
9	10.03	9.87	6.04	65.53	65.60
10	8.08	7.98	5.97	47.56	47.68
11	8.33	8.18	6.04	48.98	49.11
12	10.20	9.90	6.40	62.13	62.70
13	14.65	14.11	7.93	86.51	97.94
14	8.99	8.83	6.35	49.18	51.28
15	9.32	9.18	6.32	54.55	55.88
16	9.65	9.49	6.07	66.67	66.74
17	8.09	7.98	6.17	44.62	45.40
18	15.07	14.60	8.09	92.26	104.55
19	8.47	8.35	6.12	49.72	49.94
20	10.56	10.33	6.83	58.85	64.29
Mean	10.07	9.87	6.48	60.83	63.41
Std Dev	2.16	2.02	0.65	14.07	17.88

Table C.8: Distortion Ratios (%, subject VS).

	DR (overall)		Frequency Range (Hz)	
	Time Domain	**Frequency Domain**	**0.5 to 25**	**25 to 100**
1	6.90	6.87	5.31	72.62
2	6.69	6.67	5.22	61.95
3	6.89	6.86	5.17	63.50
4	6.62	6.61	5.07	65.66
5	6.92	6.89	5.27	61.35
6	6.90	6.88	5.13	59.67
7	6.57	6.56	5.11	63.58
8	6.74	6.73	5.23	62.27
9	7.52	5.98	5.16	50.42
10	7.03	7.02	5.23	63.39
11	6.63	6.61	5.23	65.17
12	7.10	6.72	5.08	62.72
13	6.70	6.68	5.17	62.87
14	6.24	6.23	5.14	61.38
15	6.51	6.49	5.21	58.28
16	6.92	6.90	5.10	68.36
17	6.12	6.12	5.08	65.39
18	6.12	6.11	5.15	58.74
19	6.58	6.52	4.99	73.99
20	7.73	7.49	5.22	61.08
Mean	6.38	6.36	5.38	73.46
Std Dev	0.48	0.47	0.19	9.58

Table C.9: Distortion Ratios (%, Subject MH).

	DR (overall)		Frequency Range (Hz)	
	Time Domain	**Frequency Domain**	**0.5 to 25**	**25 to 100**
1	8.25	8.21	5.90	46.09
2	8.16	8.13	5.86	48.43
3	8.02	7.96	5.88	46.94
4	8.27	8.24	5.95	44.39
5	8.28	8.21	5.87	50.56
6	8.10	8.10	5.68	53.21
7	7.91	7.90	5.81	47.57
8	7.96	7.91	5.87	49.41
9	7.92	7.91	5.87	49.41
10	8.05	8.01	5.81	53.41
11	8.10	8.06	5.88	54.14
12	7.86	7.83	5.80	47.57
13	7.49	7.48	5.87	42.37
14	7.36	7.33	5.76	45.74
15	7.90	7.86	5.91	43.06
16	8.16	8.15	5.86	47.26
17	7.87	7.85	5.75	48.99
18	7.86	7.80	5.78	47.59
19	7.92	7.87	5.84	47.41
20	8.07	8.03	5.85	50.04
Mean	6.77	6.65	5.16	63.12
Std Dev	0.40	0.35	0.08	5.03

Table C.10: Distortion Ratios (%, subject MJ).

	TDR (overall)		Frequency Range (Hz)	
	Time Domain	Frequency Domain	0.5 to 25	25 to 100
1	5.76	5.76	5.14	67.19
2	5.81	5.81	5.18	76.17
3	5.73	5.72	5.13	64.37
4	5.63	5.63	5.07	59.44
5	5.48	5.48	5.01	57.64
6	5.77	5.76	5.14	70.92
7	6.39	6.38	5.33	76.06
8	6.50	6.49	5.42	74.15
9	6.40	6.37	5.46	61.26
10	6.69	6.65	5.57	69.57
11	6.59	6.56	5.54	65.05
12	6.66	6.64	5.61	71.80
13	6.65	6.62	5.43	79.16
14	6.84	6.83	5.50	89.96
15	6.57	6.56	5.44	74.78
16	6.75	6.74	5.47	90.84
17	6.84	6.81	5.51	85.83
18	6.91	6.89	5.49	78.04
19	6.91	6.87	5.48	84.88
20	6.71	6.69	5.57	72.15
Mean	7.98	7.94	5.84	48.18
Std Dev	0.23	0.23	0.06	3.16

Table C.11: Relative spectral contribution above and below 25 Hz (subjects: RJ, EG, VS - normal heart rates).

	Relative Contribution (%)							
	RJ			EG			VS	
	< 25 Hz	> 25 Hz		< 25 Hz	> 25 Hz		< 25 Hz	> 25 Hz
1	92.42	7.58		92.23	7.77		95.49	4.51
2	92.29	7.71		91.61	8.39		94.54	5.46
3	92.32	7.68		91.68	8.32		93.93	6.07
4	92.10	7.90		92.07	7.93		94.54	5.46
5	92.09	7.91		91.15	8.85		94.16	5.84
6	92.58	7.42		91.74	8.26		93.53	6.47
7	92.35	7.65		91.44	8.56		94.42	5.58
8	91.95	8.05		91.48	8.52		94.43	5.57
9	92.09	7.91		91.88	8.12		95.52	4.48
10	92.39	7.61		92.26	7.74		93.80	6.20
11	92.00	8.00		92.01	7.99		94.76	5.24
12	92.26	7.74		91.63	8.37		95.49	4.51
13	92.37	7.63		91.76	8.24		94.40	5.60
14	92.09	7.91		91.75	8.25		95.18	4.82
15	92.15	7.85		91.66	8.34		94.52	5.48
16	91.97	8.03		92.40	7.60		94.02	5.98
17	91.99	8.01		92.38	7.62		95.37	4.63
18	92.38	7.62		91.92	8.08		95.34	4.66
19	92.55	7.45		92.15	7.85		94.82	5.18
20	92.34	7.66		91.76	8.24		95.38	4.62
Mean	**92.23**	**7.77**		**91.85**	**8.15**		**94.68**	**5.32**
Std Dev	**0.19**	**0.19**		**0.33**	**0.33**		**0.62**	**0.62**

Table C.12: Relative spectral contribution above and below 25 Hz (subjects: MH, MJ - tachycardia).

	Relative Contribution (%)				
	MH			MJ	
	< 25 Hz	> 25 Hz		< 25 Hz	> 25 Hz
1	91.35	8.65		96.10	3.90
2	92.09	7.91		96.27	3.73
3	92.32	7.68		95.77	4.23
4	91.77	8.23		95.93	4.07
5	92.19	7.81		96.21	3.79
6	92.15	7.85		96.20	3.80
7	92.34	7.66		95.06	4.94
8	92.67	7.33		94.76	5.24
9	92.67	7.33		94.66	5.34
10	92.67	7.33		94.58	5.42
11	92.64	7.36		94.44	5.56
12	92.70	7.30		94.07	5.93
13	92.70	7.30		94.62	5.38
14	91.35	8.65		94.84	5.16
15	91.87	8.13		94.51	5.49
16	91.83	8.17		95.06	4.94
17	92.77	7.23		94.65	5.35
18	92.24	7.76		94.28	5.72
19	92.41	7.59		94.74	5.26
20	92.60	7.40		94.52	5.48
Mean	**92.27**	**7.73**		**95.06**	**4.94**
Std Dev	**0.44**	**0.44**		**0.72**	**0.72**

Table C.13: Input/output waveform dissimilarity (1-r_{MSP}).

	RJ		EG		VS		MH		MJ
1	0.00304		0.00318		0.00225		0.00312		0.00062
2	0.00322		0.00362		0.00211		0.00320		0.00060
3	0.00317		0.00411		0.00212		0.00298		0.00056
4	0.00322		0.00749		0.00208		0.00350		0.00054
5	0.00320		0.00453		0.00224		0.00302		0.00046
6	0.00315		0.00432		0.00216		0.00285		0.00060
7	0.00307		0.00429		0.00198		0.00290		0.00110
8	0.00344		0.00498		0.00219		0.00290		0.00110
9	0.00328		0.00475		0.00184		0.00290		0.00110
10	0.00310		0.00313		0.00229		0.00288		0.00110
11	0.00329		0.00333		0.00205		0.00293		0.00124
12	0.00324		0.00463		0.00207		0.00304		0.00130
13	0.00307		0.00763		0.00205		0.00289		0.00102
14	0.00330		0.00367		0.00187		0.00263		0.00120
15	0.00333		0.00393		0.00195		0.00308		0.00108
16	0.00345		0.00438		0.00212		0.00313		0.00124
17	0.00342		0.00312		0.00177		0.00288		0.00127
18	0.00340		0.00810		0.00182		0.00280		0.00136
19	0.00292		0.00341		0.00184		0.00300		0.00136
20	0.00319		0.00465		0.00629		0.00312		0.00131
Mean	**0.32%**		**0.46%**		**0.23%**		**0.30%**		**0.10%**
Std Dev	**0.000143**		**0.001488**		**0.000962**		**0.000185**		**0.000314**

Table C.14: Input/output variability of three ECG signal parameters (subject RJ).

Stat	INPUT				OUTPUT		
	Peak Ampl. (mV)	Peak Time (ms)	RMS Ampl. (mV)		Peak Ampl. (mV)	Peak Time (ms)	RMS Ampl. (mV)
	1.5576	0.2990	2.126		1.6254	0.2943	2.162
	1.6300	0.2925	2.234		1.6872	0.2875	2.271
	1.6174	0.2855	2.239		1.6908	0.2810	2.281
	1.6607	0.2826	2.298		1.7332	0.2779	2.340
	1.6626	0.3322	2.285		1.7359	0.3273	2.327
	1.4837	0.3067	2.049		1.5450	0.3023	2.088
	1.5345	0.3406	2.110		1.6037	0.3360	2.144
	1.6437	0.3199	2.228		1.6888	0.3152	2.271
	1.6472	0.2964	2.280		1.7022	0.2912	2.322
	1.6598	0.3270	2.296		1.7382	0.3222	2.337
	1.5719	0.3063	2.183		1.6628	0.3019	2.225
	1.6436	0.3190	2.257		1.7150	0.3138	2.297
	1.5663	0.3074	2.138		1.6323	0.3020	2.172
	1.6350	0.2894	2.239		1.7125	0.2844	2.279
	1.6620	0.3054	2.314		1.7353	0.3003	2.358
	1.6738	0.3134	2.291		1.7551	0.3083	2.337
	1.5803	0.2995	2.187		1.6667	0.2952	2.236
	1.6668	0.2794	2.126		1.7036	0.2749	2.162
	1.5685	0.2777	2.150		1.6437	0.2730	2.180
	1.6556	0.2699	2.257		1.7437	0.2648	2.294
Mean	1.6161	0.3025	2.214		1.6861	0.2977	2.254
Std Dev	0.0534	0.0191	0.0759		0.0543	0.0191	0.0785
* $p <$	0.9449	0.9990	0.8814				
Pearson *r*	0.9678	0.9999	0.9988				

* from the F test for variance differences

Table C.15: Input/output variability of three ECG signal parameters (subject EG).

Stat	INPUT				OUTPUT		
	Peak Ampl. (mV)	Peak Time (ms)	RMS Ampl. (mV)		Peak Ampl. (mV)	Peak Time (ms)	RMS Ampl. (mV)
	2.1646	0.4618	2.265		2.2174	0.4593	2.285
	2.2052	0.5002	2.354		2.2599	0.4976	2.375
	2.1545	0.5544	2.373		2.1928	0.5526	2.392
	2.3904	0.5695	2.387		2.7497	0.5695	2.495
	2.0681	0.5930	2.265		2.0904	0.5889	2.298
	2.1508	0.6122	2.316		2.1732	0.6098	2.340
	2.2127	0.4989	2.345		2.2844	0.4963	2.371
	2.3122	0.6224	2.368		2.4505	0.6215	2.415
	2.1787	0.5480	2.290		2.2600	0.5446	2.325
	2.2421	0.4924	2.439		2.2651	0.4891	2.465
	2.1633	0.6359	2.365		2.1998	0.6334	2.382
	2.2950	0.5242	2.344		2.3495	0.5231	2.384
	2.3853	0.5682	2.427		2.7538	0.5680	2.542
	2.3057	0.5049	2.472		2.3887	0.5035	2.505
	2.3011	0.5126	2.515		2.3874	0.5110	2.559
	2.1703	0.4924	2.336		2.1916	0.4877	2.371
	2.2793	0.6372	2.265		2.3150	0.6347	2.285
	2.3948	0.6366	2.453		2.7841	0.6365	2.570
	2.2907	0.5872	2.265		2.2787	0.5847	2.285
	2.3548	0.6169	2.480		2.5228	0.6162	2.539
Mean	2.2510	0.5585	2.366		2.3557	0.5564	2.409
Std Dev	0.0934	0.0572	0.0777		0.2021	0.0577	0.0969
* p <	0.0015	0.9743	0.3438				
Pearson r:	0.9151	0.9998	0.9560				

* from the F test for variance differences

Table C.16: Input/output variability of three ECG signal parameters (subject VS).

Stat	INPUT				OUTPUT		
	Peak Ampl. (mV)	Peak Time (ms)	RMS Ampl. (mV)		Peak Ampl. (mV)	Peak Time (ms)	RMS Ampl. (mV)
	1.4035	0.3944	1.591		1.4963	0.3895	1.582
	1.4357	0.3464	1.624		1.5187	0.3413	1.613
	1.4377	0.3488	1.611		1.4956	0.3438	1.599
	1.4562	0.3574	1.651		1.5170	0.3524	1.638
	1.4643	0.2720	1.591		1.5377	0.2667	1.582
	1.4754	0.4186	1.636		1.5519	0.4135	1.624
	1.4951	0.3783	1.702		1.5683	0.3732	1.688
	1.5006	0.3575	1.641		1.5759	0.3522	1.634
	1.5069	0.3612	1.630		1.5834	0.3558	1.625
	1.5290	0.3658	1.683		1.6225	0.3607	1.676
	1.5020	0.4485	1.591		1.5889	0.4432	1.582
	1.4912	0.4477	1.671		1.5634	0.4424	1.661
	1.5231	0.3962	1.709		1.6082	0.3912	1.696
	1.5328	0.5518	1.740		1.6061	0.5468	1.726
	1.5464	0.4681	1.756		1.6312	0.4627	1.742
	1.5704	0.4593	1.738		1.6446	0.4540	1.724
	1.5676	0.4977	1.792		1.6399	0.4928	1.774
	1.5705	0.4734	1.780		1.6418	0.4685	1.764
	1.5644	0.4693	1.785		1.6228	0.4642	1.765
	1.5884	0.4681	1.788		1.6522	0.4630	1.770
Mean	1.5081	0.4140	1.686		1.5833	0.4089	1.673
Std Dev	0.0518	0.0670	0.0715		0.0509	0.0670	0.0683
* p <	0.9395	0.9985	0.8453				
Pearson r	0.9802	1.0000	0.9994				

* from the F test for variance differences

Table C.17: Input/output variability of three ECG signal parameters (subject MH).

Stat	INPUT				OUTPUT		
	Peak Ampl. (mV)	Peak Time (ms)	RMS Ampl. (mV)		Peak Ampl. (mV)	Peak Time (ms)	RMS Ampl. (mV)
	0.5498	0.3314	0.9365		0.5674	0.3273	0.9307
	0.5020	0.3640	0.8840		0.5110	0.3589	0.8799
	0.5461	0.2644	0.9163		0.5532	0.2591	0.9136
	0.5643	0.2868	0.9579		0.5798	0.2822	0.9564
	0.6073	0.3090	0.9365		0.6228	0.3054	0.9307
	0.5290	0.2432	0.9187		0.5388	0.2367	0.9134
	0.5532	0.2772	0.9601		0.5577	0.2726	0.9552
	0.5780	0.2884	1.063		0.5867	0.2843	1.054
	0.5780	0.2884	1.063		0.5867	0.2843	1.054
	0.5534	0.2563	1.013		0.5566	0.2505	1.006
	0.5144	0.2640	0.9090		0.5210	0.2583	0.9053
	0.5570	0.2974	0.9765		0.5683	0.2931	0.9705
	0.5654	0.2779	0.9994		0.5811	0.2737	0.9928
	0.5524	0.2335	0.9515		0.5564	0.2284	0.9461
	0.5922	0.2761	1.018		0.6087	0.2714	1.015
	0.6063	0.3106	1.014		0.6134	0.3060	1.012
	0.6247	0.2459	0.9365		0.6310	0.2413	0.9307
	0.5412	0.3174	0.9681		0.5558	0.3115	0.9625
	0.5755	0.3404	1.042		0.5896	0.3361	1.036
	0.5777	0.1638	0.9823		0.5862	0.1590	0.9802
Mean	0.5634	0.2818	0.9723		0.5736	0.2770	0.9672
Std Dev	0.0306	0.0437	0.0514		0.0316	0.0439	0.05045
* $p <$	0.8993	0.9827	0.9369				
Pearson r	0.9898	0.9999	0.9993				

* from the F test for variance differences

145

Table C.18: Input/output variability of three ECG signal parameters (subject MJ).

Stat	INPUT				OUTPUT		
	Peak Ampl. (mV)	Peak Time (ms)	RMS Ampl. (mV)		Peak Ampl. (mV)	Peak Time (ms)	RMS Ampl. (mV)
	0.6045	0.2458	1.622		0.5906	0.2423	1.558
	0.6053	0.2470	1.697		0.5955	0.2431	1.628
	0.6187	0.2378	1.730		0.6035	0.2341	1.659
	0.6676	0.2438	1.861		0.6551	0.2404	1.785
	0.6938	0.2435	1.945		0.6769	0.2394	1.864
	0.5708	0.2408	1.595		0.5594	0.2375	1.530
	0.4463	0.2388	1.286		0.4457	0.2352	1.238
	0.4558	0.2346	1.246		0.4521	0.2307	1.203
	0.4615	0.2389	1.266		0.4616	0.2353	1.224
	0.4434	0.2297	1.226		0.4470	0.2262	1.188
	0.4558	0.2175	1.259		0.4611	0.2134	1.218
	0.4470	0.2265	1.220		0.4564	0.2227	1.182
	0.4562	0.2519	1.326		0.4660	0.2489	1.277
	0.4621	0.2487	1.265		0.4728	0.2456	1.221
	0.4572	0.2568	1.296		0.4701	0.2535	1.250
	0.4757	0.2703	1.277		0.4854	0.2671	1.233
	0.4542	0.2783	1.251		0.4677	0.2746	1.209
	0.4775	0.3061	1.287		0.4871	0.3025	1.245
	0.4551	0.3394	1.290		0.4658	0.3364	1.249
	0.4668	0.3305	1.291		0.4790	0.3273	1.249
Mean	0.5088	0.2564	1.412		0.5100	0.2528	1.361
Std Dev	0.0830	0.0332	0.234		0.0739	0.0334	0.220
* $p<$	0.6161	0.9830	0.7924				
Pearson r	0.9973	1.0000	1.0000				

* from the F test for variance differences

Bibliography

1. Mitchell MW, Chiao RY (1998). Causality and negative group delays in a simple bandpass amplifier, *American Journal of Physics,* 66(1):14-19.

2. Garrison JC, Mitchell MW, Chiao RY, Bolda EL (1998). Superluminal Signals: Causal Loop Paradoxes Revisited, *Physics Letters A*, 245:19-25.

3. Chiao RY, Hickmann JM, Solli D (2001). Faster-than-light effects and negative group delays in optics and electronics, and their applications, *Proceedings of SPIE, the International Society for Optical*, 4283, 16 (invited paper).

4. Kitano M, Nakanishi T, Sugiyama K (2003). Negative Group Delay and Superluminal Propagation: An Electronic Circuit Approach, *IEEE Journal. of Selected Topics in Quantum Electronics*, 9(1):43.

5. Munday JN, Henderson RH (2004), Superluminal time advance of a complex audio signal, *Applied Physics Letters,* 85(3):503-505.

6. Solli D, Chiao RY (2002). Superluminal effects and negative group delays in electronics, and their applications, *Physical Review E*, 66, 056601, 4.

7. Horowitz P, Hill W (1998). The Art of Electronics, *Cambridge University Press*, NY, 266-281.

8. Schaumann R, Van Valkenburg ME (2001). Design of Analog Filters, *Oxford Library Press,* NY.

9. Brillouin L (1960). Wave Propagation and Group Velocity (Pure and Applied Physics), *Academic Press*, New York.

10. McDonald KT (2000). Negative Group Velocity, *ArXiV:physics*.0008013 V4, 15 Sep.

11. White P (1999). Group Delay Explanations and Applications, *Applied Radio Labs*, Design File: DN004, 15 Nov.

12. The Fundamentals of Signal Analysis, *Application Note 243*, 5952-8898E, Agilent Technologies, 06/00.

13. Cao H, Dogariu A, Wang LJ (2003). Negative Group Delay and Pulse Compression in Superluminal Pulse Propagation, *IEEE Journal of Selected Topics in Quantum Electronics*, 9(1): 52-58.

14. Lee J-G, Park SM (1999), Clock signal modeling circuit with negative delay, U.S. Patent No. 5,945,861.

15. Lee J-G, Jun Y-H (2000), Negative delay circuit operable in wide band frequency, U.S. Patent No. 6,154,079.

16. Zhilu W, Zhendong Y, Gaunghui R, Zhonghao Z (2006). A Novel Method of Speeding up the Signal Processing System, *The 8th International Conference on Signal Processing*, 16-20.

17. Noto H, Yamauchi K, Nakayama M, Isota Y (2007). Negative Group Delay Circuit for Feed-Forward Amplifier, *Microwave Symposium, 2007. IEEE/MTT-S International*, 3-8 June.

18. Blaise Ravelo B, Perennec A, Le Roy M (2007). Synthesis of Broadband Negative Group Delay Active Circuits, *IEEE MTT-s 2007 International Microwave Symposium Tech. Program.*

19. Erickson SJ, Khaja M, Mojahedi M (2005). Time- and frequency-domain measurements for an active negative group delay circuit, *Antennas and Propagation Society International Symposium*, IEEE 2005, 3A:790-793.

20. Arntz BJ (1995), Method and apparatus for imparting positive phase slope to a narrow-band signal, US Patent No. 5,291,156.

21. OPA134, OPA2134, OPA4134, SoundPlus High Performance Audio Operational Amplifiers, *Literature No. PDS-1339C*, Burr-Brown, Dec. 1997.

22. LM6165/LM6265/LM6365 High Speed Operational Amplifier, *Literature No. DS009i52* May 1999, National Semiconductor.

23. MAX477 300MHz High-Speed Op Amp, *Literature No. 9-0467*; Rev 3; 11/99, Maxum Integrated Products.

24. LF353 Wide bandwidth Dual JFET Input Operational Amplifier, *Literature No. DS009152* Dec 2003, National Semiconductor.

25. AD745 Ultralow Noise, High Speed, BiFET Op Amp, *Literature475*, RevD, Analog Devices, 2004.

26. ADA4817-1/ADA4817-2 low Noise, 1 GHz *Fast FET* Op Amps, *Literature ADA4817-1/ADA4817*, Rev A, 3/09 Analog Devices.

27. ADS1271 24-Bit Wide Bandwidth Analog-to-Digital Converter, *Literature No: SBAS306D*, Nov. 2004, Revised Jul. 2006, Texas Instruments.

28. ADS1605 24-Bit Wide Bandwidth Analog-to-Digital Converter, *Literature No: SBAS274*, Mar. 2003, Texas Instruments.

29. TMS320VC5509A Fixed-Point Digital Signal Processor - Data Manual, *Literature No: SPRS205E*, Nov. 2002, Revised: Aug 2005, Texas Instruments.

30. 56F8023 Data Sheet (Preliminary Technical Data) 56F8000 - 16-Bit Digital Signal Controllers, *MC56F8023*, Rev. 3, 01/2007, Freescale Semiconductor.

31. Bendat JS, Piersol AG (1971), Random Data: Analysis and Measurement Procedures, *Wiley Intersciences*, New York.

32. Oppenheim AV, Schafer RW (1989), Discrete-Time Signal Processing (2nd Edition), *Prentice Hall*, Englewood Cliffs, NJ.

33. Aylward K (2009), Super-SPICE Gold Professional Circuit Analysis Package, http://www.anasoft.co.uk.

34. Warwick, Colin (May 2009). Everything you always wanted to know about SPICE* (*But were afraid to ask). *EMC Journal* (Nutwood UK Limited) (82): 27–29.

35. Tupe SK, Sayyad SB, Behre SH (2009). Comparative Study of Different SPICE Software's Using Astable Multivibrator in Different SPICE Software, *International Journal of Recent Trends in Engineering,* 2(6):26-29.

36. Nagel LW (1996). The Life of SPICE, in *1996 Bipolar Circuits and Technology Meeting*, Minneapolis, MN US.

37. DiStefano JJ, Stubberud AR, Williams IJ (1967). Theory and Problems of Feedback and Control Systems, Schaum's Outline Series, *McGraw-Hill,* New York.

38. Floyd, TL (1981). Principles of Electric Circuits. *Charles E. Merrill,* Columbus.

39. Albright B (2009). Chapter 3, Empirical Modeling, *Mathematical Modeling With Excel*, Jones and Bartlett Learning, Publ.

40. Kester W (2008). What the Nyquist Criterion Means to Your Sampled Data System Design, in *Analog Device*, http://www.analog.com/static/imported-files/tutorials/MT-002.pdf.

41. Donnelly D, Rust B (2005). The Fast Fourier Transform for Experimentalists, Part 1: Concepts, *IEEE Computing in Science and Engineering,* 7:80-88.

42. Electrogram Libraries, Chicago, IL USA, ECG Traces: AAEL203, AAEL 204.

43. Shih H-T (2009). Center for Cardiac Arrhythmias, Houston, TX USA.

44. Baggini A (2008). Handbook of Power Quality, *John Wiley and Sons*, New York.

45. Gerstenfeld EP, Dixit S, Callans DJ, Rajawat y, Rho R, Marchlinski FE (2003). Quantitative comparison of spontaneous and paced 12-lead electrocardiogram during right ventricular outflow tract ventricular tachycardia, *Journal of the American College of Cardiology,* 41;2046-53.

46. Schaff DP, Richards PG (2004). Repeating Seismic Events in China. *Science*, 303:1176-78.

47. Roche A, Malandain G, Pennec X, Ayache N (1998). The Correlation Ratio as a New Similarity Measure for Multimodal Image Registration, Springer Verlag. *Proceedings MICCAI'98*, Vol. 1496 of LNCS, 1115-1124.

48. Tihelka D, Romportl J (2009). Exploring Automatic Similarity Measures for Unit Selection Tuning, *INTERSPEECH 2009, Proceedings of 10th Annual Conference of International Speech Communication Association*, 736-739, ISCA, Brighton, Great Britain.

49. Chiu C-C, Lin T-H, Liau BY (2003). Using Correlation Coefficient in ECG Waveform for Arrhythmia Detection, *Biomedical Engineering Applications, Basis and Communications,* 17(3):147-152.

50. Semmlow JL (2004). Biosignal and Biomedical Image Processing: MATLAB-based Applications, Volume 1. *CRC Press,* Taylor and Francis Group, Boca Raton, FL

51. Throne RD, Jenkins JM, DiCarlo AL (1990). Intraventricular Electrogram Analysis for Ventricular Tachycardia Detection: Statistical Validation, Part I, P*ACE*, 13:1596-1601.

52. Han C-P (1989). Combining Tests for Correlation Coefficients, *The American Statistician*, Vol. 43, No. 4 (Nov., 1989), pp. 211-215.

53. Amann A, Tratnig R, Unterkofler K (2005).Reliability of old and new ventricular fibrillation detection algorithms for automated external defibrillators, *Biomedical Engineering OnLine,* 4:60:1-15.

54. Witham MK (2008), Foundation Doctor's Guide to Medicine and Surgery, Elsevier Health Sciences, Philadelphia, PA.

55. Algra A, Tijssen JG, Roelandt JR, Pool J, Lubsen J (1993), Heart Rate Variability From 24-Hour Electrocardiography and the 2-Year Risk for Sudden Death, *Circulation,* 88:180-185.

56. Vikman S, Mäkikallio TH, Yli-Mäyry S, Pikkujämsä S, Koivisto AM, Reinikainen P, Airaksinen KEJ, Huikuri HV (1999), Altered Complexity and Correlation Properties of R-R Interval Dynamics Before the Spontaneous Onset of Paroxysmal Atrial Fibrillation, *Circulation* 1999;100;2079-2084.

57. Whitsel EA, Raghunathan TE, Pearce RM, Lin D, Rautaharju PM, Lemaitre R, Siscovick DS (2001), RR interval variation, the QT interval index and risk of primary cardiac arrest among patients without clinically recognized heart disease, *European Heart Journal* 22:165-173.

58. Homoud MK (2008), Introduction to Electrocardiography, Tufts-New England Medical Center, Boston, MA.

59. An Aging, Fatter Population Drives Demand for New Medical Devices, *Wharton Communications,* March 2003, University of Pennsylvania, Philadelphia PA.

60. Shih H-T (2008), electrocardiologist/researcher in a private communication stated: "Signal Advance technology … can revolutionize the non-pharmacological treatment of cardiac arrhythmias and epilepsy."

61. Malmivuo J, Plonsey R (1995). Bioelectromagnetism – Principles and Applications of Bioelectric and Biomagnetic Fields, Chapter 23 – *Cardiac Pacing*, Oxford University Press, NY.

62. Trohman RG, Kim MH, Pinski SL (2004). Cardiac pacing: the state of the art, *Lancet*; 364:1701-19.

63. Ermis C (2007). Optimal programming in cardiac resynchronization therapy, *The Anatolian Journal of Cardiology, 7* Suppl (1):50-2.

64. Boriani G, Diemberger I,Biffi M, Martignani C, Valzania C, Ziacchi M, Bertini M, Specchia S, Grigioni F, Rapezzi C, Branzi A (2006). Cardiac resynchronization therapy in clinical practice: Need for electrical, mechanical, clinical and logistic synchronization, *Journal of Interventional Cardiac Electrophysiology,* 17:215-224.

65. Phillippon F (2004). Cardiac Resynchronization Therapy: Device-based Medicine for Heart Failure, *Journal of Cardiac Surgery*, 19:270-274.

66. Bhatia A, Cooley R, Berger M, Blanck Z, Dahla A, Sra J, Axtell-McBride K, VanderVort C, Akhtar M (2004). The Implantable Cardioverter Defibrillator: Technology, Indications, And Impact On Cardiovascular Survival, *Current Problems in Cardiology*, June.

67. McPherson CA, Manthous C (2004). Permanent Pacemakers and Implantable Defibrillators, Considerations for Intensivists, *American Journal of Respiratory and Critical Care Medicine*, 170:933-940.

68. Gura MT (2005). Implantable Cardioverter Defibrillator Therapy, *Journal of Cardiovascular Nursing,* 20(4):276-287.

69. Padeletti L, Michelucci A, Frohlig G, Corbucci G, van Oort, G, Barold SS (2005). Digital technology in Cardiac Pacing: methods for Morphology Analysis of Sensed Endocavity Signals, *Journal of Interventional Cardiac Electrophysiology*, 14(1):9-16.

70. Blaauw Y, Van Gelder IC, Crijns HJGM (2002). Treatment of atrial fibrillation, *Heart,* 88:432-437.

71. Irwin ME (2004). Cardiac Pacing Device Therapy for Atrial Dysrhythmias, How Does It Work?, *AACN Clincal Issues* 15(3):377-390.

72. Agarwal A, York M, Kantharia BK, Ezekowitz M (2005). Atrial Fibrillation: Modern Concepts and Management, *Annual Review of Medicine,* 65:475-94.

73. Knight BP, Gersh BJ, Carlson MD, Friedman PA, McNamara RL, Strickberger SA, Tse HF, Waldo AL (2005). Role of Permanent Pacing to Prevent Atrial Fibrillation, *Circulaton*, 111:240-243.

74. Kirchhof P, (2009), Can we improve outcomes in AF patients by early therapy?, *BMC Medicine*, 7:72.

75. Bollman A, Mende M, Neugebauer A, Pfieffer D (2003), Atrial Fibrillatory Frequency Predicts Atrial Defibrillation Threshold and Early Arrhythmia Recurrence in Patients Undergoing Internal Cardioversion of Persistent Atrial Fibrillation, *Pacing and Clinical Electrophysiology*, 25(8):1179-1184.

76. Shin H, Lee C, Kim J, Lee M (2006). Development of Arrhythmia Diagnosis Algorithm for Effective Control of Antitachycardia Pacing and High Energy Shock of ICD, *Conference Proceeding of IEEE Engineering in Medicine and Biology Society,* 1:4366-4369.

77. Ravelli F, Masè M, Del Greco M, Faes L, Disertori M (2007). Deterioration of organization in the first minutes of atrial fibrillation: a beat-to-beat analysis of cycle length and wave similarity. *Journal of Cardiovascular Electrophysiology,* 18(1):60-5.

78. Jekova I (2003). Estimation of Electrocardiogram Peak Frequency and Periodicity During Ventricular Fibrillation, *Computers in Cardiology* 30:225–228.

79. Marill KA, Kazzi AA, Khalil MK, Bright AA (2010). Ventricular Fibrillation http://emedicine.medscape.com/article/760832-overview.

80. Hoppe BL, Kahn Am, Feld GK, Hassankhani A, Narayan SM (2005). Separating Atrial Flutter From Atrial Fibrillation With Apparent Electrocardiographic Organization Using Dominant and Narrow F-Wave Spectra, *Journal of the American College of Cardiology,* 46:2079-2087.

81. Haïssaguerre M, Derval N, Sacher F, Jesel L, Deisenhofer I, de Roy L, Pasquié J-L, Nogami A, Babuty D, Yli-Mayry S, De Chillou C, Scanu P, Mabo P, Matsuo S, Probst V, Le Scouarnec S, Defaye P, Schlaepfer J, Rostock T, Lacroix D, Lamaison D, Lavergne T, Aizawa Y, Englund A, Anselme F, O'Neill, M, Hocini, M, Lim KT, Knecht S, Veenhuyzen G D, Bordachar P, Chauvin, M, Jais P, Coureau G, Chene G, Klein GJ, Clémenty J (2008). Sudden Cardiac Arrest Associated with Early Repolarization, *New England Journal of Medicine,* 358(19):2016-23.

82. Gillberg J (2007). Detection of cardiac tachyarrhythmias in implantable devices, *Journal of Electrocardiology,* 40:S123-S128.

83. Seiler J, Lee JC, Roberts-Thomson KC (2008). Regular wide QRS tachycardia complicating treatment for atrial fibrillation, *Kardiovaskuläre Medizin,* 11(5):166-167.

84. Amann A, Tratnig R, Unterkofler K (2007). Detecting Ventricular Fibrillation by Time-Delay Methods, *IEEE Transactions on Biomedical Engineering*, 54:174-177.

85. Ruiz J, Aramendi E, Ruiz de Gauna S, Lazkano A, Leturiondo LA, Gutiérrez JJ (2003), Distinction of Ventricular Fibrillation and Ventricular Tachycardia Using Cross Correlation, *Computers in Cardiology*, 30:729-732.

86. Tsipouras MG, Fotiadis DI Sideris D (2005). An arrhythmia classification system based on the RR-interval signal, *Artificial Intelligence in Medicine,* 33:237-250.

87. Chen S-W (2007), Complexity-Measure-Based Sequential Hypothesis Testing for Real-Time Detection of Lethal Cardiac Arrhythmias, EURASIP *Journal on Advances in Signal Processing*, Vol 2007, Article ID 20957:1-8.

88. Brazdzionyte J, Bluzaite I, Bluzhas J, Mickeviciene A (1996). Dynamics of the Data of Signal-Averaged Electrocardiogram and their Relation to Ventricular Rhythm Disturbancies in Myocardial Infarction *Journal of the Hong Kong College of Cardiology,* 4:72-76.

89. Yamada T, Watanabe I, Okumura Y, Takagi Y, Okubo K, Hashimoto K, Shindo A, Nakai T, Kasamaki Y, Saito S (2006). Atrial Electrophysiological Abnormality in Patients With Brugada Syndrome Assessed by P-Wave Signal-Averaged ECG and Programmed Atrial Stimulation, *Circulation Journal,* 70:1574-1579.

90. Sasaki T, Niwano S, Sasaki S, Imaki R, Yuge M, Hirasawa S, Satoh D, Moriguchi M, Fujiki A, Izumi T, (2006). Long-Term Follow-up of Changes in Fibrillation Waves in Patients With Persistent Atrial Fibrillation -Spectral Analysis of Surface ECG, *Circulation Journal*, 70: 169-173.

91. Poli S, Barbaro V, Bartolini P, Calcagnini G, Censi F, (2003). Prediction of atrial fibrillation from surface ECG: review of methods and algorithms, *Annals of the First Super Sanità,* 39(2):195-203.

92. Khadra L, Friwan A, Shahab W (2002). Neural wavelet analysis of cardiac arrhythmia, presented at the *Third International Conference on Neural Networks and Applications,* Interlaken, Switzerland, Feb 2002.

93. Durka PJ, Klekowicz H, Blinowska KJ, Szelenberger W, Niemcewicz Sz (2003). A Simple System for Detection of EEG Artifacts in Polysomnographic Recordings, *IEEE Transactions on Biomedical Engineering*, 50(4):526-528.

94. Knight JA (2003). Signal Fraction Analysis and Artifact Removal in the EEG, Master of Science Thesis, Colorado State University.

95. Benbadis SR, Rielo D, (2010). eMedicine Neurology - EEG Artifacts, URL:http://emedicine.medscape.com/article/1140247-overview.

96. Molina GN, Ebrahimi T, Vesin J-M (2003). Joint Time-Frequency-Space Classification of EEG in a Brain-Computer Interface Application, *EURASIP Journal on Applied Signal Processing*, 7:713-729.

97. Boudet S, Peyrodie L, Gallois P, Vasseur C (2006). A global approach for automatic artifact removal for standard EEG record, *Conf Proc IEEE Engineering in Medicine and Biology Society,* 1:5719-22.

98. Brunner DP, Vasko RC, Detka CS, Monahan JP, Reynolds CF 3rd, Kupfer DJ (1996). Muscle artifacts in the sleep EEG: automated detection and effect on all-night EEG power spectra, *Journal of Sleep Research*, 5(3):155-64.

99. Ochoa JB (2002). EEG Signal Classification for Brain Computer Interface Applications, Ecole Polytechnique Federale de Lausanne (Thesis).

100. Park H-J, Jeong D-U, Park K-S (2002). Automated Detection and Elimination of Periodic ECG Artifacts in EEG Using the Energy Interval Histogram Method, *IEEE Transactions on Biomedical Engineering*, 49(12):1526-1533.

101. Guerrero-Mosquera C, Vazquez AN (2009). Automatic Removal of Ocular Artifacts from EEG Data using Adaptive Filtering and Independent Components Analysis, *17th European Signal Processing Conference,* (EUSIPCO 2009*).*

102. Wang J, Xu G (2009). Some Highlights on EEG Signal Processing, *Recent patents on Biomedical Engineering,* 2:1-10.

103. Garreffa G, Carnì M, Gualniera G, Ricci GB, Bozzao L, De Carli D, Morasso P, Pantano P, Colonnese C, Roma V, Maraviglia B (2003). Real-time MR artifacts filtering during continuous EEG/fMRI acquisition, *Magnetic Resonance Imaging,* 21:1175-1189.

104. Kim K, Yoon H, Song M, Park H (2004). Ballistocardiac artifact removal algorithm for simultaneous EEG/fMRI, *Proceedings of the international Society for Magnetic Resonance in Medicine*, 11:1044.

105. Negishi M, Abildgaard M, Nixon T, Constable RT (2004). Removal of time-varying artifacts from EEG data acquired during continuous fMRI, *Clinical Neurophysiology,* 115: 2181-2192.

106. Suresh HN, Puttamadappa C (2008). Removal of time-varying gradient artifacts from EEG data acquired during continuous fMRI, *International Journal of Physical Sciences*, 3(5):120-125.

107. Rasheed T, Lee Y-K, Lee S (2009). Principal Subspace Analysis Based BCG Artifact Removal in Single Channel EEG Signal Measured Inside MRI Scanner, *Communications in Computer and Information Science*, 57:24-30.

108. Pedersen MS, Larsen J, Kjems U, Parra LC (2007). A Survey of Convolutive Blind Source Separation Methods, In *Springer Handbook of Speech,* Springer Press, URL: http://www2.imm.dtu.dk/pubdb/p.php?4924.

109. Choi S, Cichocki A, Park H-M, Lee S-Y (2005). Blind Source Separation and Independent Component Analysis: A Review, *Neural Information Processing - Letters and Reviews*, 6(1):1-57.

110. Delorme A, Sejnowski T, Makeig T (2007). Enhanced detection of artifacts in EEG data using higher-order statistics and independent component analysis, *NeuroImage* 34:1443-1449.

111. De Clercq W, Vergult, Vanrumste B, Van Paesschen W, Van Huffel S (2006). Canonical Correlation Analysis Applied to Remove Muscle Artifacts from the Electroencephalogram, *IEEE Transactions on Biomedical Engineering,* 53:2583-2587.

112. Vergult A, de Clercq W, Palmini A, Vanrumste B, Dupont P, Van Huffel S, Van Paesschen W (2007). Improving the Interpretation of Ictal Scalp EEG - BSS-CCA algorithm for muscle artifact removal, *Epilepsia*, 48:950-958.

113. Mohammed A, Ballal T, Grbic N (2007). Blind Source Separation Using Time-Frequency Masking, *Radio Engineering,* 16(4):96-100.

114. Kumar PS, Arumuganathan R, Sivakumar K, Vimal C (2008). Removal of Ocular Artifacts in the EEG through Wavelet Transform without using an EOG Reference Channel, *International Journal of Open Problems in Computational Mathematics*, 1(3):188-200.

115. DeCoster J (1998). Overview of Factor Analysis, http://www.stat-help.com/notes.html.

116. Schetinin V (2001). Polynomial Neural Networks Learnt to Classify EEG Signals, NIMIA-SC2001 - 2001 NATO *Advanced Study Institute on Neural Networks for Instrumentation, Measurement, and Related Industrial Applications: Study Cases*, Crema, Italy, 9-20 Oct.

117. Robert C, Gaudy JF, Limoge A (2002). Electroencephalogram processing using neural networks, *Clinical Neurophysiology,* 113(5):694-701.

118. Halder S, Bensch M, Mellinger J, Bogdan M, Kübler A, Birbaumer N, Rosenstiel W (2007). Online Artifact Removal for Brain-Computer Interfaces Using Support Vector Machines and Blind Source Separation, *Computational Intelligence and Neuroscience,* Vol. 2007, Article ID 82069.

119. Peterson DA, Knight JN, Kirby MJ, Anderson CW, Thaut MH (2005). Feature Selection and Blind Source Separation in an EEG-Based Brain-Computer Interface, *EURASIP Journal on Applied Signal Processing,* 19:3128-3140.

120. Molgedey L, Schuster HG (1994), Separation of a mixture of independent signals using time delayed correlations, *Physics Review Letters*, 72:3634-3636.

121. Bruhn J, Bouillon TW, Hoeft A, Shafer SL (2002). Artifact Robustness, Inter- and Intraindividual Baseline Stability, and Rational EEG Parameter Selection, *Anesthesiology,* 96:54-9.

122. Gharieb RR, Cichocki A (2003). Second-order statistics based blind source separation using a bank of sub-band filters, *Digital Signal Processing*, 13:252-274.

123. Miwakeichi F, Martınez-Montes E, Valdés-Sosa PA, Nishiyama, Mizuhara H, Yamaguchi Y (2004). Decomposing EEG data into space–time–frequency components using Parallel Factor Analysis, *NeuroImage,* 22:1035-1045.

124. Lakmal SR, Zhu B (2007). Blind Source Separation in Real Time using Second Order Statistics, (THESIS), Blekinge Institute of Technology.

125. Smaragdis P (998). Blind Separation of Convolved Mixtures in the Frequency Domain, *Neurocomputing*, 22:21-34.

126. Dichter MA, Brodie MJ (1996), New Antiepileptic Drugs, *New England Journal of Medicine*, 334(24):1583-90.

127. Coenen AML, van Luijtelaar ELJM (2003). Genetic Animal Models for Absence Epilepsy - A Review of the WAG/Rij Strain of Rats, *Behavior Genetics*, 33(6):635-655.

128. Meeren H, van Luijtelaar G, Lopes da Silva F, Coenen A (2005). Evolving Concepts on the Pathophysiology of Absence Seizures, *Archives of Neurology,* 62:371-376.

129. Mormann F, Elger CE, Lehnertz K (2006), Seizure anticipation: from algorithms to clinical practice, *Current Opinion in Neurology*, 19:187-193.

130. Litt B, Echauz J (2002), Prediction of Epileptic Seizures, *The Lancet, Neurology*, 1(1):22-30.

131. Meng L, Frei MG, Osorio I, Strang G, Nguyen TQ (2004). Gaussian mixture models of ECoG signal features for improved detection of epileptic seizures, *Medical Engineering and Physics,* 26(5):379-93.

132. Alkan A, Koklukaya E, Subasi A (2005). Automatic seizure detection in EEG using logistic regression and artificial neural network, *Journal of Neuroscience Methods* 148:167-176.

133. Michel JAM, Van Putten MJAM, Kind T, Visser F, Lagerburg V (2005). Detecting temporal lobe seizures from scalp EEG recordings: A comparison of various features, *Clinical Neurophysiology,* 116:2480-2489.

134. Päivinen N, Lammi S, Pitkänen A, Nissinen J, Penttonen M, Grönfors T (2005). Epileptic seizure detection: A non-linear viewpoint, *Computer Methods and Programs in Biomedicine,* 79:151-159.

135. Saab ME, Gotman J (2005). A system to detect the onset of epileptic seizures in scalp EEG, *Clinical Neurophysiology*, 116:427-442.

136. Aarabi A, Wallois F, Grebe R (2006). Automated neonatal seizure detection: A multistage classification system through feature selection based on relevance and redundancy analysis, *Clinical Neurophysiology,* 117:328-340.

137. Mohseni HR, Maghsoudi A, Shamollahi MB (2006). Seizure Detection in EEG Signals: A Comparison of Different Approaches, In the *Proceedings of the 28th Annual International Conference of the IEEE Engineering in Medicine and Biology Society*, Vol. Suppl. 6724-6727.

138. Shoeb A, Edwards H, Connolly J, Bourgeois B, Treves ST, Guttag J (2004). Patient-specific seizure onset detection, *Epilepsy & Behavior,* 5:483-498.

139. Grewal S, Gotman J (2005). An automatic warning system for epileptic seizures recorded on intracerebral EEGs, *Clinical Neurophysiology,* 116:2460-2472.

140. Wilson SB (2005). A neural network method for automatic and incremental learning applied to patient-dependent seizure detection, *Clinical Neurophysiology,* 116:1785-1795.

141. Wilson SB (2006). Algorithm architectures for patient dependent seizure detection, *Clinical Neurophysiology,* 117:1204-1216.

142. Esteller R, Echauz J, D'Alessandro M, Vachtsevanos G, Litt B (2001). Feature parameter optimization for seizure detection/prediction, *Engineering in Medicine and Biology Society, 2001. Proceedings of the 23rd Annual International Conference of the IEEE*, 2:1711-1714.

143. Osorio I, Frei MG, Manly BF, Sunderam S, Bhavaraju NC, Wilkinson SB (2001). An introduction to contingent (closed-loop) brain electrical stimulation for seizure blockage, to ultra-short-term clinical trials, and to multi-dimensional statistical analysis of therapeutic efficacy, *Journal of Clinical Neurophysiology*, 18(6):533-44.

144. Osorio I, Frei MG, Sunderam S, Giftakis J, Bhavaraju NC, Schaffner SF, Wilkinson SB (2005). Automated Seizure Abatement in Humans Using Electrical Stimulation, *Annals of Neuroscience,* 57:258-268.

145. Gardner AB, Krieger A, Vachtsevanos G, Litt B (2006). One-Class Novelty Detection for Seizure Analysis from Intracranial EEG, *Journal of Machine Learning Research,* 7:1025-1044.

146. Wong S, Gardner AB, Krieger AM, Litt B (2007), A Stochastic Framework for Evaluating Seizure Prediction Algorithms Using Hidden Markov Models, *Journal of Neurophysiology,* 97: 2525-2532.

147. Haas SM, Frei MG, Osorio I (2007). Strategies for adapting automated seizure detection algorithms, *Medical Engineering & Physics,* 29:895–909.

148. Hammond DC (2006). What is neurofeedback? *International Society for Neuro-feedback and Research*, (http://www.isnr.org/uploads/whatisnfb.pdf).

149. Heinrich H, Gevensleben H, Strehl U (2007). Annotation: Neurofeedback - train your brain to train behaviour, *Journal of Child Psychology and Psychiatry,* 48:1:3-16.

150. Schneider TR, Debener S, Oostenveld R, Engel AK (2008). Enhanced EEG gamma-band activity reflects multisensory semantic matching in visual-to-auditory object priming, *NeuroImage*, 42(3):1244-1254.

151. Gevensleban H, Holl B, Albrecht B, Schlamp D, Kratz O, Studer P, Wangler S, Rothenberger A, Moll G, Heinrich H (2009). Distinct EEG effects related to neurofeedback training in children with ADHD: A randomized controlled trial, *International Journal of Psychophysiology,* 74:149-157.

152. Barnea A, Rassisa A, Zaidel E (2005). Effect of neurofeedback on hemispheric word recognition, *Brain and Cognition,* 59:314-321.

153. Walker JE, Lawson R, Kozlowski G, (2007). Current status of QEEG and neurofeedback in the treatment of depression. Chapter in J. R. Evans (Ed.), *Handbook of Neurofeedback.* Haworth Medical Press, Binghampton, NY, 341-351.

154. Walker JE (2010). Recent Advances in Quantitative EEG as an Aid to Diagnosis and as a Guide to Neurofeedback Training for Cortical Hypofunctions, Hyperfunctions, Disconnections, and Hyperconnections- Improving Efficacy in Complicated Neurological and Psychological Disorders, *Applied Psychophysiology and Biofeedback*, 35:25–27.

155. Barry RJ, Clarke AR, Johnstone SJ (2003). A review of electrophysiology in attention-deficit - hyperactivity disorder, I Qualitative and quantitative electroencephalography, *Clinical Neurophysiology*, 114:171-183.

156. Rossiter T (2004). The Effectiveness of Neurofeedback and Stimulant Drugs in Treating AD/HD: Part II. Replication, *Applied Psychophysiology and Biofeedback*, 29,(4):233-243.

157. Butnik S (2005). Neurofeedback in Adolescents and Adults with Attention Deficit Hyperactivity Disorder, *Journal of Clinical Psychology*, 61:621-625.

158. Fox DJ, Tharp DF, Fox LC (2005). Neurofeedback: An Alternative and Efficacious Treatment for Attention Deficit Hyperactivity Disorder, *Applied Psychophysiology and Biofeedback*, 30 (4):365-373.

159. Loo SK, Barkley RA (2005). Clinical Utility of EEG in Attention Deficit Hyperactivity Disorder, *Applied Neuropsychology,* 12:64-76.

160. Leins U, Hinterberger T, Kaller T, Schober S, Weber C, Strehl U (2007). Neurofeedback for Children with ADHD: A Comparison of SCP and Theta/Beta Protocols, *Prax Kinderpsychol Kinderpsychiatr*, 55(5):384-407.

161. Russell H, Turow G (2010). Rhythmic Sensory Stimulation of the Brain: The Possible Use of Inexpensive Sensory Stimulation Technologies to Improve IQ Test Scores and Behavior, Chapter 11, *The Rhythmic Brain*, Turow G, Berger G, Eds. (In Press).

162. Sterman MB (2000). Basic Concepts and Clinical Findings in the Treatment of Seizure Disorders with EEG Operant Conditioning, *Clinical Electroencephalography*, 31(1):45-55.

163. Walker JE, Kozlowski GP (2005). Neurofeedback Treatment of Epilepsy, *Child Care & Adolescent Psychiatric Clinics of North America*, 14(1):163-176.

164. Egner T, Sterman MB (2006), Neurofeedback treatment of Epilepsy: from basic rationale to practical application, *Expert Review of Neurotherapy,* 6:247-257.

165. Sterman MB, Egner T (2006). Foundation and Practice of Neurofeedback for the Treatment of Epilepsy, *Applied Psychophysiology & Biofeedback*, 31(1):21-35.

166. Thatcher RW (2000). EEG operant conditioning (biofeedback) and traumatic brain injury, *Clinical Electroencephalography,* 31(1):38-44.

167. Bounias M, Laibow RE, Bonaly A, Stubblebine AN (2002). EEG-Neurofeedback treatment of patients with brain injury: Part 4: Duration of treatments as a function of both initial load of clinical symptoms and the rate of rehabilitation, *Journal of Neurotherapy*, 6(1):23-28.

168. Bearden TS, Cassisi JE, Pineda M (2003). Neurofeedback training for a patient with thalamic and cortical infarctions, *Applied Psychophysiology & Biofeedback*, 28(3):241-253.

169. Thornton KE, Carmody DP (2009), Traumatic Brain Injury Rehabilitation: QEEG Biofeedback Treatment Protocols, *Applied Psychophysiol Biofeedback,* 34:59-68.

170. Peniston EG, Kulkosky PJ (1990). Alcoholic personality and alpha–theta brainwave training, *Medical Psychotherapy,* 3:37-55.

171. Saxby E, Peniston EG (1995). Alpha-theta brainwave neurofeedback training: an effective treatment for male and female alcoholics with depressive symptoms. *Journal of Clinical Psychology*, 51:685-693.

172. Trudeau DL (2005). Applicability of brain wave biofeedback to substance use disorder in adolescents. *Child & Adolescent Psychiatric Clinics of North America*, 14(1):125-136.

173. Kelly MJ (1997). "Native Americans, neurofeedback, and substance abuse theory" Three year outcome of alpha/theta neurofeedback training in the treatment of problem drinking among Dine' (Navajo) people. *Journal of Neurotherapy*, 2(3):24-60.

174. Scott WC, Brod TM, Sideroff S, Kaiser D, Saga M (2002). Type-specific EEG biofeedback improves residential substance abuse treatment. Presented at the *American Psychiatric Association* Annual Meeting.

175. Bodehnamer-Davis E, Callaway T (2003). Extended follow-up of Peniston protocol results with chemical dependency, Presentation at the *International Society of Neuronal Regulation*, September, Houston, Texas, USA.

176. Burkett VS, Cummins JM, Dickson RM, Skolnick MH (2005). An open clinical trial utilizing real-time EEG operant conditioning as an adjunctive therapy in the treatment of crack cocaine dependence, *Journal of Neurotherapy*, 6(10):23-28.

177. Moore NC (2000). A review of EEG Biofeedback treatment of Anxiety Disorders, *Clinical Electroencephalography*, 31(1):1-6.

178. Sattlberger E, Thomas JE (2000). Treatment of anxiety disorder with slow-wave suppression EEG feedback: A case study. *Biofeedback*, 28(4):17-19.

179. Hammond DC (2005). Neurofeedback with anxiety and affective disorders, *Child & Adolescent Psychiatric Clinics of North America,* 14:105-123.

180. Baehr E, Rosenfeld JP, & Baehr R (2001). Clinical use of an alpha asymmetry neurofeedback protocol in the treatment of mood disorders: Follow-up study one to five years post therapy. *Journal of Neurotherapy*, 4(4):11-18.

181. Ham LP, Packard RC (1996). A retrospective, follow-up study of biofeedback assisted relaxation therapy in patients with posttraumatic headache. *Biofeedback and Self-Regulation*, 21(2): 93-104.

182. Siniatchkin, M., Hierundar, A., Kropp, P., Kuhnert, R., Gerber, W-D., & Stephani, U (2000). Self-regulation of slow cortical potentials in children with migraine: An exploratory study. *Applied Psychophysiology & Biofeedback*, 25(1):13-32.

183. Sime, A (2004). Case study of trigeminal neuralgia using neurofeedback and peripheral biofeedback. *Journal of Neurotherapy*, 8(1):59-71.

184. Nestoriuc Y, Martin A, Rief W, Andrasik F (2008). Biofeedback Treatment for Headache Disorders: A Comprehensive Efficacy Review, *Applied Psychophysiology and Biofeedback,* 33(3):125-40.

185. Coben R, Padolsky I (2007). Assessment-Guided Neurofeedback for Autistic Spectrum Disorder. *Journal of Neurotherapy*, 11(1):5-22.

186. Coben R, Linden M, Myers TE (2010). Neurofeedback for Autistic Spectrum Disorder: A Review of the Literature. *Applied Psychophysiology and Biofeedback,* 35:83-105.

187. Ayers ME (2004). Neurofeedback for cerebral palsy, *Journal of Neurotherapy,* 8(2):93-94.

188. Evans JR, Park N-S (1996). Quantitative EEG Abnormalities in a Sample of Dyslexic Persons, *Journal of Neurotherapy*, 2 (1):1-5.

189. Breteler MHM, Arns M, Peters S, Giepmans I, Verhoeve L (2010). Improvements in Spelling after QEEG-based Neurofeedback in Dyslexia: A Randomized Controlled Treatment Study, *Applied Psychophysiology and Biofeedback,* 35:5-11.

190. Surmeli T, Ertem A (2010). Post WISC-R and TOVA improvement with QEEG guided neurofeedback training in mentally retarded: a clinical case series of behavioral problems, *Clinical EEG and Neuroscience*, 41(1):32-41.

191. Budzynski TH (1996). Brain Brightening: Can neurofeedback improve cognitive process?, *Biofeedback,* 24(2):14-17.

192. Vernon D, Egner T, Cooper N, Compton T, Neilands C, Sheri A, Gruzelier J (2003). The effect of training distinct neurofeedback protocols on aspects of cognitive performance, *International Journal of Psychophysiology*, 47(1):75-85.

193. Hanslmayer S, Sauseng P, Doppelmayr M, Schabus M, Klimesch W (2005). Increasing individual upper alpha by neuro-feedback improves cognitive performance in human subjects, *Applied Psychophysiology & Biofeedback*, 30(1):1-10.

194. Angelakis E, Stathopoulou S, Frymiare JL, Green DL, Lubar JF, Kounios J (2007). EEG neurofeedback: a brief overview and an example of peak alpha frequency training for cognitive enhancement in the elderly. *Clinical Neuropsychology,* 21(1):110-29.

195. Egner T, Gruzelier JH (2003). Ecological validity of neurofeedback: modulation of slow-wave EEG enhances musical performance, *NeuroReport* 14:1225-1228.

196. Edge J, Lancaster L (2004). Enhancing musical performance through neurofeedback: playing the tune of life, *Transpersonal Psychology,* Rev. 8:2-35.

197. Raymond J, Sajid I, Parkinson LA, Gruzelier JH (2005). Biofeedback and Dance Performance: A Preliminary Investigation, *Applied Psychophysiology and Biofeedback*, 30(1):65-73.

198. Vernon DJ (2005). Can Neurofeedback Training Enhance Performance? An Evaluation of the Evidence with Implications for Future Research, *Applied Psycho-physiology and Biofeedback*, 30(4):347-64.

199. Gruzelier J, Egner T (2005). Critical validation studies of neurofeedback, *Child & Adolescent Psychiatric Clinics of North America*, 14:83-104.

200. Gruzelier J, Egner T, Vernon D (2006). Validating the efficacy of neurofeedback for optimising performance, *Progress in Brain Research,* 159:421-31.

201. Gruzelier J (2009). A theory of alpha/theta neurofeedback, creative performance enhancement, long distance functional connectivity and psychological integration, *Cognitive Processing,* 10:S101–S109.

202. Rockstroh, B., Birbaumer, N., Elbert, T., & Lutzenberger, W. (1984). Operant control of spontaneous EEG, evoked potentials and slow potentials of the brain. *Biofeedback & Self-Regulation*, 9(2):139-160.

203. Rosenfeld, JP, Cha G, Blair T, Gotlib I (1995). Operant biofeedback control of left-right frontal alpha power differences. *Biofeedback & Self-Regulation*, 20:241-258.

204. Egner T, Strawson E, Gruzelier JH (2002). EEG Signature and Phenomenology of Alpha/theta Neurofeedback Training Versus Mock Feedback, *Applied Psycho-physiology and Biofeedback*, 27(4):261-270.

205. Egner T, Zech TF, Gruzelier JH (2004). The effects of neurofeedback training on the spectral topography of the electroencephalogram, *Clinical Neurophysiology,* 115: 2452-2460.

206. Masterpasqua F, Healey KN (2003). Neurofeedback in Psychological Practice, *Professional Psychology: Research and Practice*, 34(6):652-656.

207. Monsma BR, Glaros AG, Lumley MA (1988), Feedback delays and relaxation expectancies in EMG biofeedback, *Biofeedback and Self Regulation,* 13(2):113-22.

208. Maddox WT, Ashby FG, Bohil CJ (2003). Delayed Feedback Effects on Rule-Based and Information-Integration Category Learning, *Journal of Experimental Psychology: Learning, Memory, and Cognition*, 29(4):650-662.

209. Val Robertson V, Ward A, Low J, Reed A (2006). Electrotherapy explained: principles and practice, Ed. 4, Butterworth-Heinemann, London, (*Principles of Using Biofeedback Clinically*), p. 225.

210. Williamson DA, Blanchard EB (2007). Effect of Feedback Delay Upon Learned Heart Rate Control, *Psychophysiology*, 16(2):108-115.

211. Rolnick A, (2009). Biofeedback, [Internet]. Version 13. Knol. 2009 Aug 12, (http://knol.google.com/k/arnon-rolnick/biofeedback/hbmfmvc8awy/40).

212. Russell H (2009), clinical neuropsychologist/researcher, in a private communication stated: "Signal Advance technology could significantly improve the precision of timing of the stimulation, improving treatment efficiency and thus, significantly decreasing treatment time."

213. Navarro X, Krueger TB, Lago N, Micera S, Stieglitz T, Dario P. (2005). A critical review of interfaces with the peripheral nervous system for the control of neuroprostheses and hybrid bionic systems, *Journal of the Peripheral Nervous System,* 10:229-258.

214. Leuthardt EC, Schalk G, Wolpaw JR, Ojemann JG, Moran DW (2004). A brain–computer interface using electrocorticographic signals in humans, *Journal of Neural Engineering,* 1:63-71.

215. Kawato M (2008). Brain controlled robots, *HFSP Journal.* 2(3):136-142.

216. Wolpaw, JR (2004) Brain-computer interfaces (BCIs) for communication and control: a mini-review. Suppl. *Clinical Neurophysiology*, 57:607-613.

217. Schwartz A, Cui X, Weber D, Moran D (2006). Brain-Controlled Interfaces: Movement Restoration with Neural Prosthetics, *Neuron*, 52(1):205-220.

218. Achtman N, Afshar A, Santhanam G, Yu BM, Ryu SI, Shenoy KV (2007). Free-paced high-performance brain - computer interfaces, *Journal of Neural Engineering.* 4(3):336-47.

219. Pfurtscheller G (2004). Brain-Computer Interfaces: State of the Art and Future Prospects, *Proceedings of the 12th European Signal Processing Conference*, EUROSIPCO'04, 509-510.

220. Lebedev MA, Nicolelis MAL (2008), Brain–machine interfaces; past, present and future, *Trends in Neurosciences,* 29(9):536-546.

221. Meek SG, Fetherston SJ (1992). Comparison of signal-to-noise ratio of myoelectric filters for prosthesis control, *Journal of Rehabilitation Research and Development*, 29(4):9-20.

222. Bashashati A, Fatourechi M, Ward RK, Birch GE (2007). A survey of signal processing algorithms in brain–computer interfaces based on electrical brain signals, *Journal of Neural Engineering,* 4:R32-R57.

223. Van Gerven M, Farquhar J, Schaefer R, Vlek R, Geuze J, Nijholt A, Ramsey N, Haselager P, Vuurpijl L, Gielen S, Desain P (2009). The brain-computer interface cycle, *Journal of Neural Engineering,* 6(4)041001.

224. Pfurtscheller G, Müller-Putz GR, Scherer R, Neuper C (2008). Rehabilitation with Brain-Computer Interface Systems, *IEEE Computer Magazine,* 41:58-65.

225. Müller K-R, Krauledat M, Dornhege G, Curio G and Blankertz B (2004). Machine learning techniques for brain-computer interfaces, *Biomedizinische Technik,* 49:11-22.

226. Lotte F, Congedo M, L´ecuyer A, Lamarche F and Arnaldi B (2007). A Review of Classification Algorithms for EEG-based Brain-Computer Interfaces, *Journal of Neural Engineering,* 4:R1–R13.

227. Desain P, Farquhar J, Haselager P, Hesse C and Schaefer RS (2008). What BCI research needs *Proc. ACM CHI 2008 Conf. on Human Factors in Computing Systems (Venice,Italy).*

228. Dornhege G, Blankertz B, Curio G, Müller KR (2004). Boosting bit rates in non-invasive EEG single-trial classifications by feature combination and multi-class paradigms, *IEEE Transactions in Biomedical Engineering*, 51(6):993-1002.

229. Kennedy PR, Kirby MT, Moore MM, King B, Mallory A (2004). Computer Control Using Human Intracortical Local Field Potentials, *IEEE Transactions on neural Systems and Rehabilitation Engineering*, 12(3):339-344.

230. Zhou P, Lowery MM, Englehart KB, Huang H, Li G, Hargrove L, Dewald JPA, Kuiken TA (2007), Decoding a New Neural–Machine Interface for Control of Artificial Limbs, *Journal of Neurophysiology,* 98:2974-2982.

231. Shenoy KV, Santhanam G, Ryu SI, Afshar A, Yu BM, Gilja V, Linderman MD, Kalmar RS, Cunningham JP, Kemere CT, Batista AP, Churchland MM, Meng TH, (2006). Increasing the Performance of Cortically-Controlled Prostheses, *Engineering in Medicine and Biology Society, 2006. EMBS '06. 28th Annual International Conference of the IEEE*, Suppl:6652-6656.

232. Barreto AB, Scargle SD, Adjouadi M (2000). A practical EMG-based human-computer interface for users with motor disabilities, *Journal of Rehabilitation Research and Development*, 37(1):53-63.

233. Hochberg LR, Serruya MD, Friehs GM, Mukand JA, Saleh M, Caplan AH, Branner A, Chen D, Penn RD, Donoghue JP (2006). Neuronal ensemble control of prosthetic devices by a human with tetraplegia, *Nature,* 442:164-171.

234. Hatsopoulos NG, Donoghue JP (2009). The Science of Neural Interface Systems, *Annual Review of Neuroscience,* 32:249-266.

235. Larson AC, White RD, Laub G, McVeigh ER, Li D, Simonetti OP (2004), Self-Gated Cardiac Cine MRI, *Magnetic Resonance in Medicine*, 51(1):92-102,

236. Earls JP, Ho VB, Foo TK, Castillo E, Flamm SD (2002), Cardiac MRI: Recent Progress and Continued Challenges, *Journal of Magnetic Resonance*, 16:111-127.

237. Desjardins B, Kazerooni EA (2004), ECG-Gated Cardiac CT, *American Journal of Roentgenology*, 182:993-1010.

238. Arens R, Sin S, McDonough JM, Palmer JM, Dominguez T, Meyer H, Wootton DM, Pack Ai (2005), Changes in Upper Airway Size during Tidal Breathing in Children with Obstructive Sleep Apnea Syndrome, *American Journal of Respiratory Critical Care Medicine*, 171: 1298-1304.

239. Jiang SB (2006), Radiotherapy of Mobile Tumors, *Seminars in Radiation Oncology*, 16:239-248.

240. Underberg RWM, van Sörnsen de Koste JR, Lagerwaard FJ, Vincent A, Slotman BJ, Senan S (2006), A Dosimetric Analysis of Respiration-gated Radiotherapy in Patients with Stage III Lung Cancer, *Radiation Oncology* 1:8.

241. Park HD, Cho Sp, Lee KJ (2006), A Method for Generating MRI Cardiac and Respiratory Gating Pulse Simultaneously based on Adaptive Real-Time Digital Filters, *Computers in Cardiology.* 33:813-816.

242. Thompson RB, McVeigh ER (2004), Flow-Gated Phase-Contrast MRI Using Radial Acquisitions, *Magnetic Resonance in Medicine*. 52(3):598-604.

243. Nijm GM, Sahakian AV, Swiryn S, Larson AC (2007), Comparison of Signal Peak Detection Algorithms for Self-Gated Cardiac Cine MRI, *Computers in Cardiology,* 34:407-41.

244. Berbeco RI, Nishioka S, Shirato H, Chen GTY, Jiang SB (2005), Residual Motion of Lung Tumors in Gated Radiotherapy with External Respiratory Surrogates, *Physics in Medicine and Biology*, 50:3655-3667.

245. Jiang SB (2006), Technical Aspects of Image-Guided Respiration-gated Radiation Therapy, *Medical Dosimetry*, 31(2):141-151.

246. Shirato H, Shimizu S, Kunieda T, Kitamura K, Van Herk M, Kagei K, Nishioka T, Hashimoto S, Fujita K, Aoyama H, Tsuchiya K, Kudo K, Miyasaka K (2000), Physical Aspects of a Real-Time Tumor-Tracking System for Gated Radiotherapy, *International Journal of Radiation Oncology • Biology • Physics*, 48(4): 1187-1195.

247. Webb S (2006), Motion Effects in (Intensity Modulated) Radiation Therapy: A Review, *Physics in Medicine and Biology*, 51: R403-R425.

248. Jiang SB, Nishioka S, Shirato H, Berbeco RI (2007), Internal-External Correlation Investigations of Respiratory Induced Motion of Lung Tumors, *Medical Physics*, 34(10):3893-3903.

249. Tsunashima Y, Sakae T, Shioyama Y, Kagei K, Terunuma T, Nohtomi A, Akine Y (2004), Correlation between the Respiratory Waveform Measured Using a Respiratory Sensor and 3D Tumor Motion in Gated Radiotherapy, *International Journal of Radiation Oncology • Biology • Physics*, 60 (3):951-958.

250. Senana S, De Ruysscherb D, Giraudc P, Mirimanoffd R, Budache V, on behalf of the Radiotherapy Group of the European Organization for Research and Treatment of Cancer (EORTC) (2004), Literature-based Recommendations for Treatment Planning and Execution in High-dose Radiotherapy for Lung Cancer, *Radiotherapy and Oncology,* 71(21):139-146.

251. Sharp GC, Lu HM, Trofimjov A, Tang X, Jiang SB, Turcotte J, Gierga DP, Chen GTY, Hong TS (2007), Assessing Residual Motion for Gated Proton-Beam Radiotherapy, *Journal or Radiation Research*, Suppl: A55-A59.

252. Jin JY, Yin FF (2006), Time Delay Measurement for Linac-based Treatment Delivery in Synchronized Respiratory Gating Radiotherapy. *Medical Physics.* 32**:**1293-6.

Curriculum Vitae

Chris M. Hymel

Education:

University of Texas Health Science Center at Houston, Graduate School of Biomedical Sciences, Doctorate: Biomedical Sciences, 2010.

Texas A&M University, Master of Engineering: Electrical Engineering, 1982.

Texas A&M University, Bachelor of Science: Electrical Engineering, 1980

Appointments/Positions:

Signal Advance, Inc, Houston, TX (formerly Biodyne Development Company) (1992-Present): President/CEO, Director. Scientific/ biomedical systems development; Engineering consulting, Training/educational systems, Biomedical/scientific animations/modeling/simulations.

Educational Enrichment Center, Inc, Houston, TX (1990-Present): Director - non-profit corporation, Application of technology to the improvement of education, and enhancement of neurocognitive function and memory processing.

CH Systems, Houston, TX (1985-93) - Microcomputer systems consulting, Research automation and data acquisition systems development, Graphics systems development.

University of Texas Health Science Center at Houston, Neurophysiology Research Center, Houston, TX (1984-88), Engineering consultant.

Shell Oil & Shell Development Company, Houston, TX (1982-85), Control systems engin engineering.

Texas A&M University, Dept. of Electrical Engineering, College Station, TX (1979-81), Research assistant.

Johnson Controls, Inc., Houston, TX, (1977-1979) Engineering support.

Awards:

- International Who's Who of Entrepreneurs (1996).
- Sterling Who's Who: Executive Edition (1996).
- Outstanding Young Men of America (1988).
- Special Recognition Award, Shell Oil Company (1985).
- Distinguished Student, Texas A&M University (1982).
- Outstanding Achievement, Texas A&M University, (1977-78).

Patents:

Voltage, Current and Frequency Measuring of Non-Standard Waveforms. U.S. Patent No.4,779,044, Israel Patent No. 85,371 (1988).

Pulse Generation and Tracking System, Great Britain Patent No. 2,223,856 (1993).

A Method for the User-Friendly Customization of Either or Both Sides with any Image, Including Text or Photographs, of Cards for Multiple Purposes, Patent pending.

Method for Actuarial Determination if the Cost of One-Time Procedural or Professional Liability Insurance Policy, Patent pending.

Utility and Method for the Application of Signal advance Technology to Analog Signal Detection, Acquisition and Processing, Patent pending.

PUBLICATIONS:

Doctoral Dissertation:

Application of Signal Advance Technology to Electrophysiology, Doctor of Philosophy, University of Texas Health Science Center at Houston, Graduate School of Biomedical Sciences, 2010.

Master's Thesis:

E.P.I. Feeder Protection Relay Monitoring System, Masters of Engineering, Electrical Engineering, Texas A&M University, 1982.

Abstracts:

DeFrance JF, Degioanni J, Hymel C, Kutyna F, Calkins R (1991). Topographical event-related potential (ERP) analysis of the effects on social/environmental isolation, *American Society for Gravitational and Space Biology*, Washington DC.

Hymel C, Schweitzer F, Defrance J, Joe H, Skolnick M (1991), Low Current Transcranial Electrostimulation Decreases Frequency Response in Human EEG's, *FASEB Journal*, 5 (4): A861, #2856. Atlanta, GA.

Trachtenberg M, DeFrance JF, Ginsberg L, Hymel C, Blume J, Sharma A, Blum K (1991), Effects of Tropamine+ on attentional processing, *American. Society of Addictive Medicine*, New York, NY.

Trachtenberg M, DeFrance, JF, Ginsberg L, Blackwell J, Hymel C (1991), Electrophysiological and cognitive measures of recovery in cocaine patients*, American Society of Addictive Medicine,* Boston, MA.

DeFrance JF, Degioanni J, Hymel C, Kutyna F, Calkins R (1991), Topographical event-related potential (ERP) analysis of the effects on social/environmental isolation, *American Society For Gravitational and Space Biology*, Washington, DC.

Hymel C, Skolnick, M (1989), Transcranial Electrostimulation Potential Field Distribution in the Brain and the Effect on Somatosensory Evoked Potentials, *7th Annual Conference Houston Society for Engineering in Medicine and Biology*, February 17-18.

Hymel C, Jenkins P, Sands S, Skolnick M, Wilson O (1988), Investigation of the Propagation and Waveform Characteristics of Transcranial Electrostimulation in the Brain, *FASEB Journal.* 2(5): A1070, #4503.

Hamilton RF, Collard CD, Hymel C, Wilson O, Skolnick M (1988), Characteristics of Low Current Transcranial Electrostimulation (TCES) in the Production of Naloxone-Reversible Analgesia in Male Rats, FASEB Journal, 2(5): A1071, #4504.

Hymel C, Jenkins P, Skolnick M (1988), Transcranial Electrostimulation Energy Density Distribution in the Brain and Effects on Somatosensory and Limbic Nuclei, *Journal for Society of Neuroscience,.*14(1):175, #75.8.

Skolnick M., Collard CD., Hamilton RF, Hudson-Howard L., Hymel C, Wilson O (1987), Transcranial Electrostimulation Increases Tail Flick Latencies After Nociceptive Challenge. *Journal for Society of Neuroscience,* 13:1304.

Journal Articles:

DeFrance JF, Hymel C, Trachtenberg MC, Ginsberg LD, Schweitzer FC, Estes S, Chen TJ, Braverman ER, Cull JG, Blum K (1997). Enhancement of Attention Processing by Kantroll in Healthy Humans: A pilot Study. *Clinical Electroencephalography.* 28:68-75.

DeFrance JF, Hymel C, Degionanni J, Kutyna F, Calkins DS, Estes S, Schweitzer FC (1997). Evidence of temporal lobe Activation by Discriminative Spatial Orientation, *Brain Topography,* 6(2):137-42.

Wilson OB, Hamilton RF, Warner RL, Johnston CM, deFriece R, Harter L, Schweitzer C, Talaverra J, Hymel CM, Skolnick MH (1989). The Influence of Electrical Variables on Analgesia Produced by Low Current Transcranial Electro-Stimulation of Rats, *Anesthesia & Analgesia.* 68(5):673-81.

Skolnick MH, Wilson OB, Hamilton RF, Collard CD, Hudson-Howard L, Hymel C, Malin DH (1989). Low Current Electrostimulation Produces Naloxone-reversible Analgesia in Rats, *Stereotactic Functional Neurosurgery*, 53(2):125-40.

Chapters/Proceedings:

DeFrance JF, Hymel C, Degioanni J, Calkins DS, Estes S, and Schweitzer FC, Assessment of Cognitive Function: Exploration of Memory Processing by Topographical Mapping Techniques. C. Reynolds (Ed.). Plenum Publishing, New York, 1992.

Skolnick M, Collard CD, Hamilton RF, Hudson- Howard L, Hymel C, Wilson O (1988), Transcranial Electrostimulation Increases Tail Flick Latencies after Nociceptive Challenge, *Proceedings for Society of Neuroscience 17th Annual Meeting*, 13:1304.

Grants:

Potentiation of Opiate Analgesia by Electrostimulation, National Institute of Drug Abuse 1 RO3 DA06869-01A1, Co-investigator (PI: Malcolm Skolnick, Ph.D) ($125,000/year), 1986 - 87.

Lectures and Presentations:

Training Series, "Digital Control Systems", Shell Oil Company, 1981-82

Invited Speaker. "Technology in the Practice of Law" University of Houston Law School, Houston Texas, 1996.

Invited Speaker, "Animations and Demonstrative Evidence," National Conference Expert Witnesses, Litigation Consultants and Attorneys, National Forensic Center, Houston Texas, 1998.